1 ER-2 Flights

The following figures show measurements of chemical species along the flight paths of the ER-2 aircraft on 16 flights between 6 January and 16 March 2000. Flights between 20 January and 12 March started from Kiruna (Sweden) and probed the stratospheric polar vortex and surf zone, while the other flights were transfer and test flights.

Additionally, the flight path and several parameters along the flight paths that are helpful for interpretation of the measurements are shown, including pressure, temperature and solar zenith angle.

Flight parameters	
Figure 1	Flight path
Figure 2	Pressure
Figure 3	Temperature
Figure 4	Solar zenith angle
Figure 5	Potential temperature
Figure 6	Equivalent latitude
Halogen sources	
Figure 7	CFC-11
Figure 8	CFC-12
Figure 9	CFC-113
Figure 10	CCl_4
Figure 11	CH_3CCl_3
Figure 12	Halon-1211
Long-lived source gases	
Figure 13	CH_4
Figure 14	N_2O
Figure 15	H_2O
Figure 16	CO_2
Ozone	
Figure 17	O_3
Chlorine	
Figure 18	ClO
Figure 19	Cl_2O_2
Figure 20	ClO_x
Figure 21	$ClONO_2$
Figure 22	Cl_y
Nitrogen	
Figure 23	HNO_3
Figure 24	NO_y
Figure 25	NO
Figure 26	NO_2
Hydrogen	
Figure 27	OH
Figure 28	HO_2

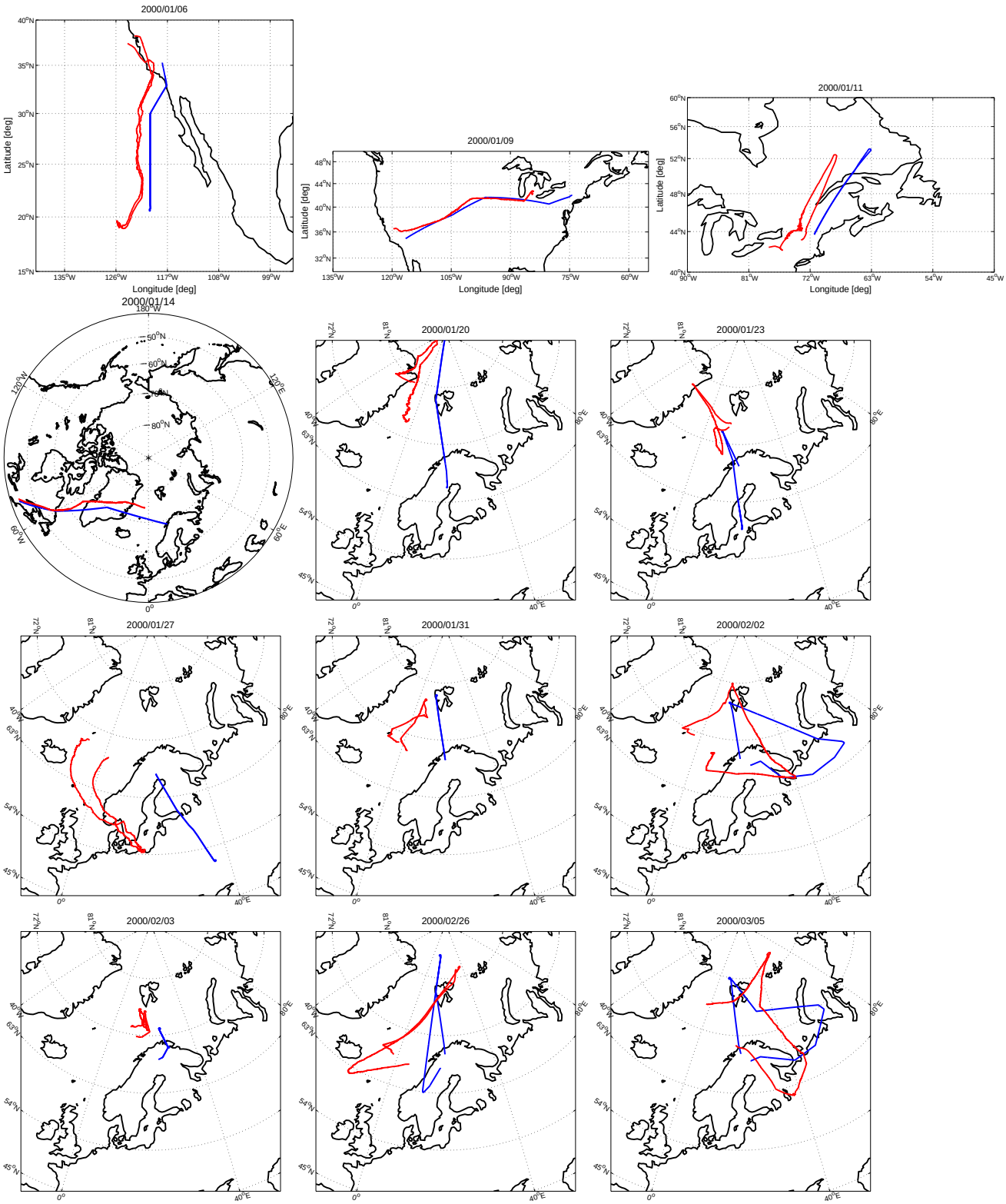

Figure 1: Flight paths of the ER-2 for all campaign flights. The blue line shows the actual flight path and the red line is the position of the probed air parcels at the last model time step before the flight (either at 00 UTC or 12 UTC).

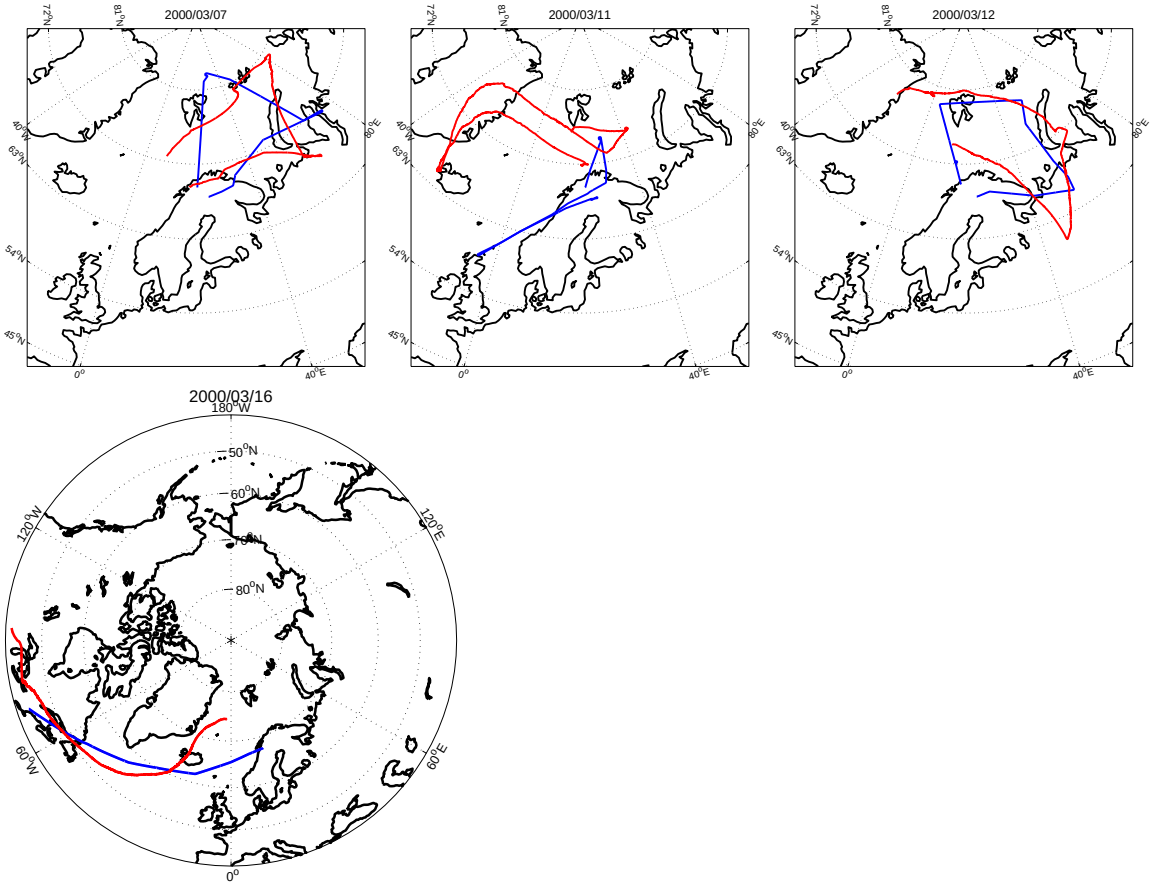

Figure 1: Flight paths of the ER-2 for all campaign flights. The blue line shows the actual flight path and the red line is the position of the probed air parcels at the last model time step before the flight (either at 00 h UTC or 12 h UTC).

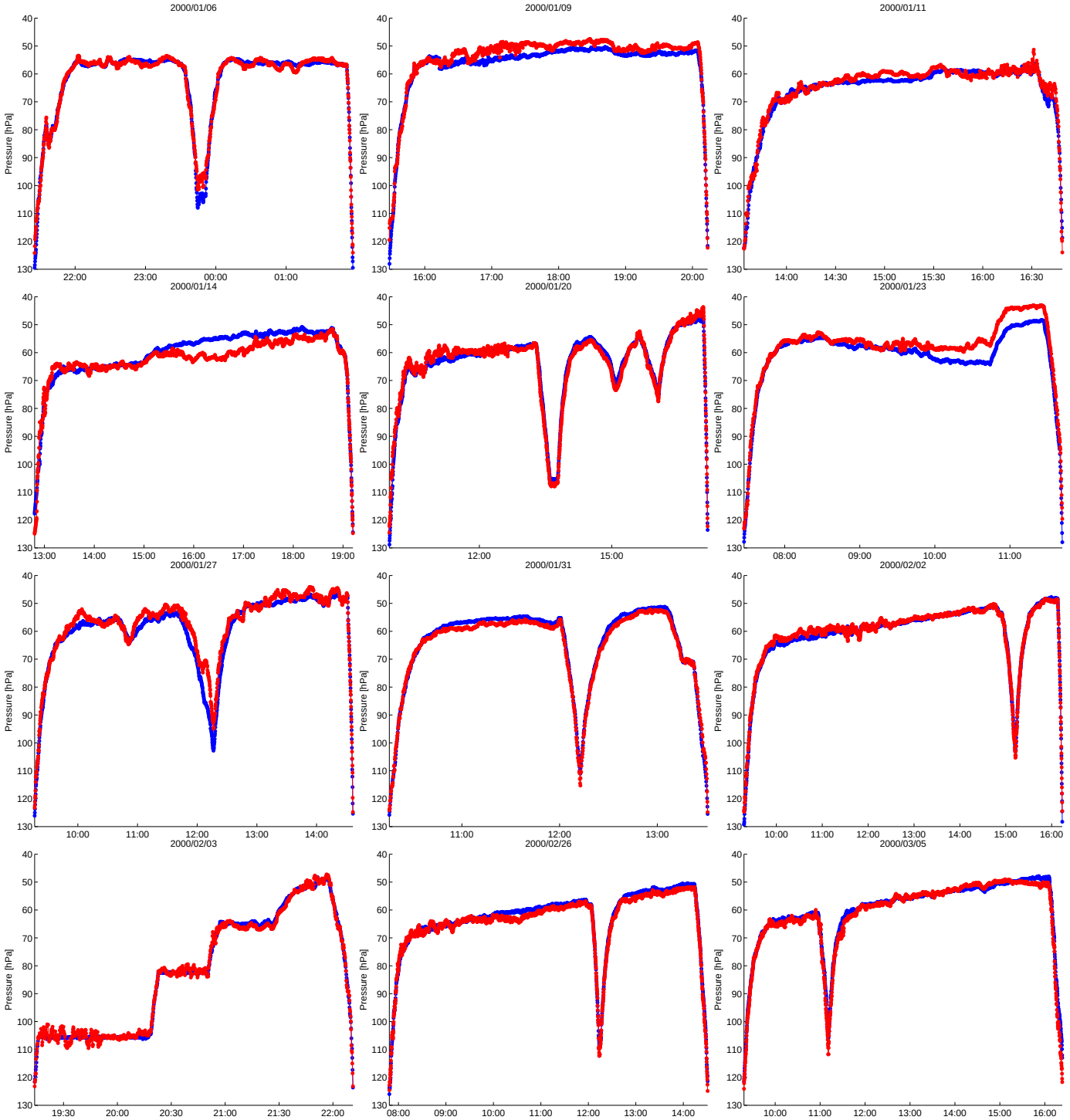

Figure 2: Pressure as a function of flight time (UTC). The blue line shows the pressure along the actual flight path (from ER-2 measurements) and the red line shows the pressure on the position of the probed air parcels at the last model time step before the flight (from the ERA Interim reanalysis, either at 00 h UTC or 12 h UTC).

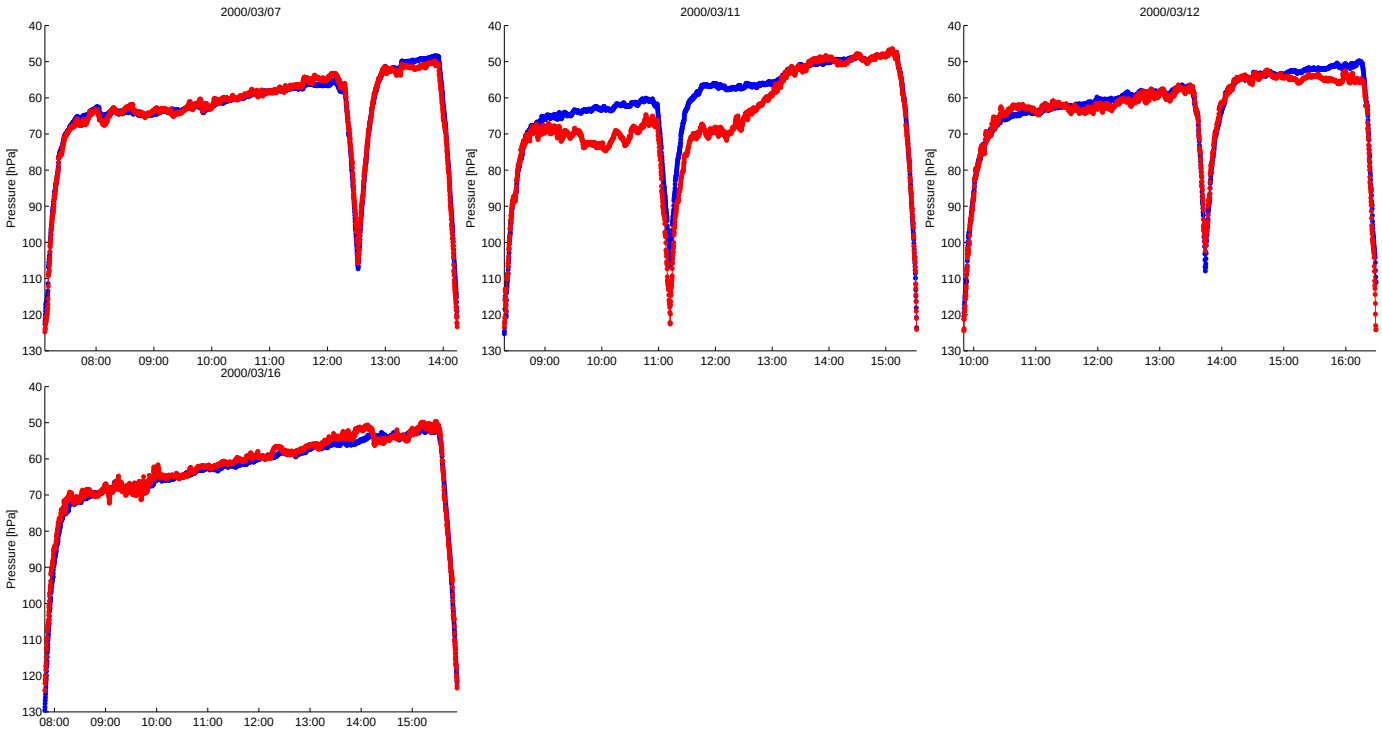

Figure 2: Pressure as a function of flight time (UTC). The blue line shows the pressure along the actual flight path (from ER-2 measurements) and the red line shows the pressure on the position of the probed air parcels at the last model time step before the flight (from the ERA Interim reanalysis, either at 00 h UTC or 12 h UTC).

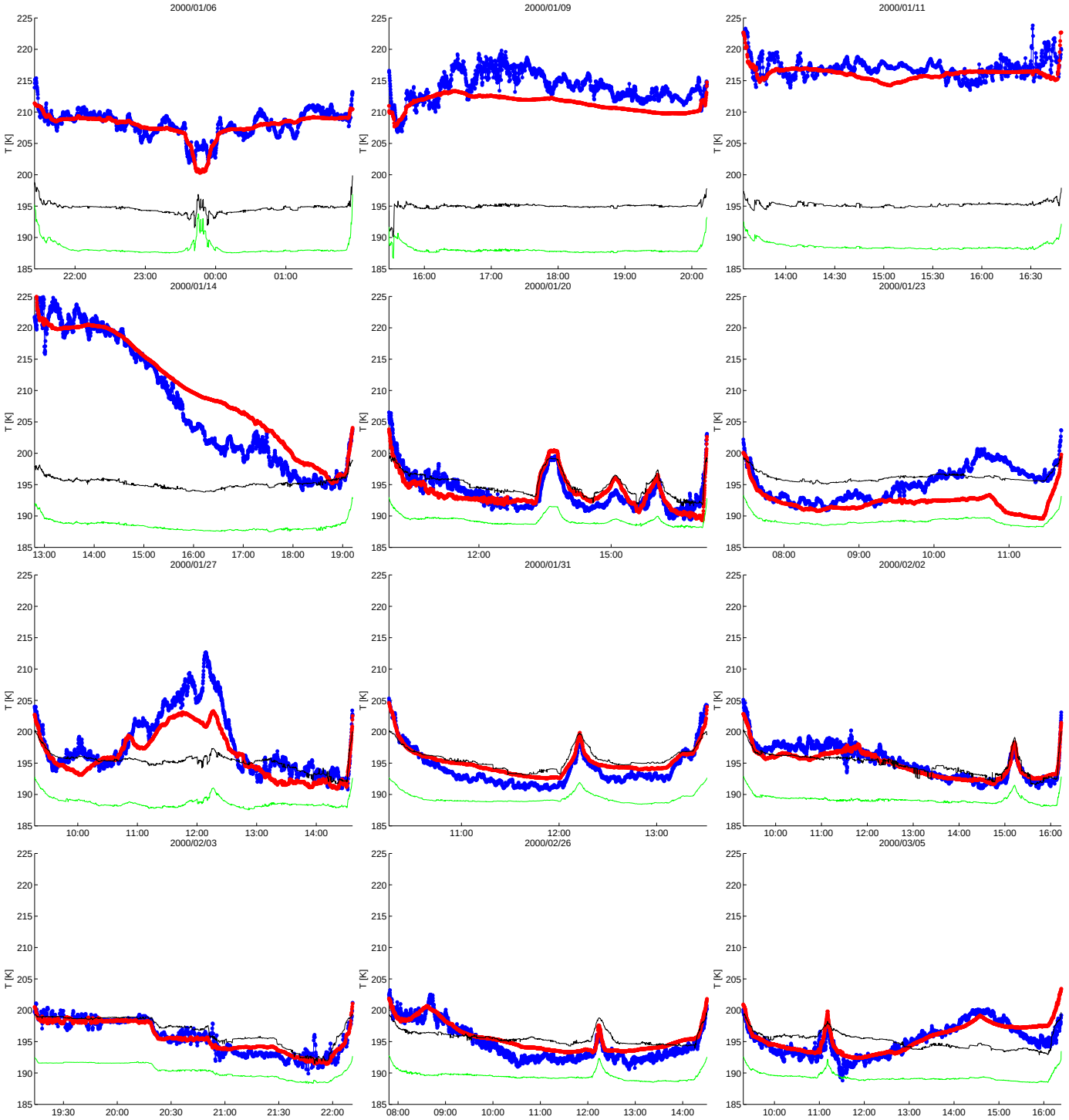

Figure 3: Temperature as a function of flight time (UTC). The blue line shows the temperature along the actual flight path (from ER-2 measurements) and the red line shows the temperature on the position of the probed air parcels at the last model time step before the flight (from the ERA Interim reanalysis, either at 00 h UTC or 12 h UTC). The thin black and green lines show the NAT and ice formation temperatures along the flight path.

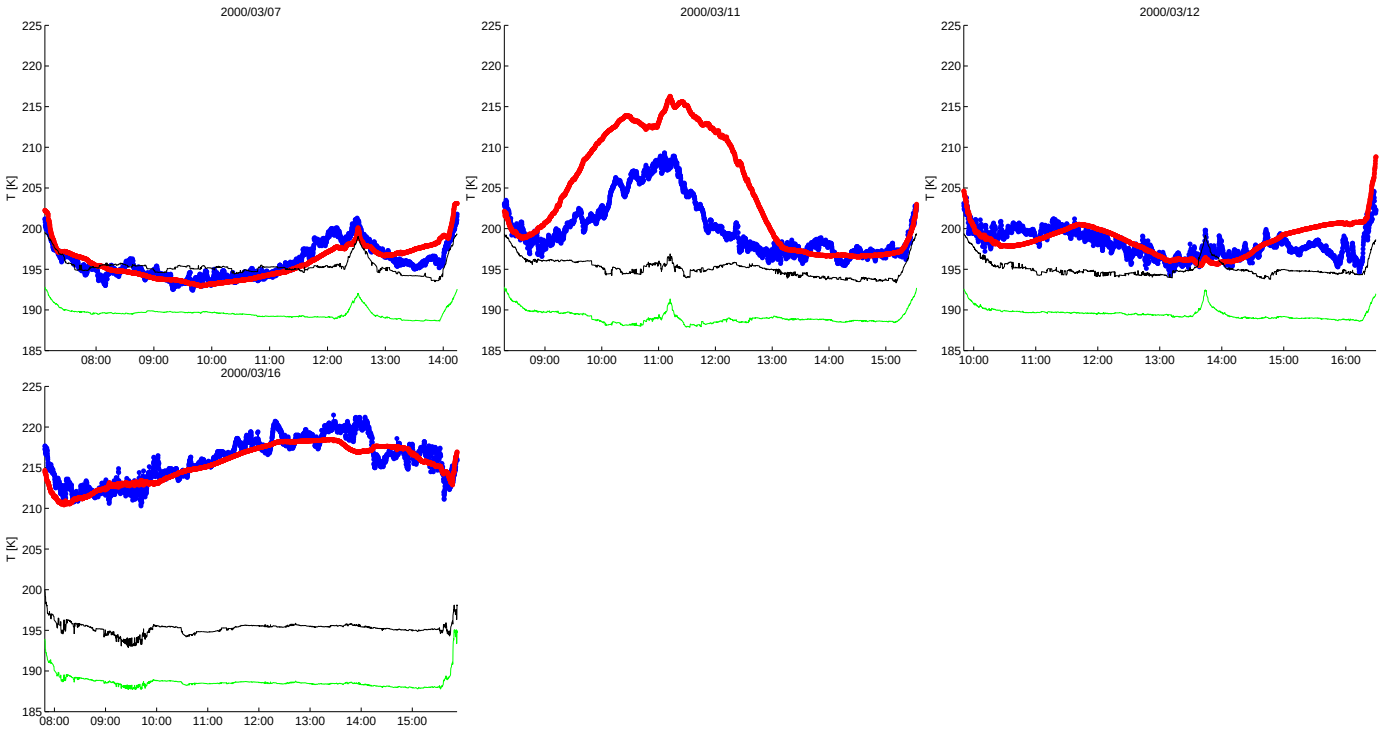

Figure 3: Temperature as a function of flight time (UTC). The blue line shows the temperature along the actual flight path (from ER-2 measurements) and the red line shows the temperature on the position of the probed air parcels at the last model time step before the flight (from the ERA Interim reanalysis, either at 00 h UTC or 12 h UTC). The thin black and green lines show the NAT and ice formation temperatures along the flight path.

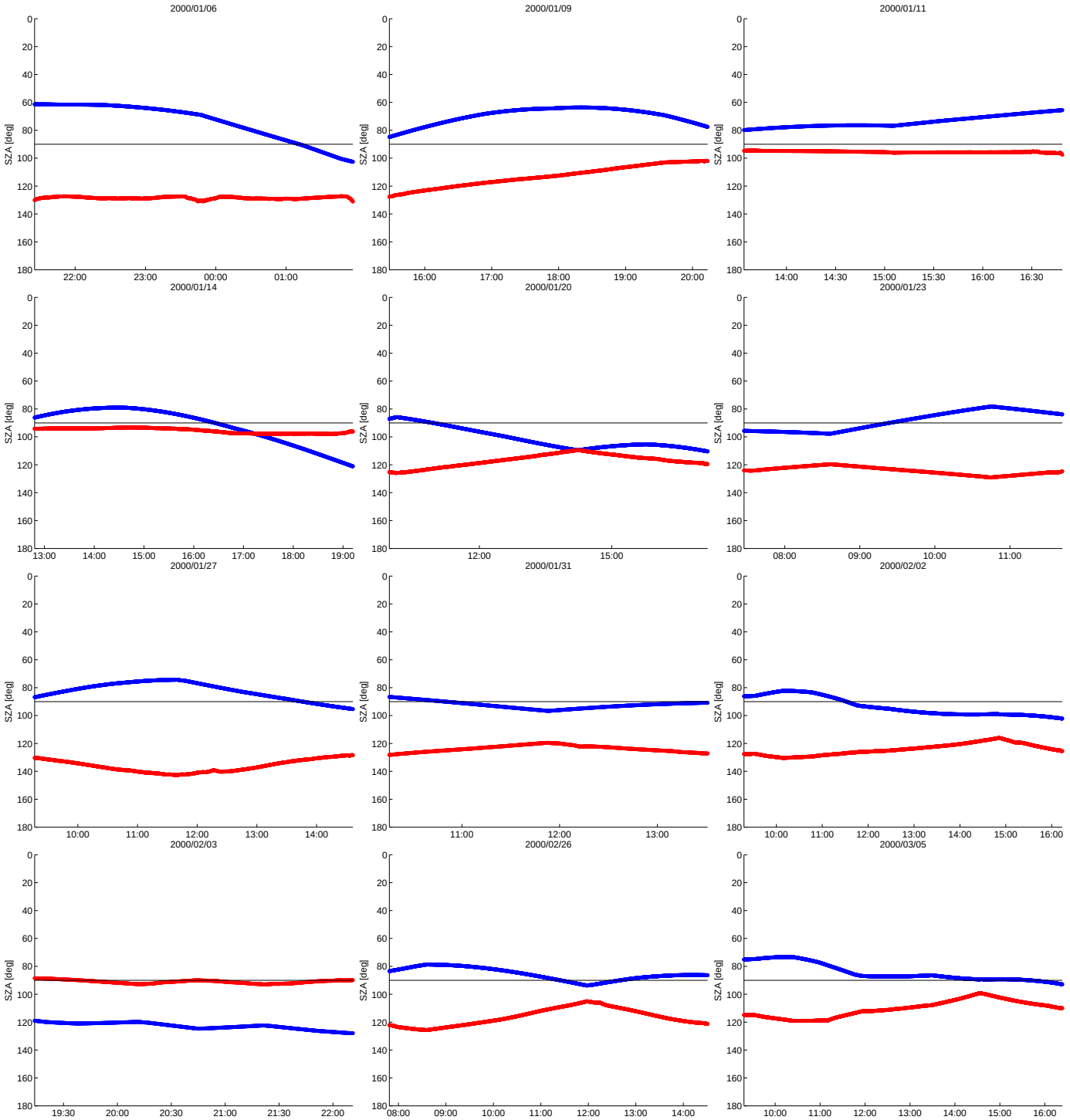

Figure 4: Solar zenith angle as a function of flight time (UTC). The blue line shows the solar zenith angle along the actual flight path and the red line shows the solar zenith angle on the position of the probed air parcels at the last model time step before the flight (either at 00 h UTC or 12 h UTC). The black line divides night and day.

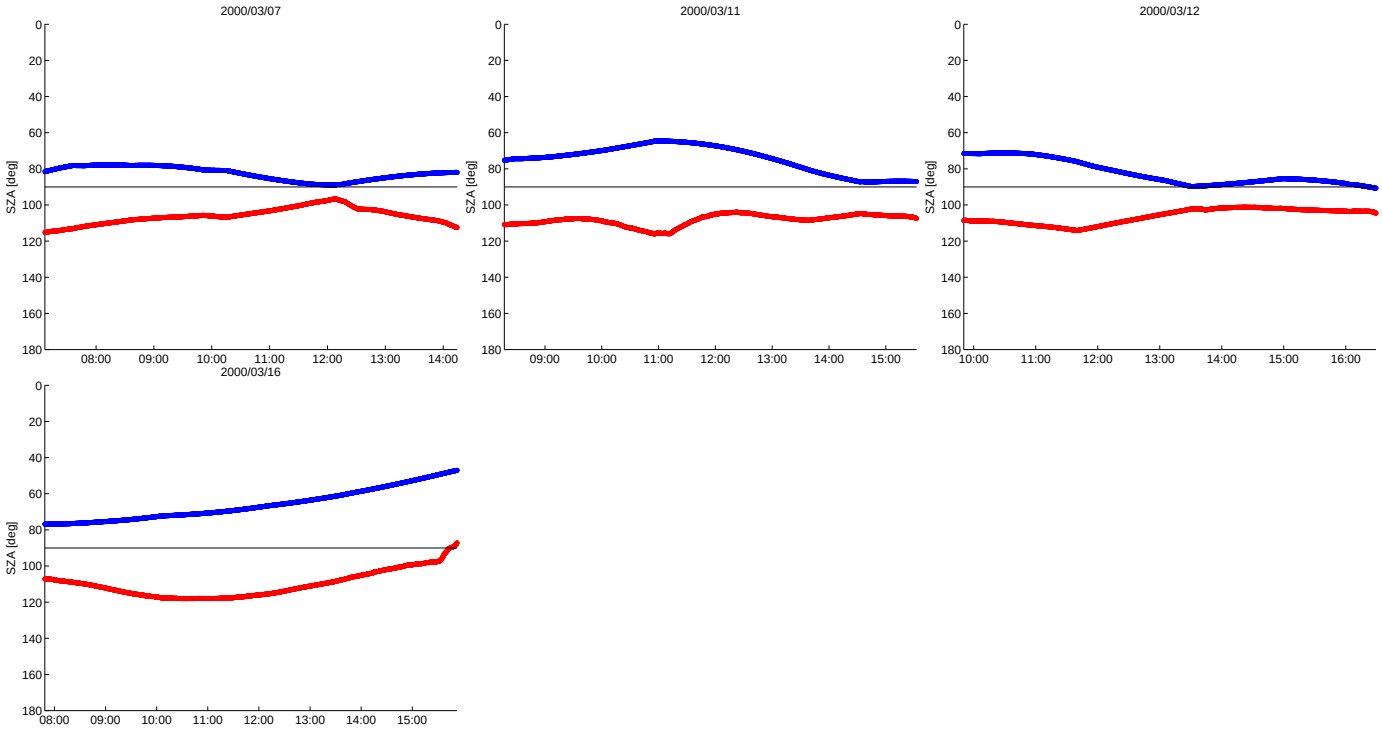

Figure 4: Solar zenith angle as a function of flight time (UTC). The blue line shows the solar zenith angle along the actual flight path and the red line shows the solar zenith angle on the position of the probed air parcels at the last model time step before the flight (either at 00 h UTC or 12 h UTC). The black line divides night and day.

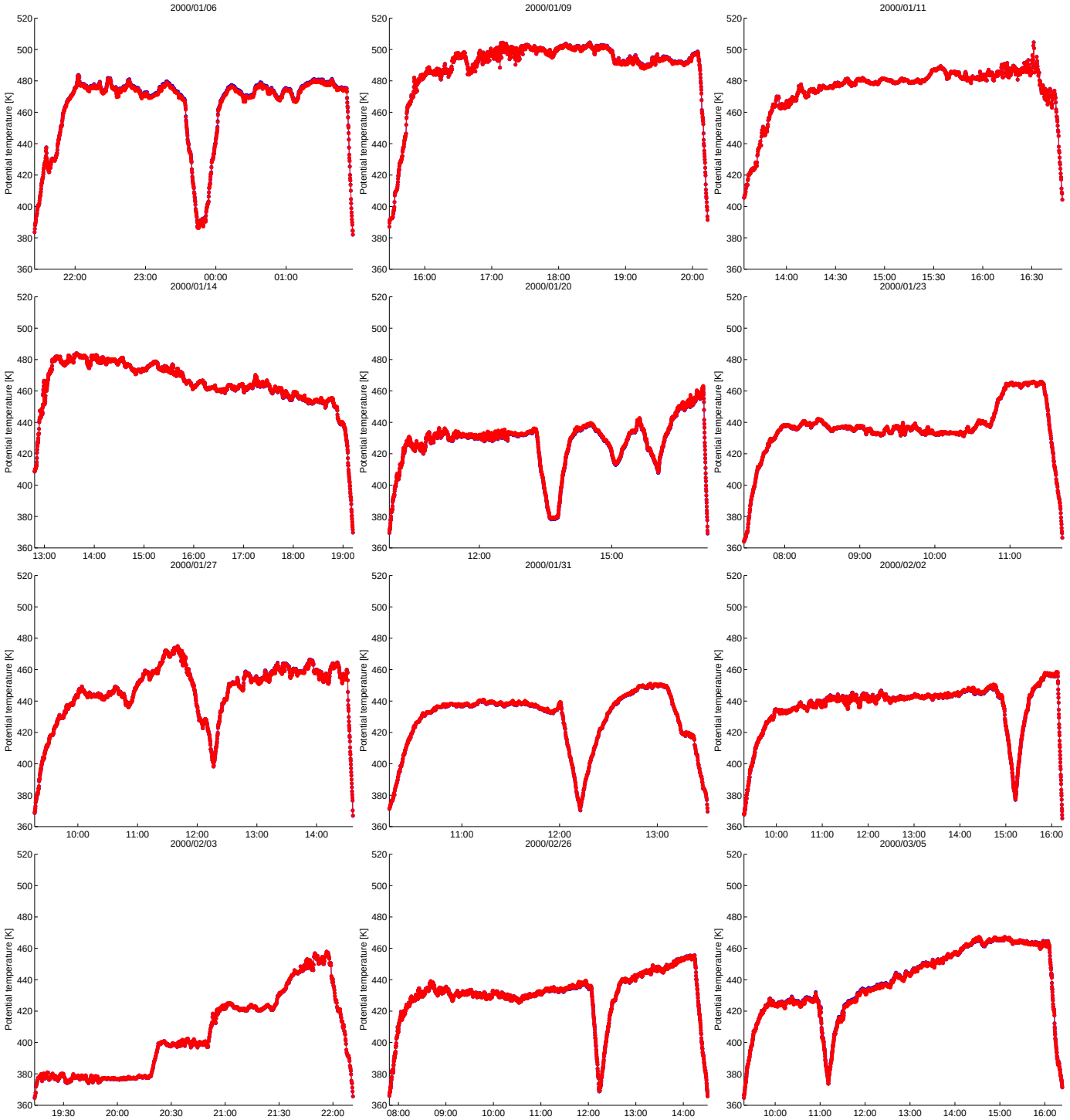

Figure 5: Potential temperature as a function of flight time (UTC). The blue line shows the potential temperature along the actual flight path (from ER-2 measurements) and the red line shows the potential temperature on the position of the probed air parcels at the last model time step before the flight (from the ERA Interim reanalysis, either at 00 h UTC or 12 h UTC).

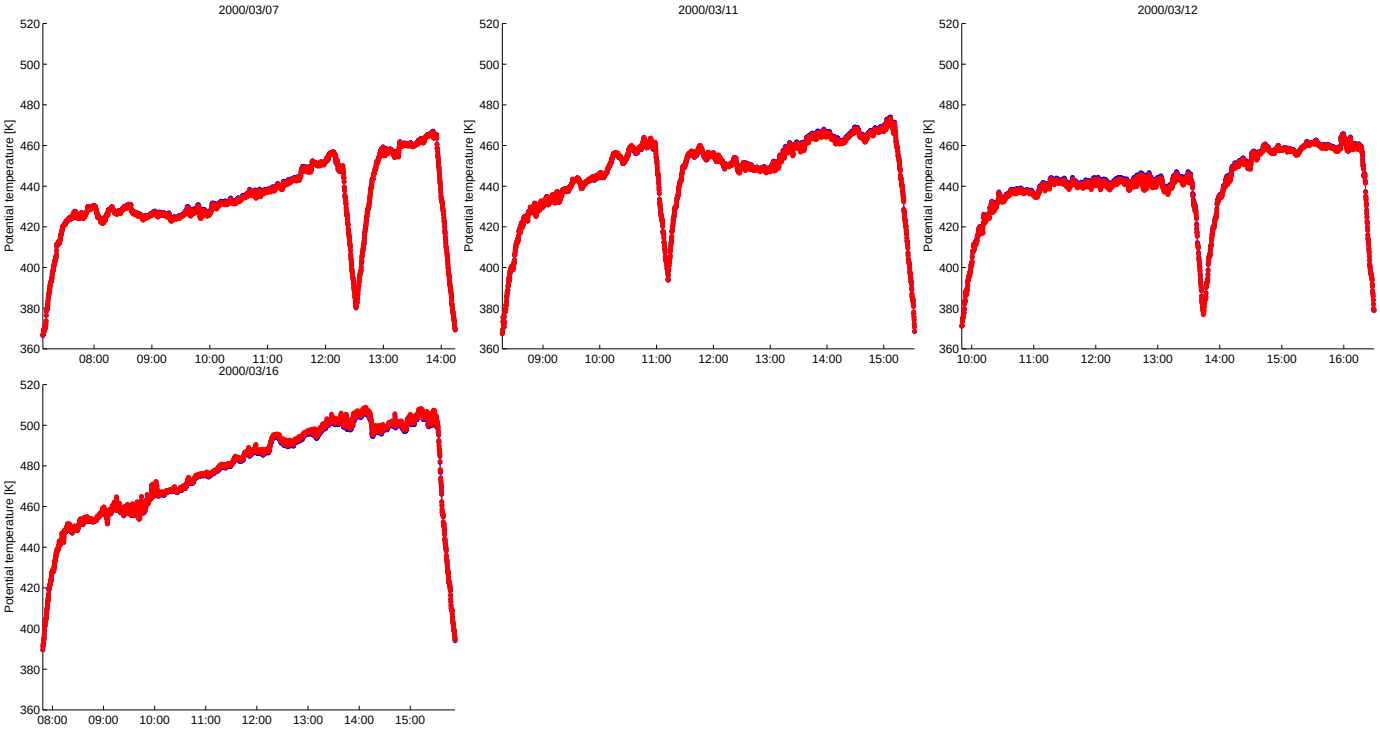

Figure 5: Potential temperature as a function of flight time (UTC). The blue line shows the potential temperature along the actual flight path (from ER-2 measurements) and the red line shows the potential temperature on the position of the probed air parcels at the last model time step before the flight (from the ERA Interim reanalysis, either at 00 h UTC or 12 h UTC).

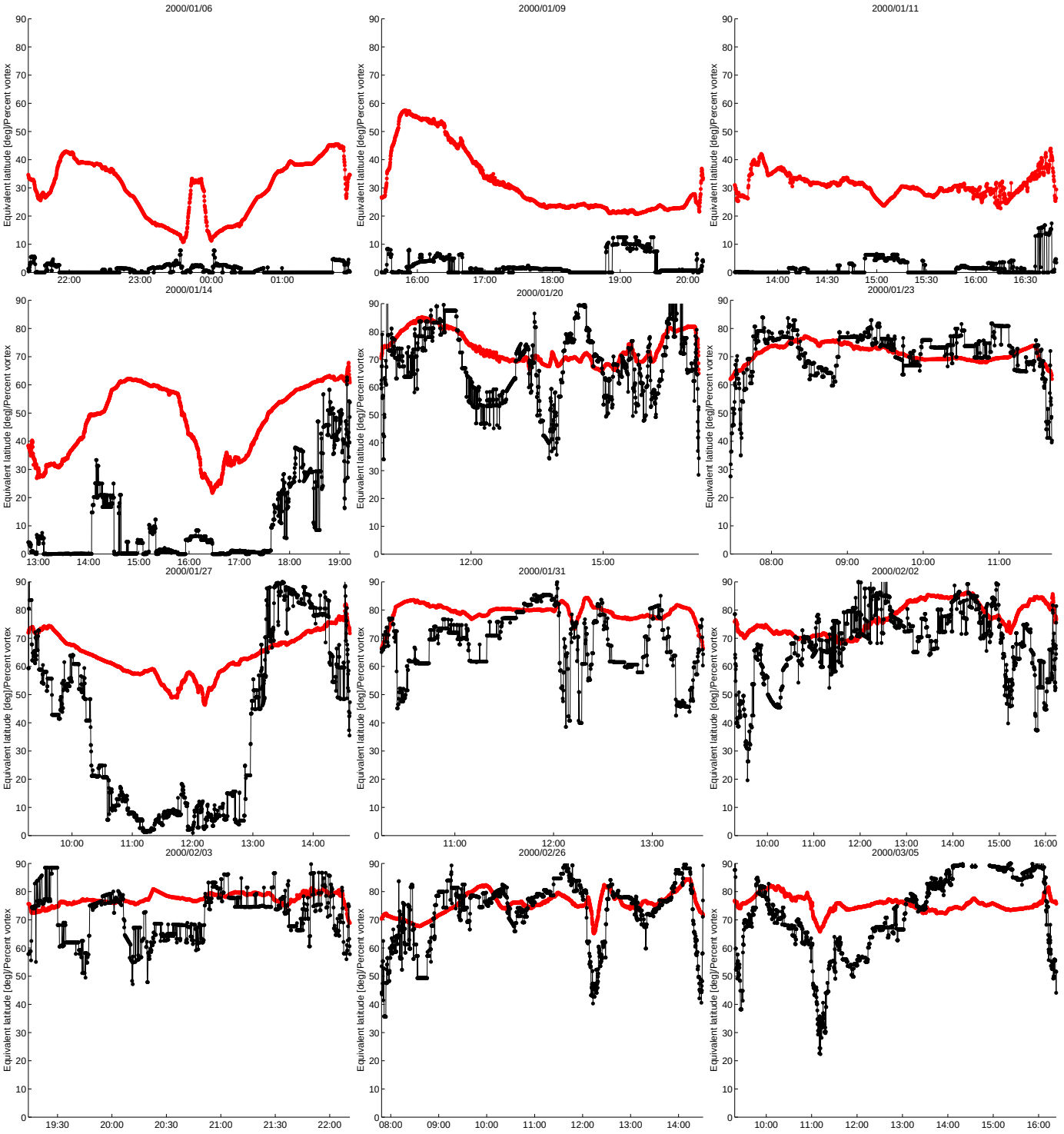

Figure 6: Equivalent latitude as a function of flight time (UTC) calculated on the position of the probed air parcels at the last model time step before the flight from potential vorticity fields of the ERA Interim reanalysis. The black line shows an approximate tracer for the vortex (initialized at 1 December with values of 100% inside 64° equivalent latitude and 0% elsewhere).

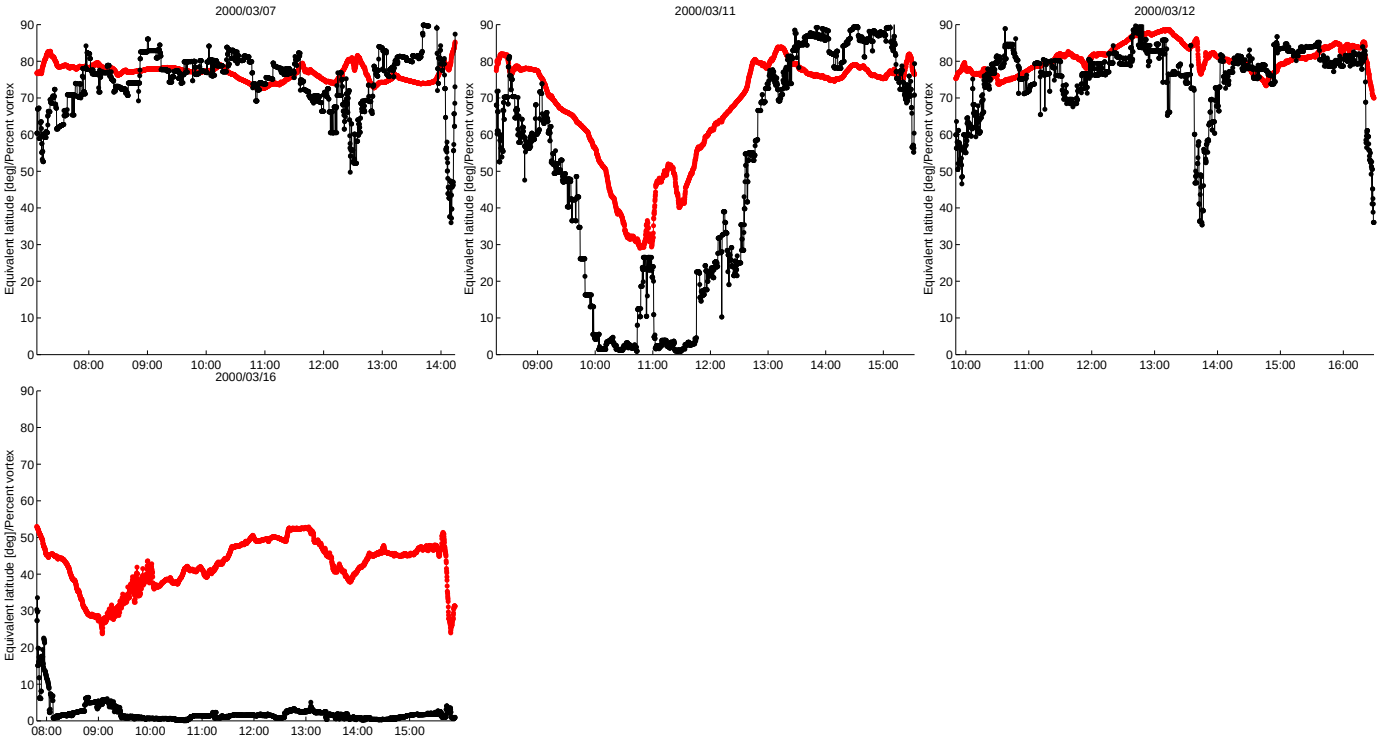

Figure 6: Equivalent latitude as a function of flight time (UTC) calculated on the position of the probed air parcels at the last model time step before the flight from potential vorticity fields of the ERA Interim reanalysis. The black line shows an approximate tracer for the vortex (initialized at 1 December with values of 100% inside 64° equivalent latitude and 0% elsewhere).

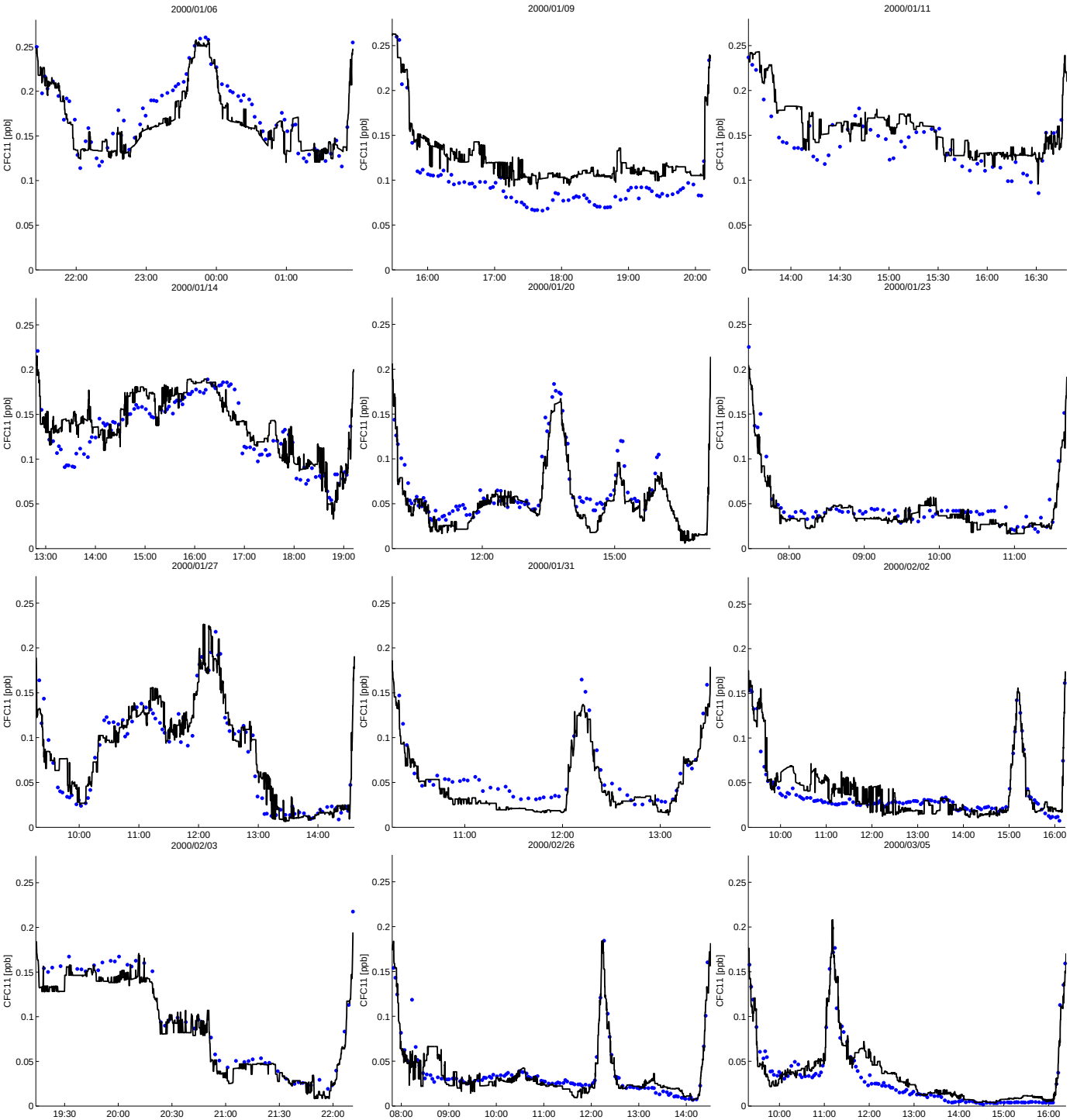

Figure 7: CFC-11 as a function of flight time (UTC) from measurements of the ACATS gas chromatograph (blue dots) compared to modeled values (black lines).

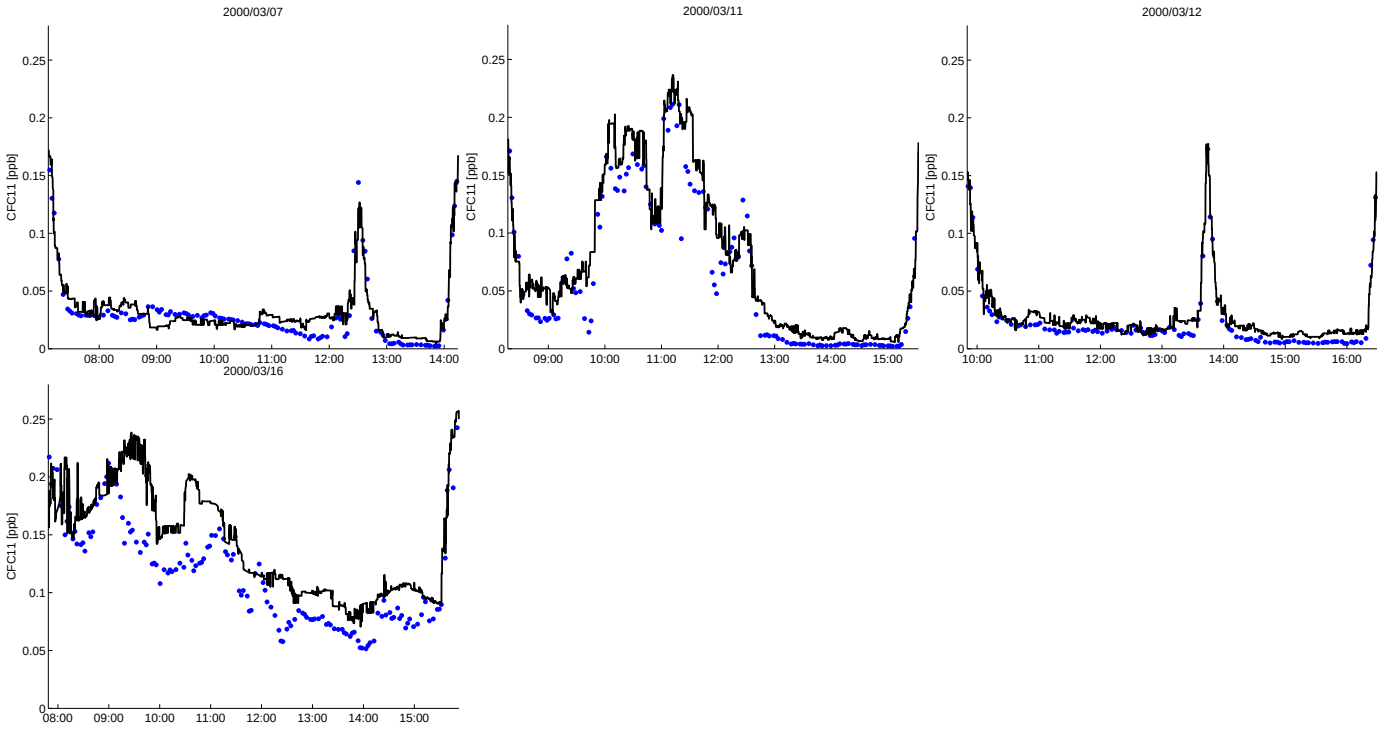

Figure 7: CFC-11 as a function of flight time (UTC) from measurements of the ACATS gas chromatograph (blue dots) compared to modeled values (black lines).

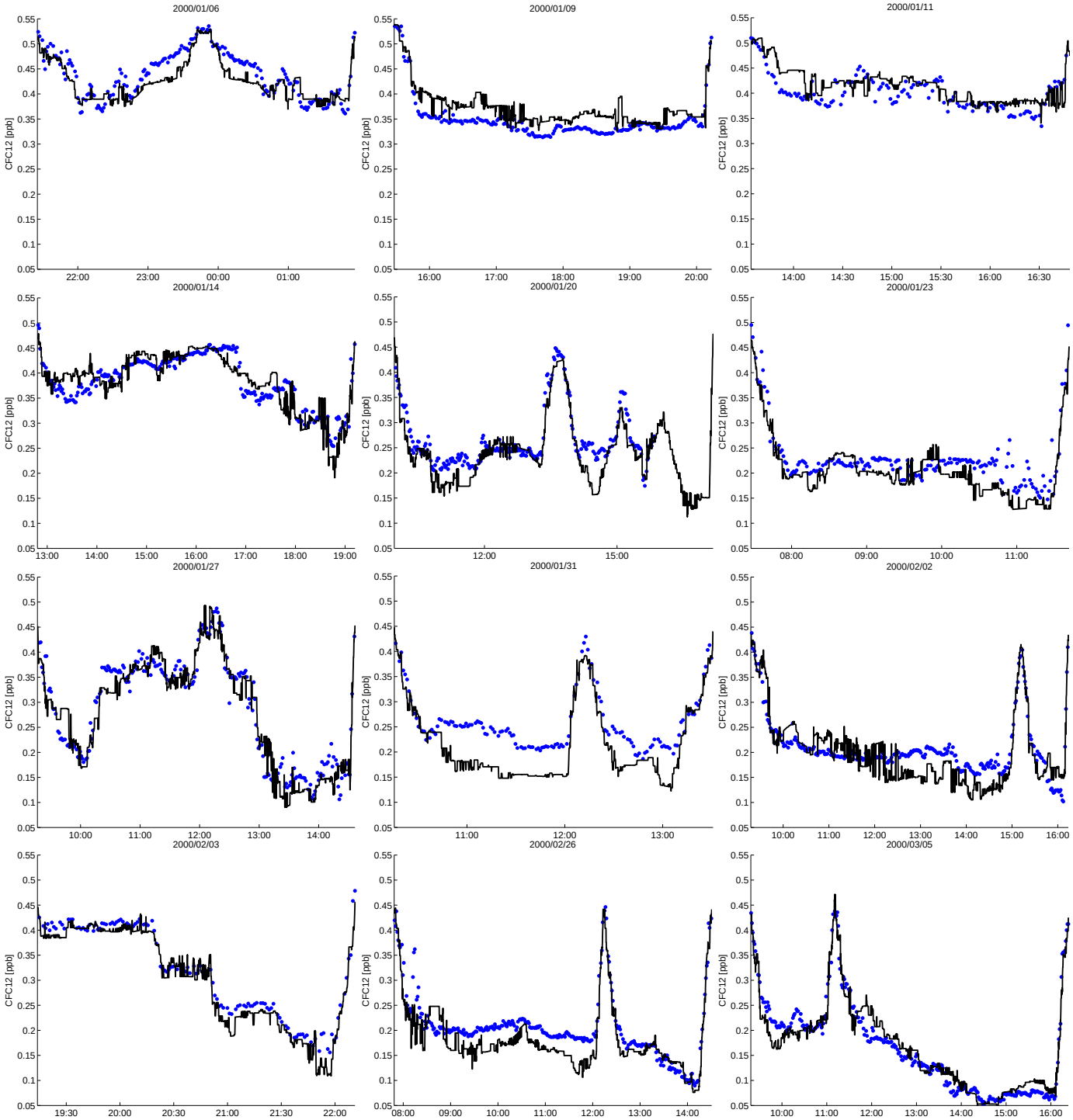

Figure 8: CFC-12 as a function of flight time (UTC) from measurements of the ACATS gas chromatograph (blue dots) compared to modeled values (black lines).

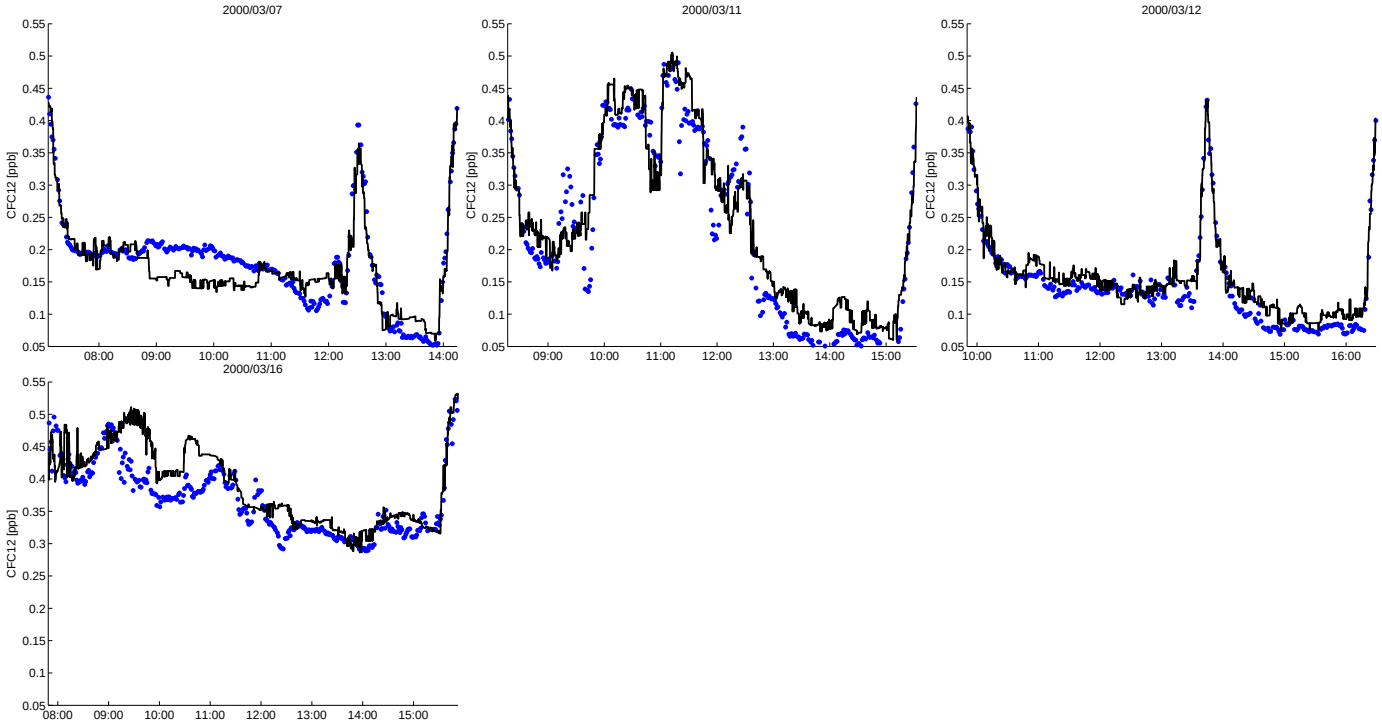

Figure 8: CFC-12 as a function of flight time (UTC) from measurements of the ACATS gas chromatograph (blue dots) compared to modeled values (black lines).

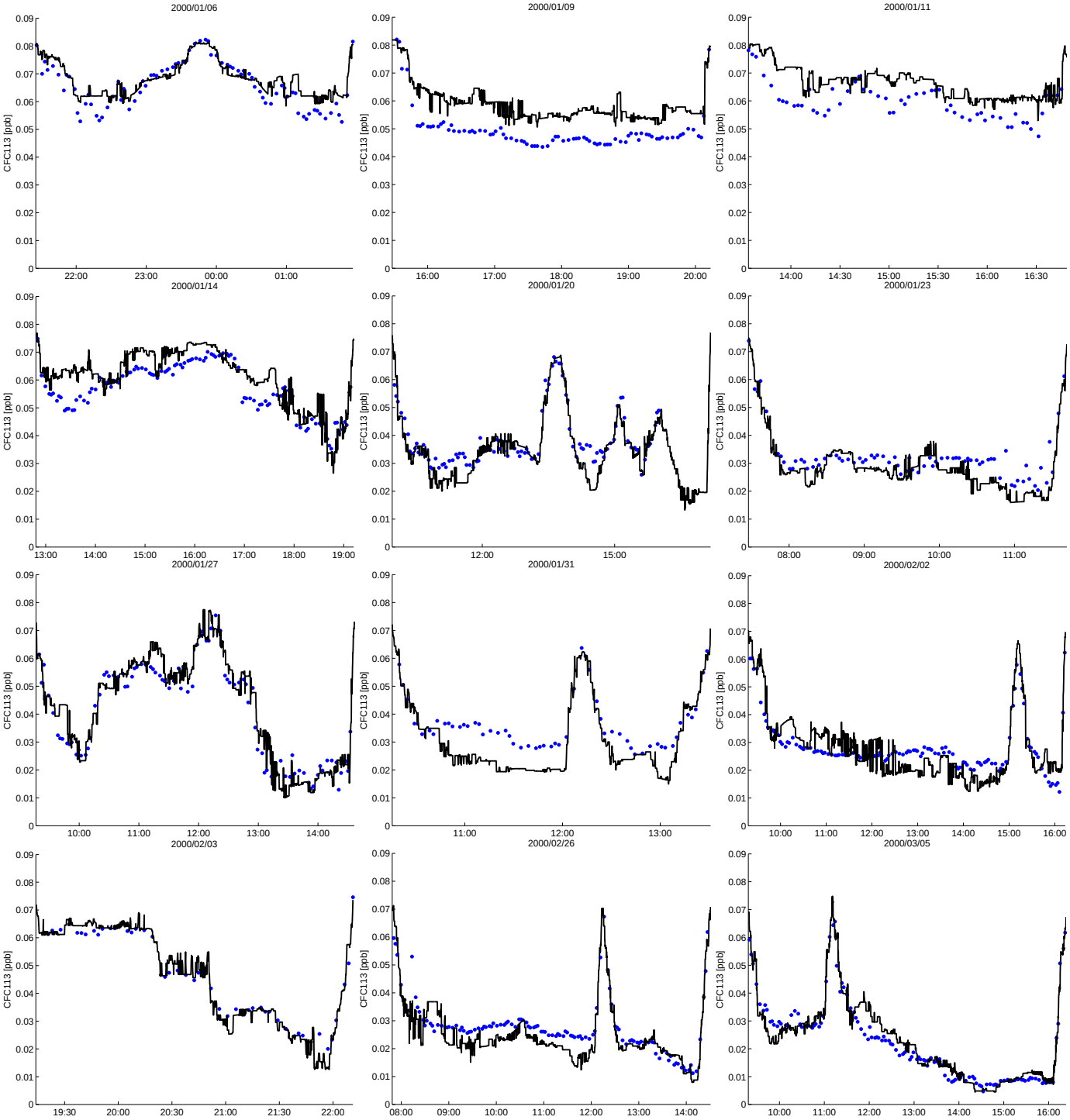

Figure 9: CFC-113 as a function of flight time (UTC) from measurements of the ACATS gas chromatograph (blue dots) compared to modeled values (black lines).

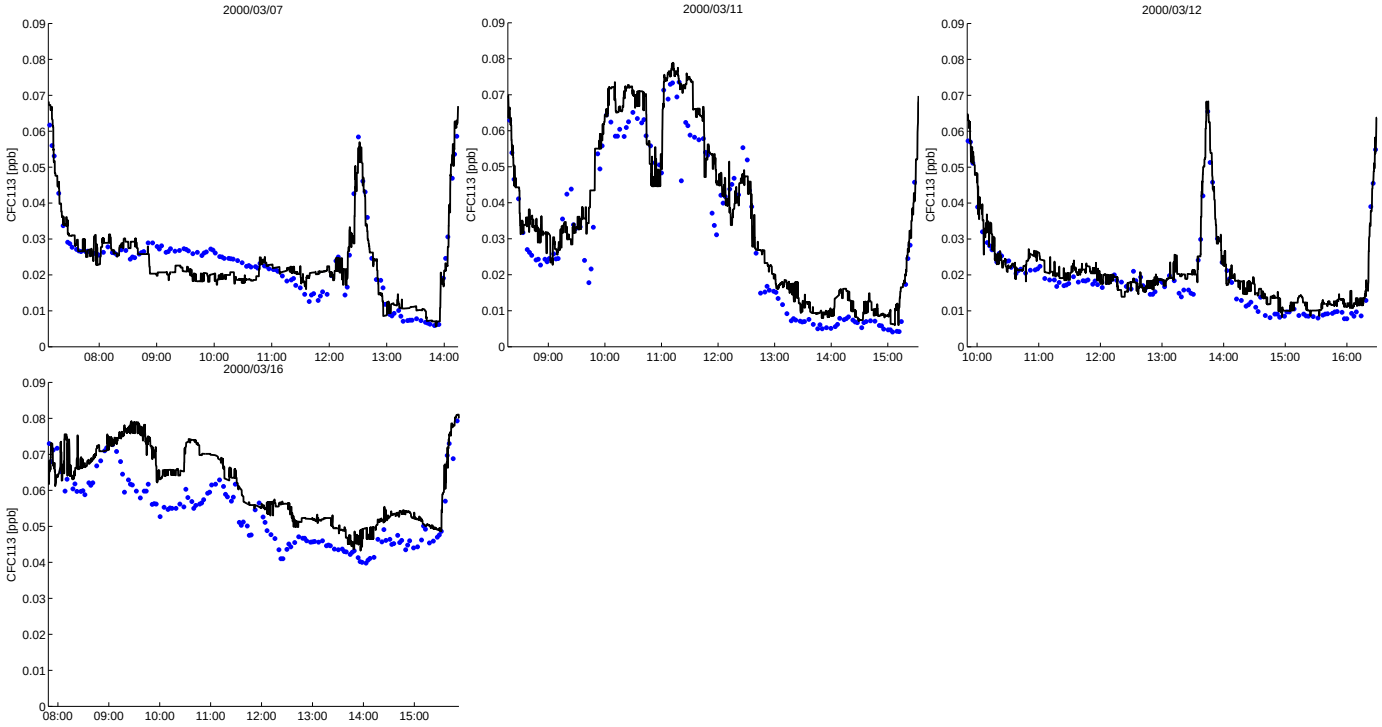

Figure 9: CFC-113 as a function of flight time (UTC) from measurements of the ACATS gas chromatograph (blue dots) compared to modeled values (black lines).

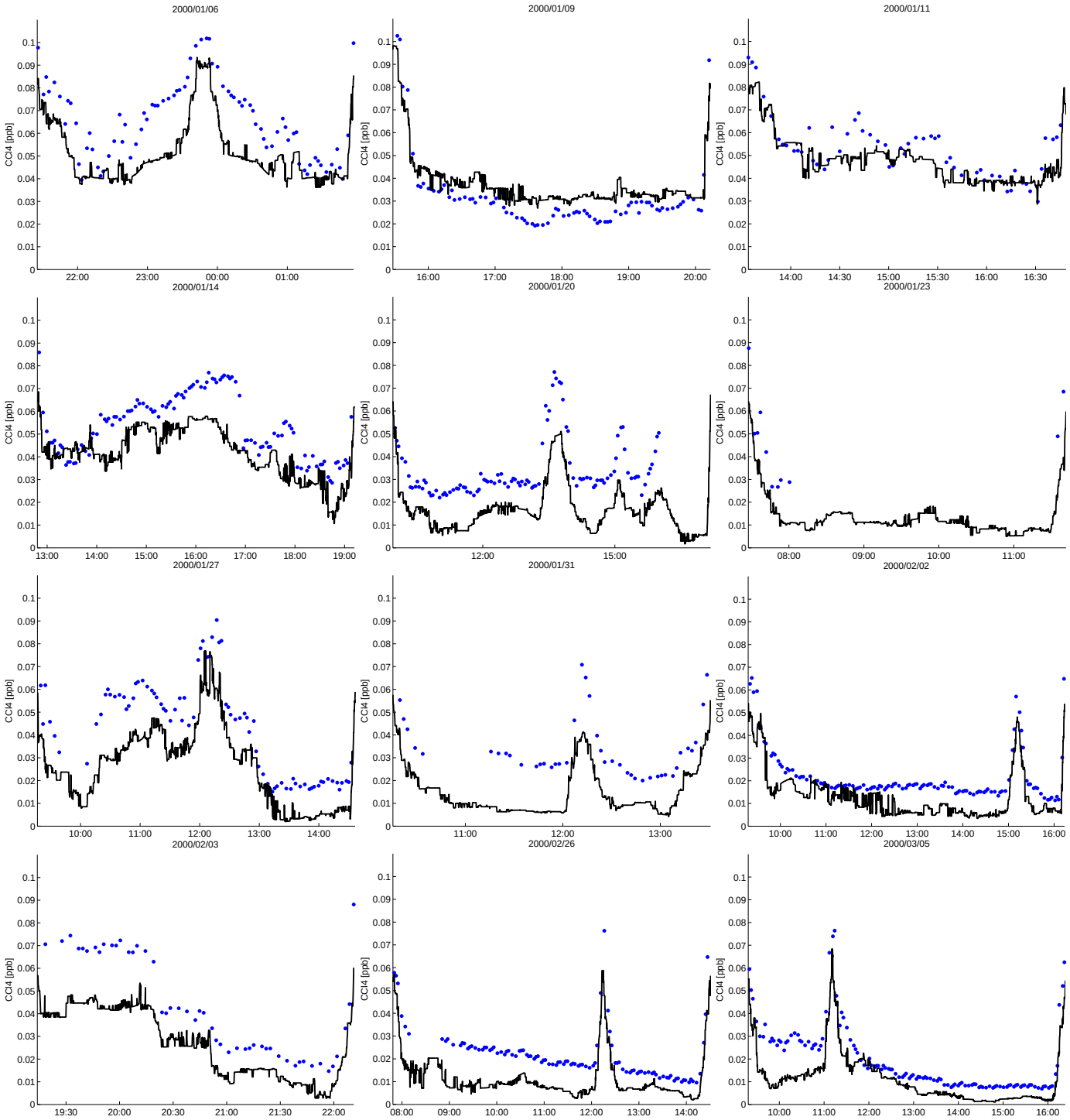

Figure 10: CCl_4 as a function of flight time (UTC) from measurements of the ACATS gas chromatograph (blue dots) compared to modeled values (black lines).

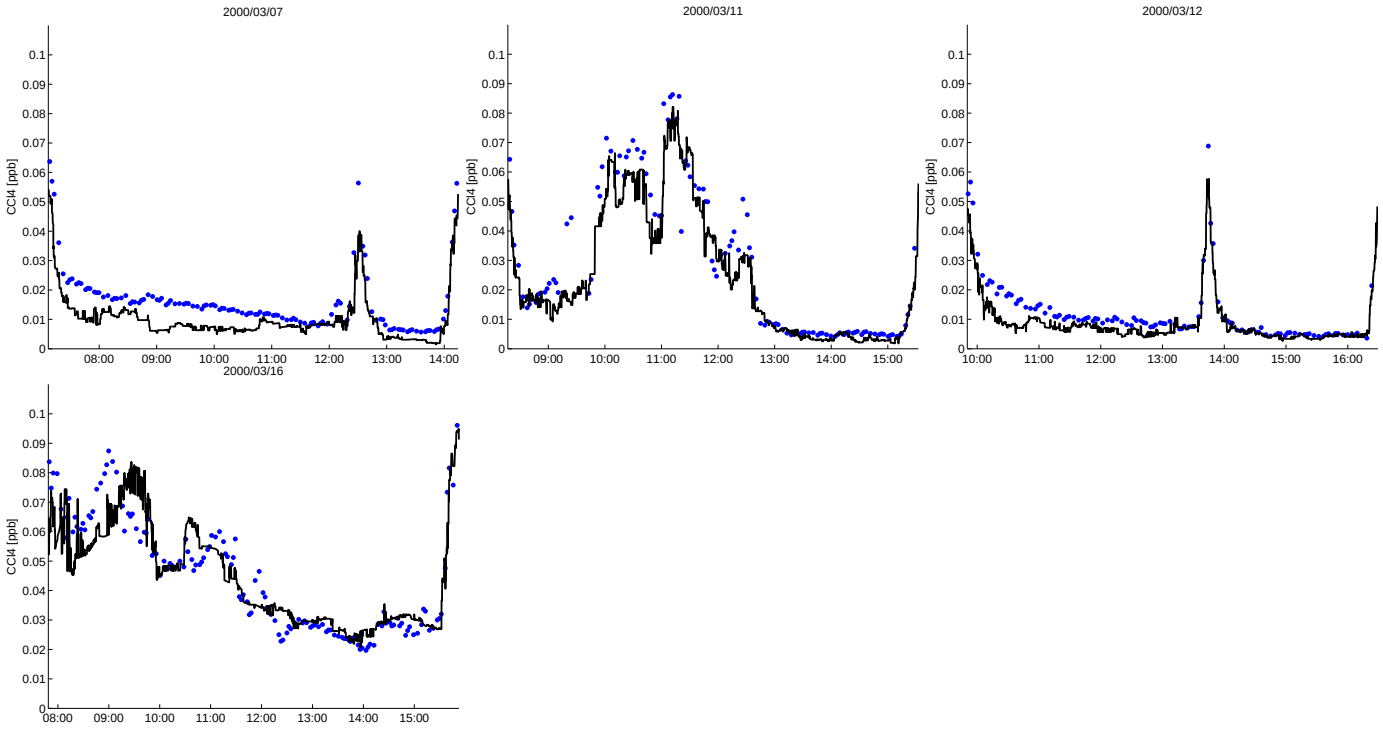

Figure 10: CCl_4 as a function of flight time (UTC) from measurements of the ACATS gas chromatograph (blue dots) compared to modeled values (black lines).

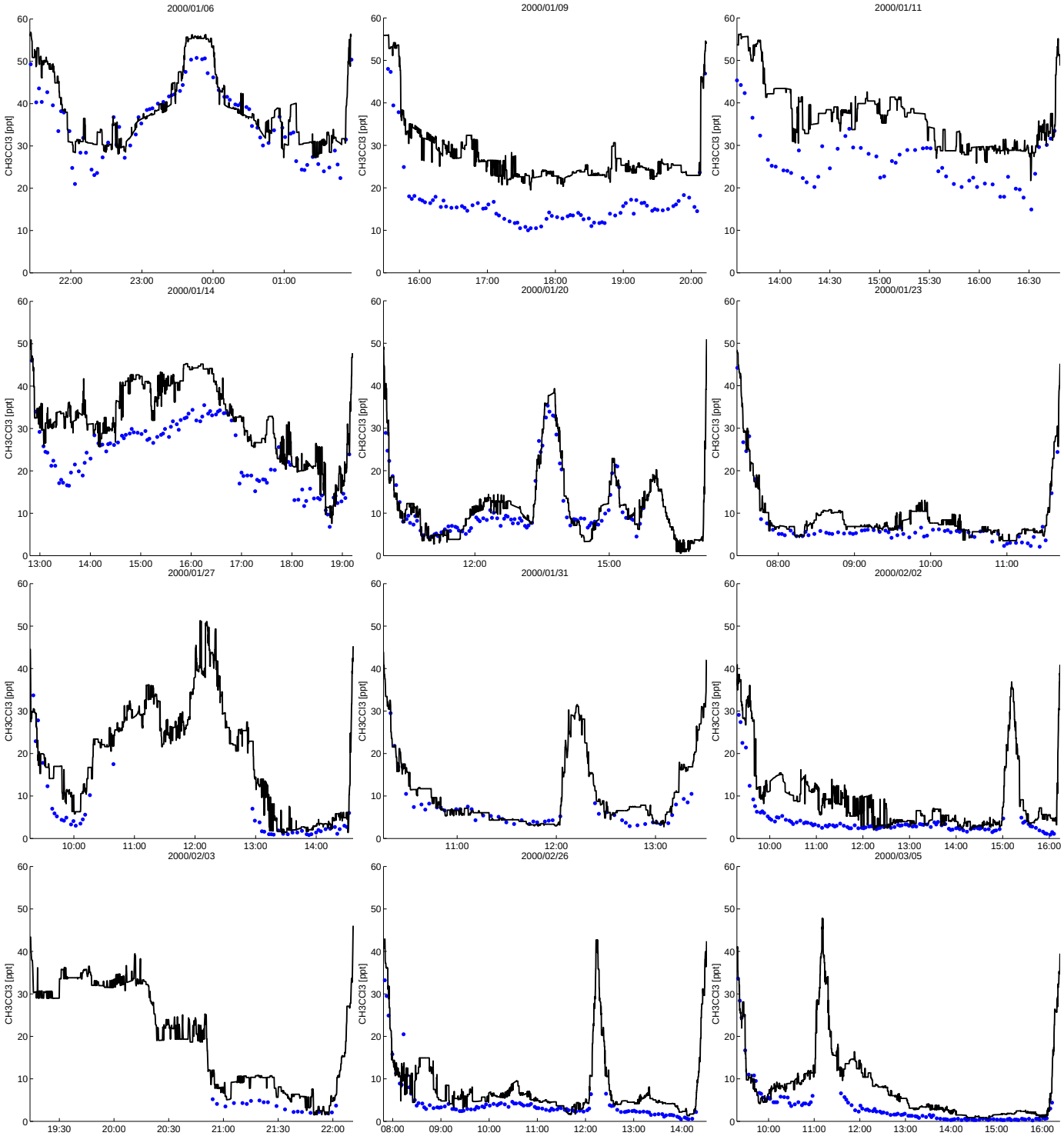

Figure 11: CH_3CCl_3 as a function of flight time (UTC) from measurements of the ACATS gas chromatograph (blue dots) compared to modeled values (black lines).

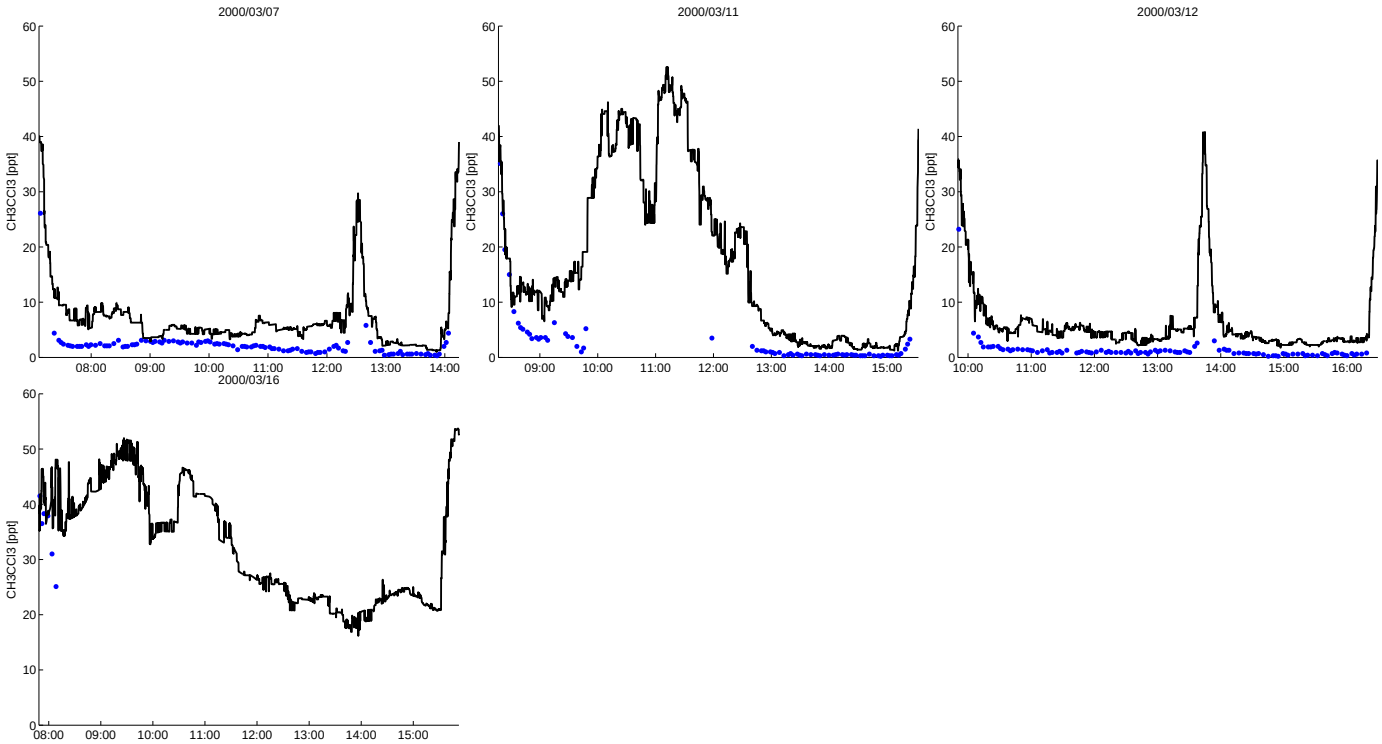

Figure 11: CH_3CCl_3 as a function of flight time (UTC) from measurements of the ACATS gas chromatograph (blue dots) compared to modeled values (black lines).

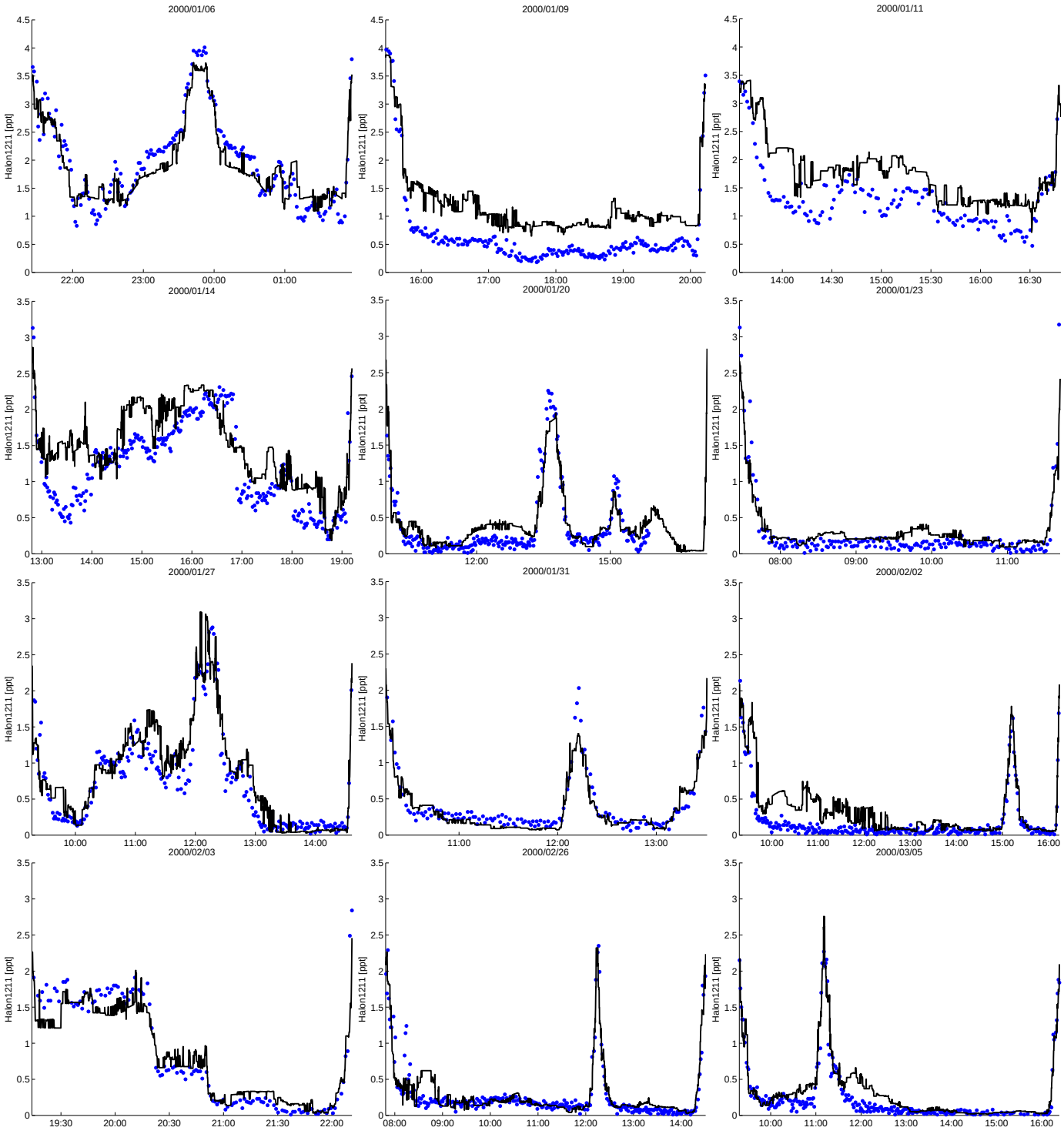

Figure 12: Halon-1211 as a function of flight time (UTC) from measurements of the ACATS gas chromatograph (blue dots) compared to modeled values (black lines).

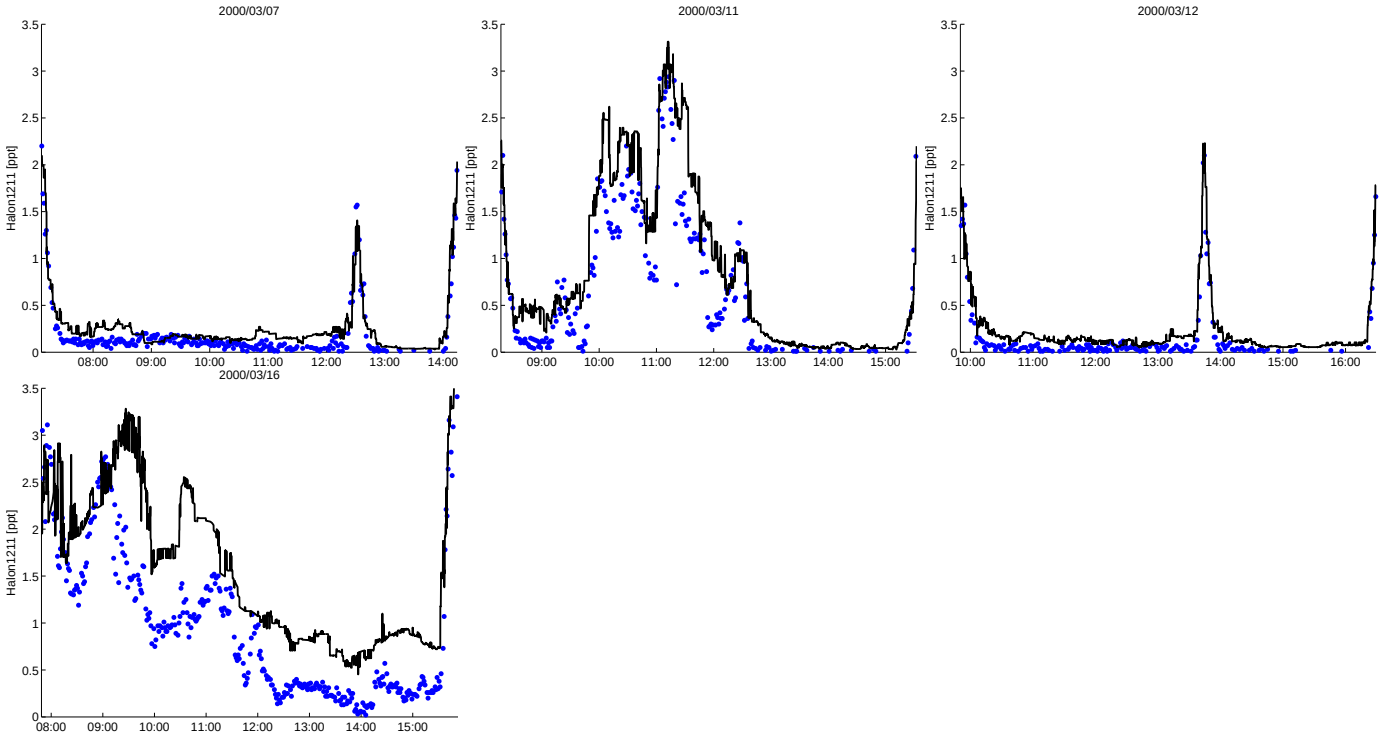

Figure 12: Halon-1211 as a function of flight time (UTC) from measurements of the ACATS gas chromatograph (blue dots) compared to modeled values (black lines).

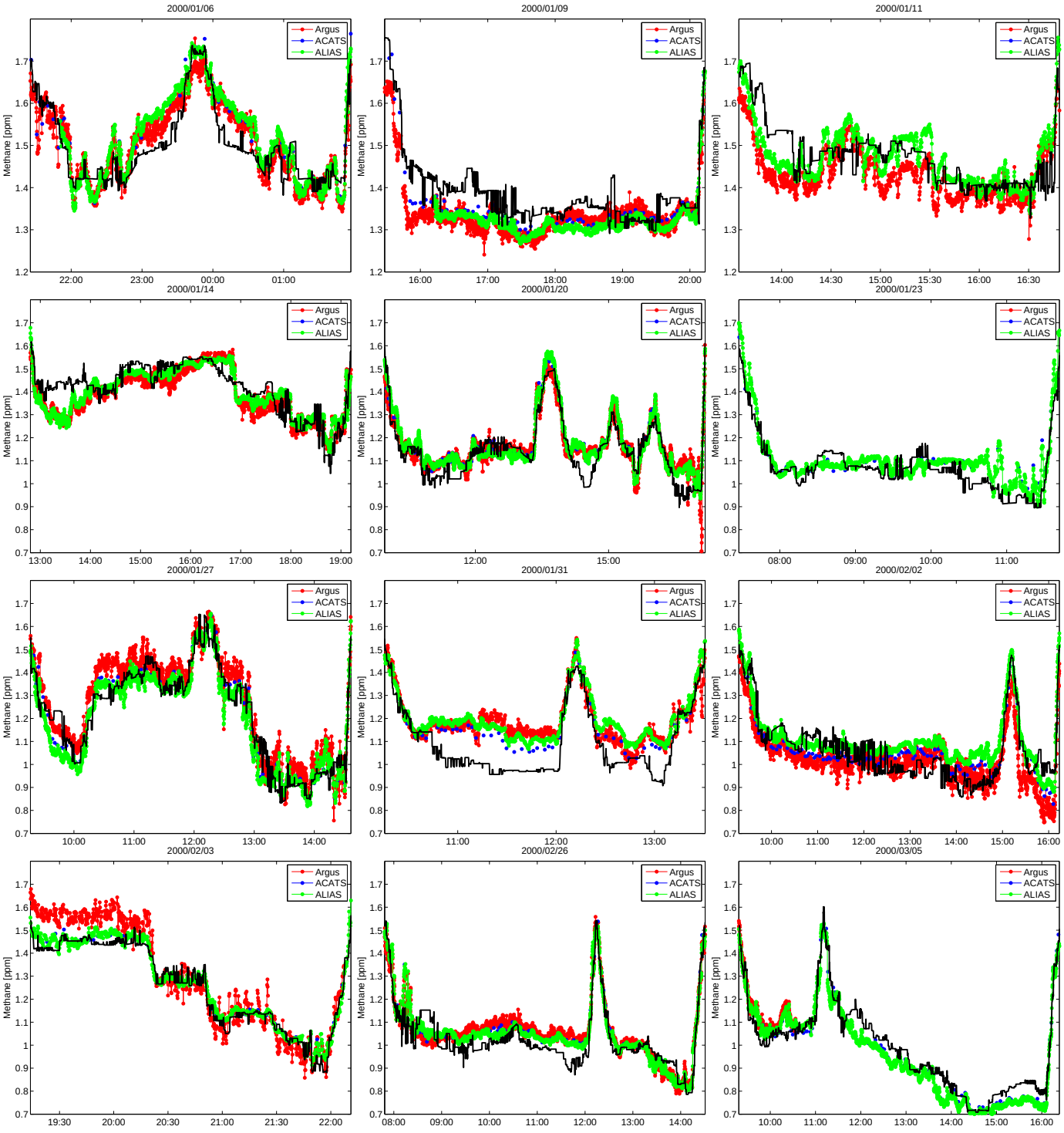

Figure 13: CH_4 as a function of flight time (UTC) from measurements of the ACATS gas chromatograph (blue dots) and the ALIAS and Argus tunable diode laser instruments (green and red dots) compared to modeled values (black lines).

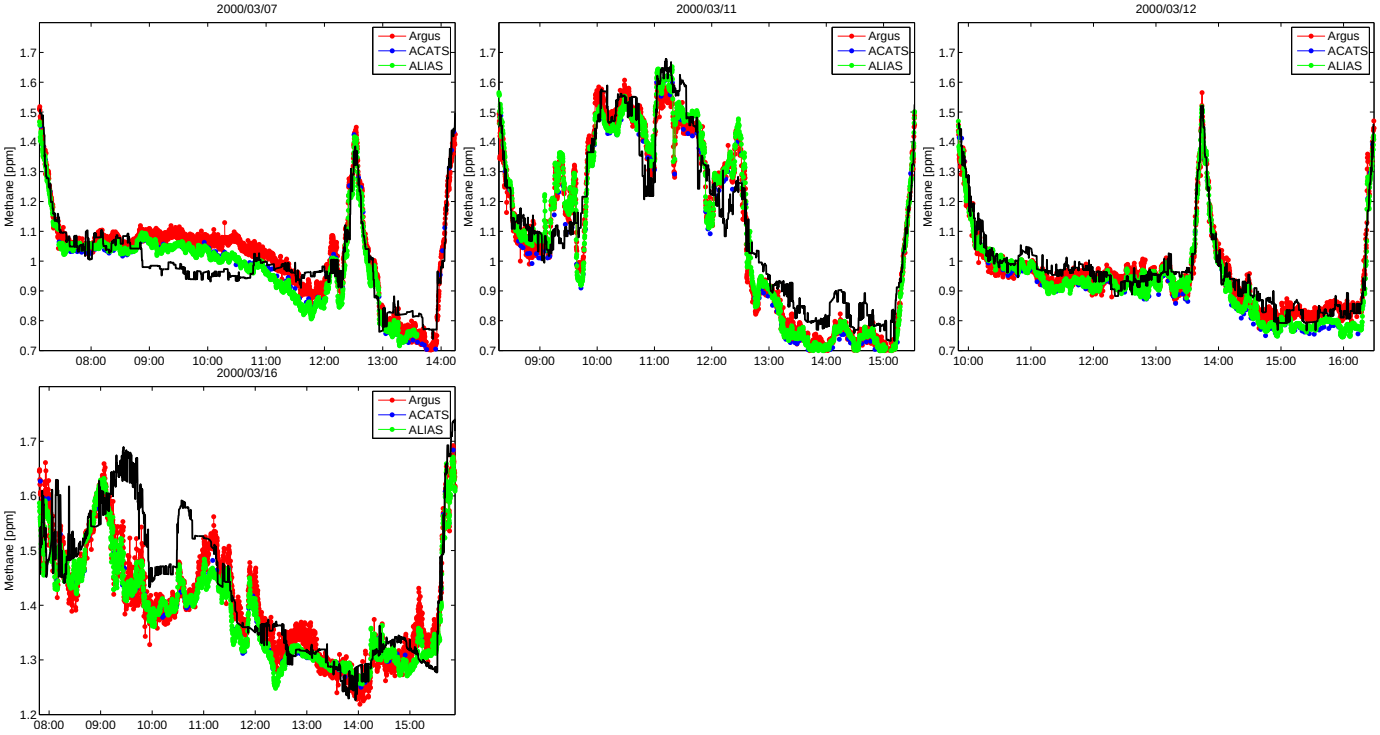

Figure 13: CH_4 as a function of flight time (UTC) from measurements of the ACATS gas chromatograph (blue dots) and the ALIAS and Argus tunable diode laser instruments (green and red dots) compared to modeled values (black lines).

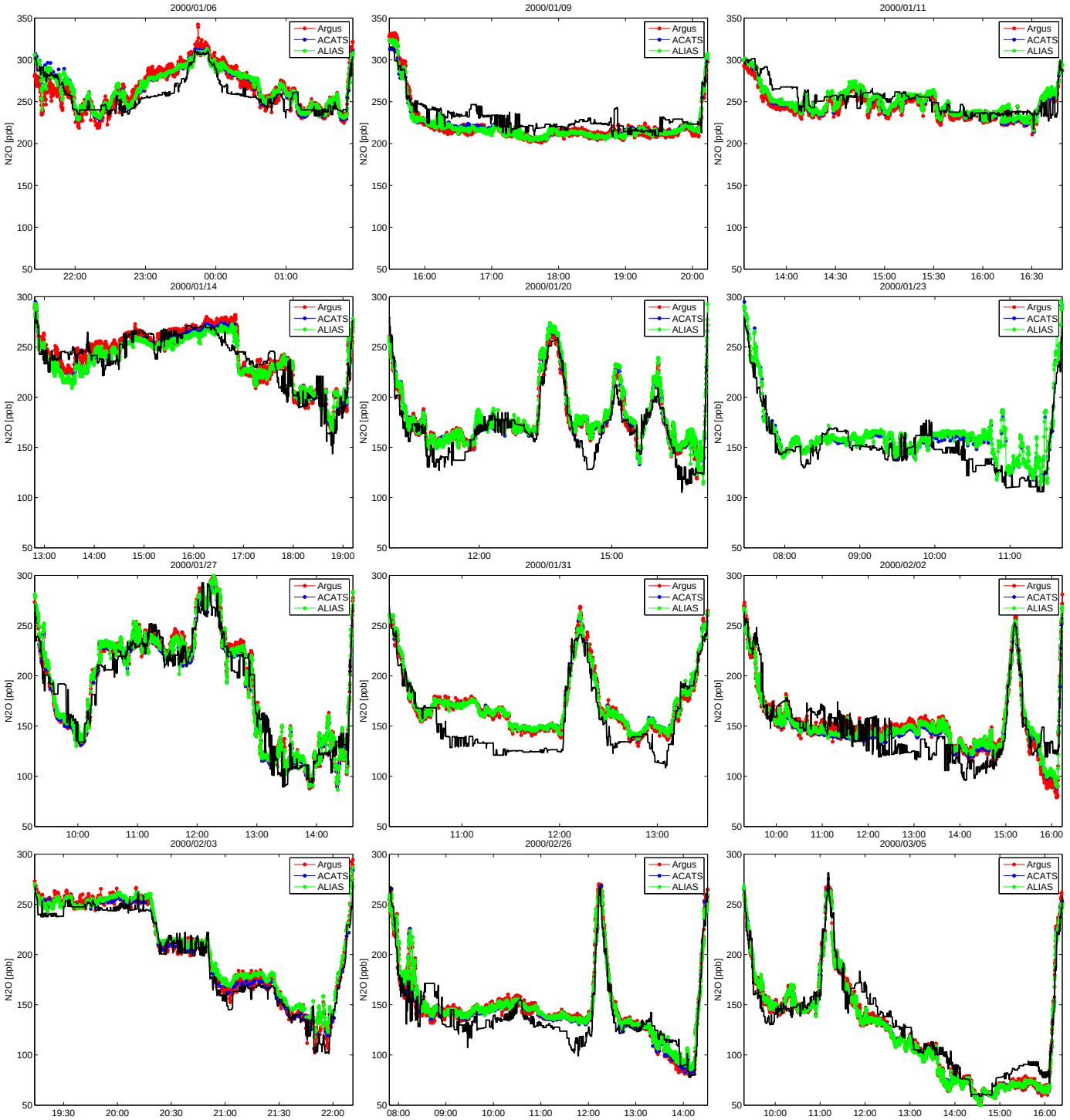

Figure 14: N_2O as a function of flight time (UTC) from measurements of the ACATS gas chromatograph (blue dots) and the ALIAS and Argus tunable diode laser instruments (green and red dots) compared to modeled values (black lines).

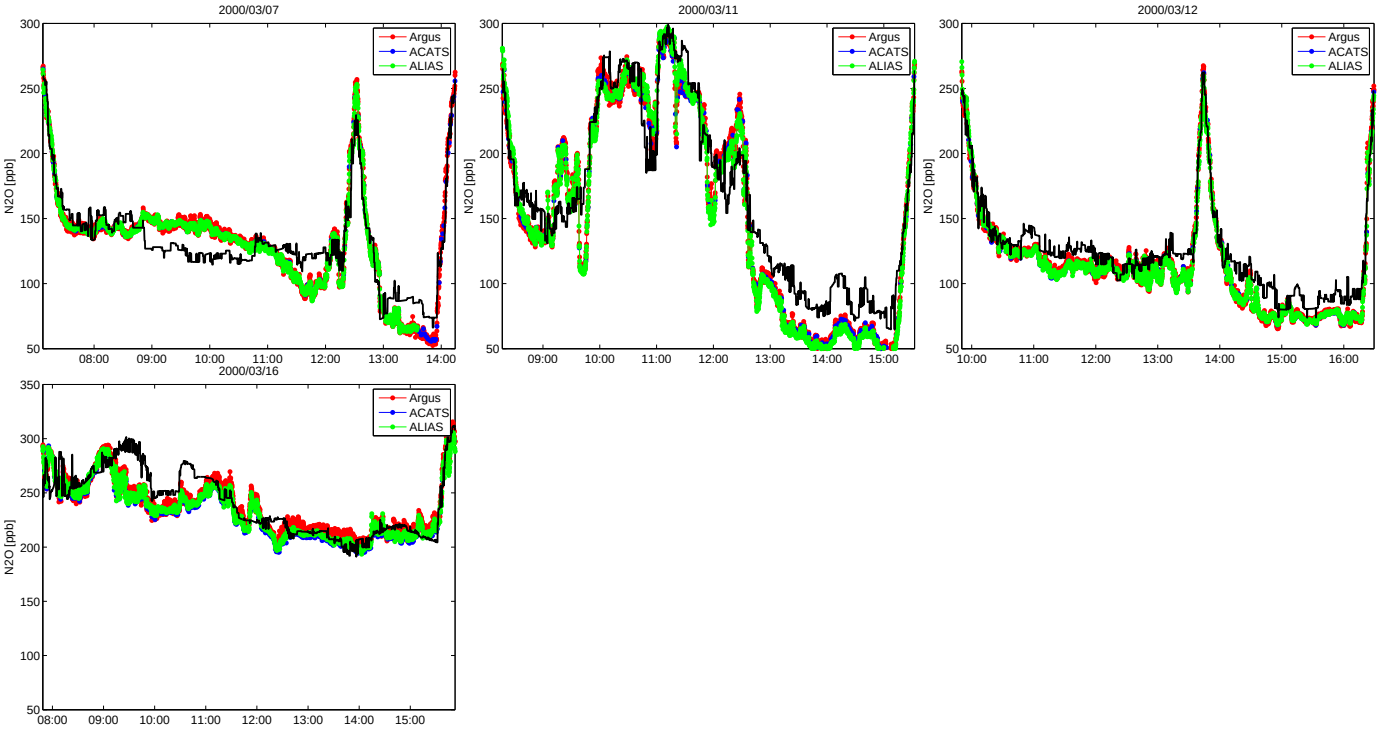

Figure 14: N_2O as a function of flight time (UTC) from measurements of the ACATS gas chromatograph (blue dots) and the ALIAS and Argus tunable diode laser instruments (green and red dots) compared to modeled values (black lines).

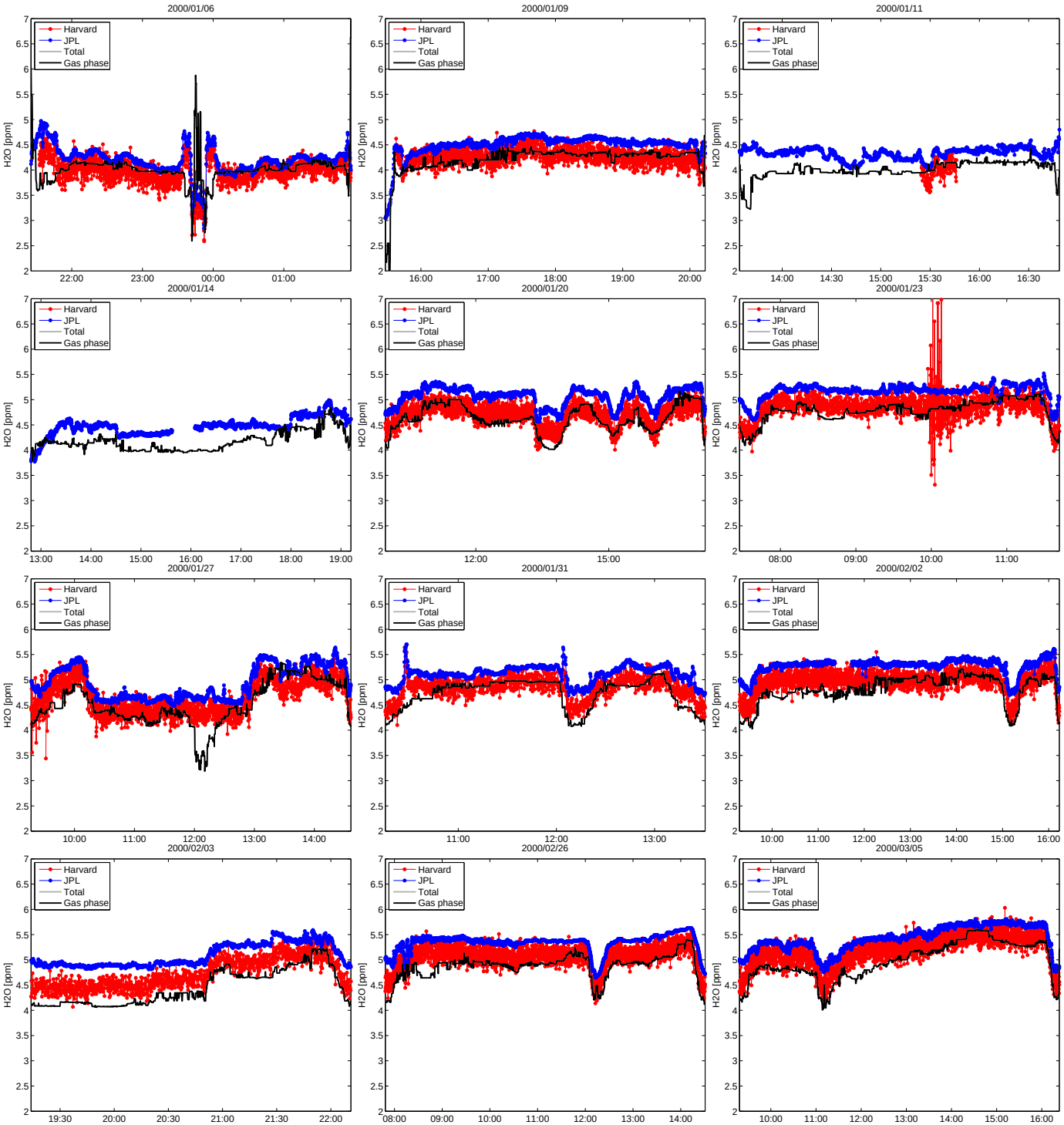

Figure 15: H_2O as a function of flight time (UTC) from measurements of the Harvard and JPL instruments (red and blue dots) compared to modeled values. Grey lines show total H_2O and black lines gas phase H_2O (practically identical for H_2O).

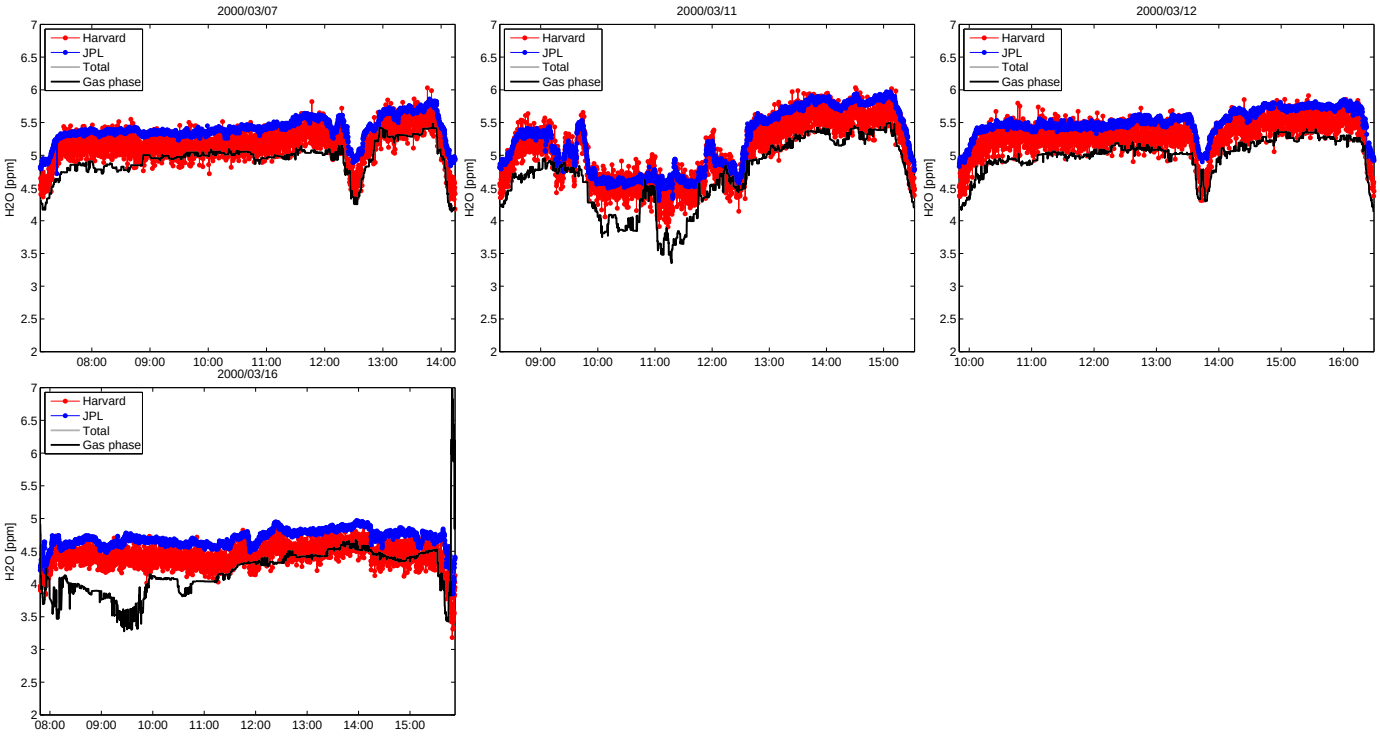

Figure 15: H_2O as a function of flight time (UTC) from measurements of the Harvard and JPL instruments (red and blue dots) compared to modeled values. Grey lines show total H_2O and black lines gas phase H_2O (practically identical for H_2O).

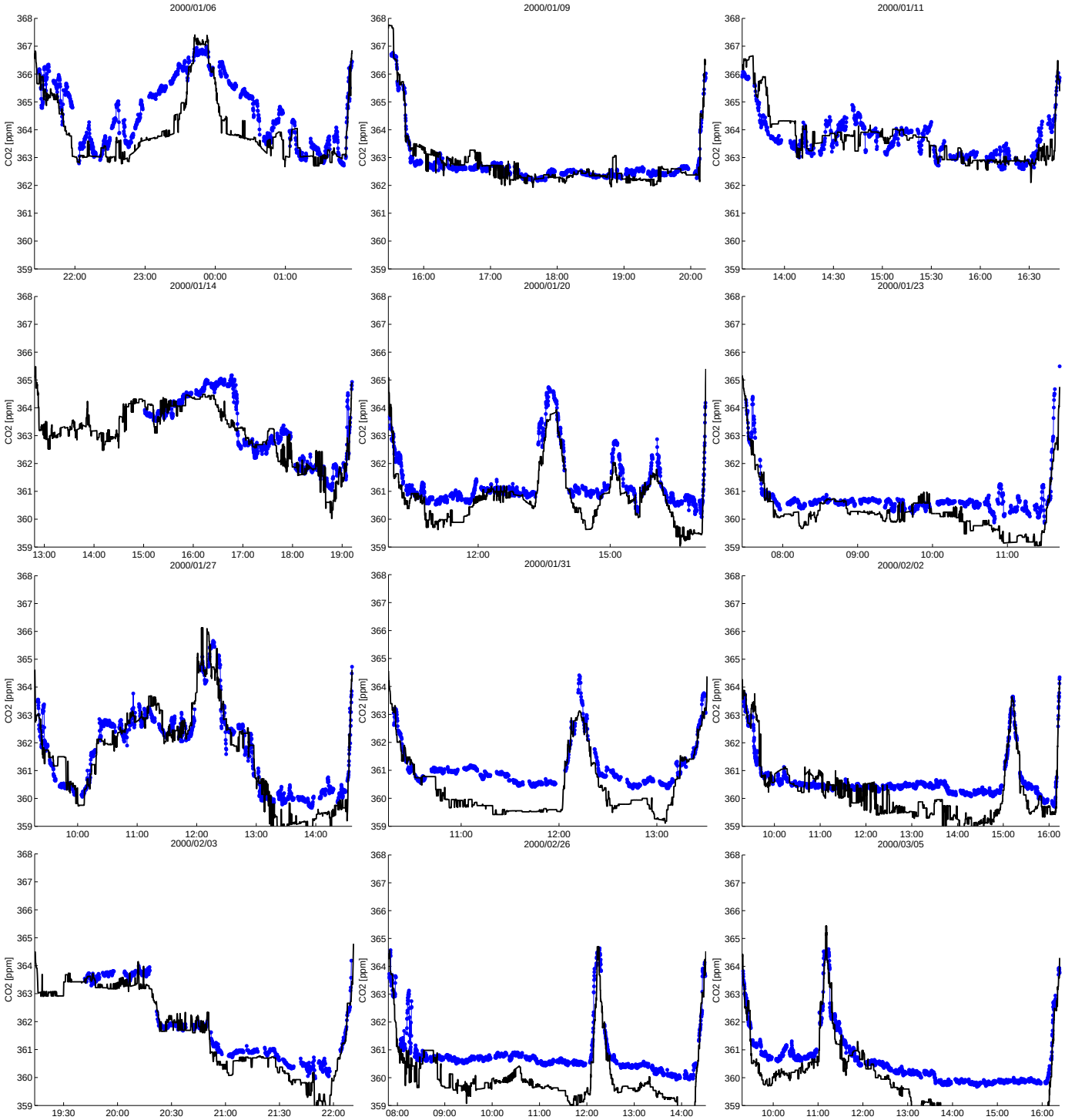

Figure 16: CO_2 as a function of flight time (UTC) from measurements of the Harvard CO_2 instrument (blue dots) compared to modeled values (black lines).

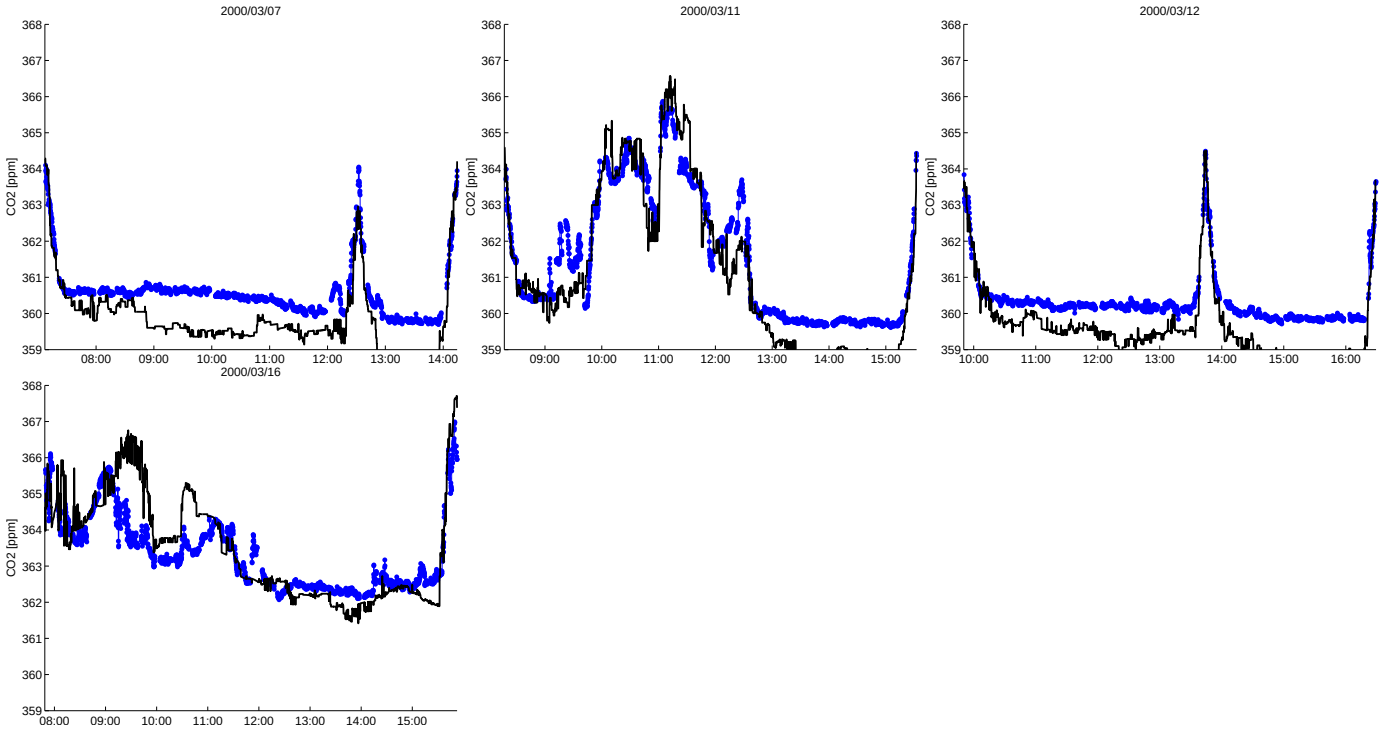

Figure 16: CO_2 as a function of flight time (UTC) from measurements of the Harvard CO_2 instrument (blue dots) compared to modeled values (black lines).

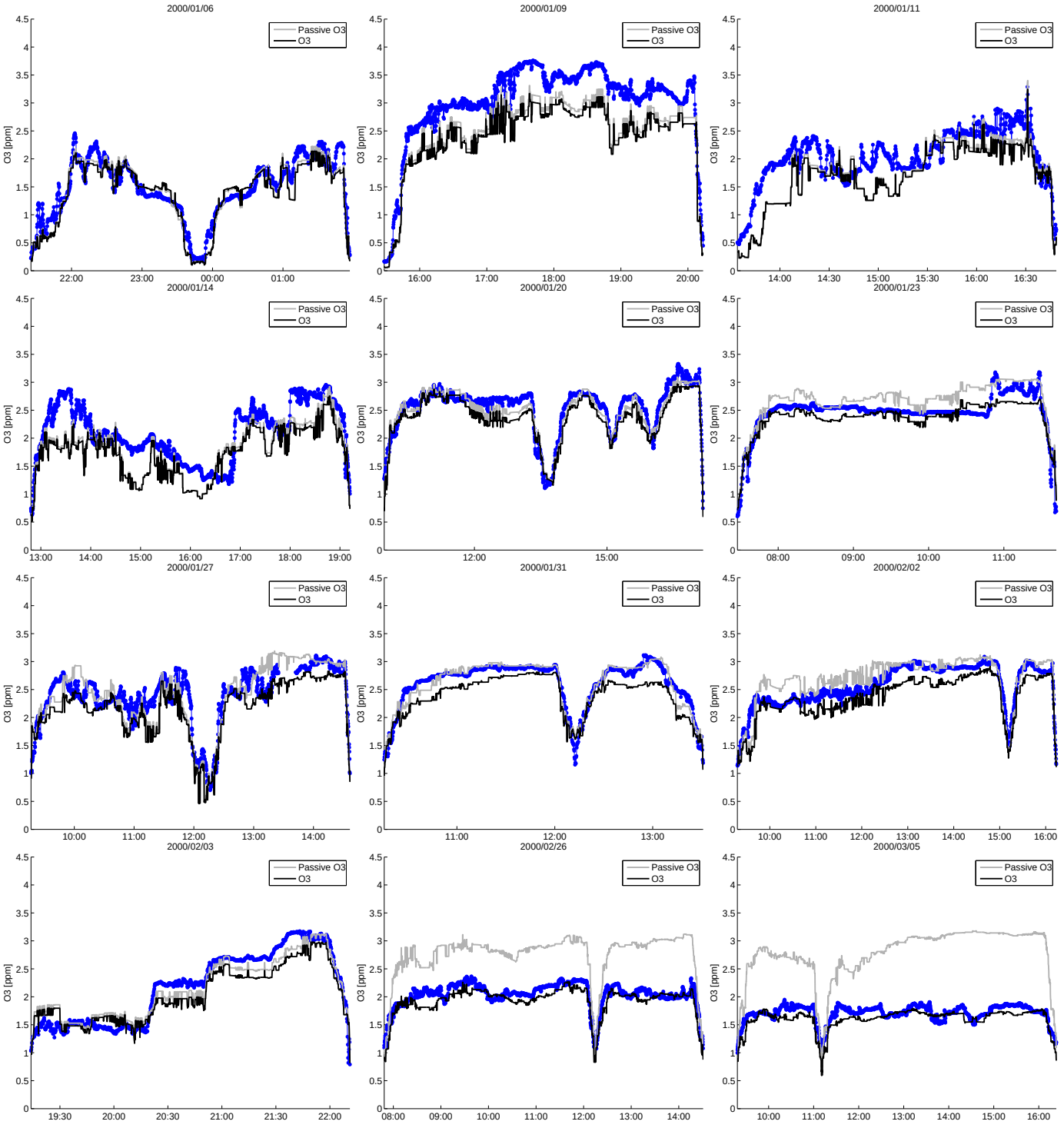

Figure 17: O_3 as a function of flight time (UTC) from measurements of the NOAA O_3 instrument (blue dots) compared to modeled values (black lines). The grey lines show the passive ozone tracer as a measure for ozone loss.

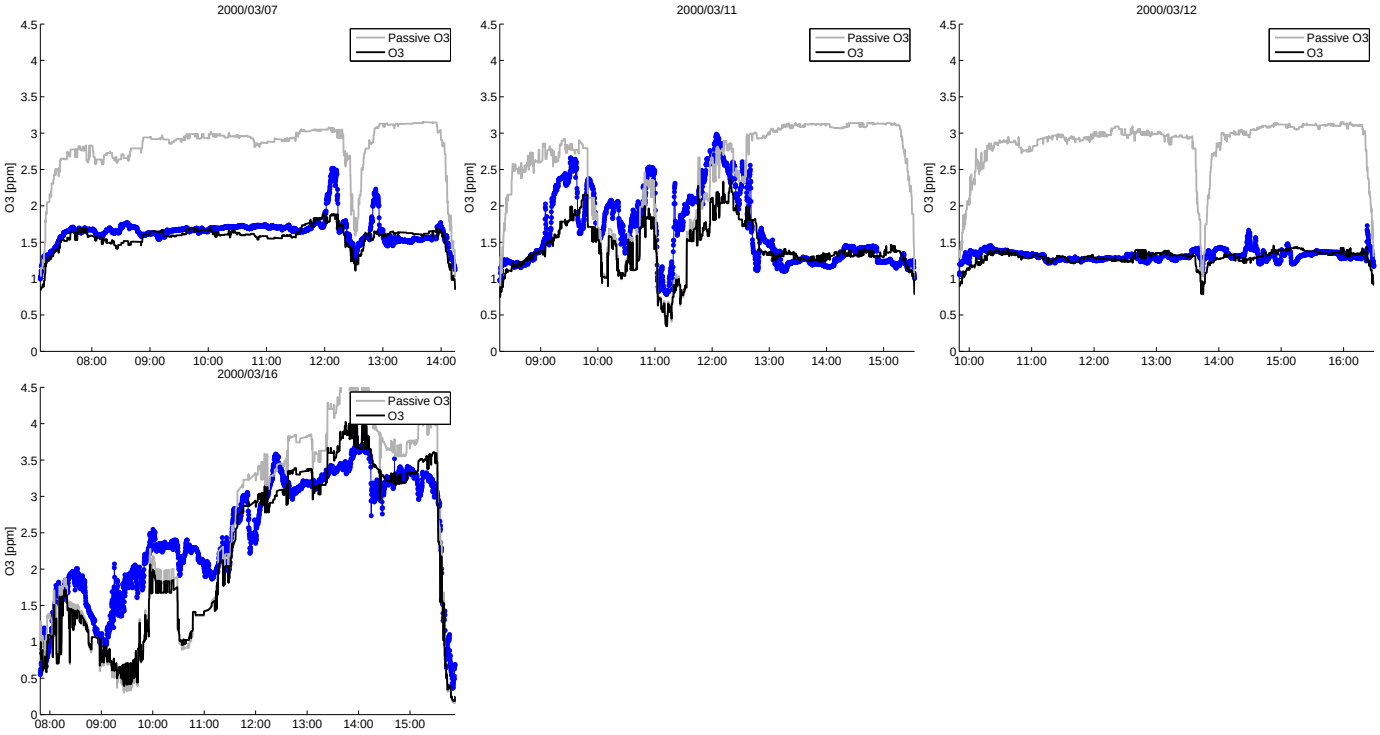

Figure 17: O_3 as a function of flight time (UTC) from measurements of the NOAA O_3 instrument (blue dots) compared to modeled values (black lines). The grey lines show the passive ozone tracer as a measure for ozone loss.

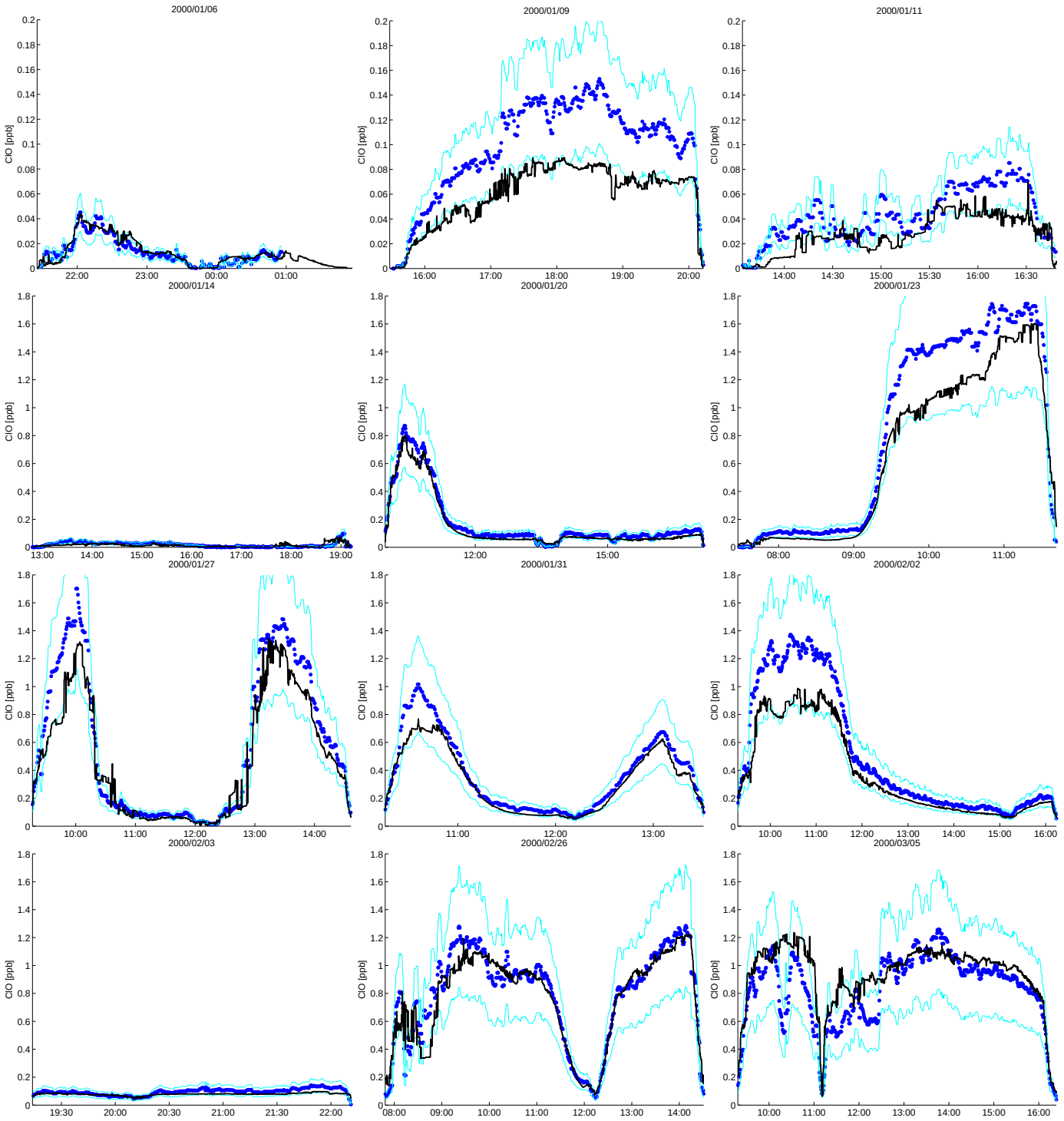

Figure 18: ClO as a function of flight time (UTC) from measurements of the Harvard $ClONO_2$-NO_2-ClO-Cl_2O_2 instrument (blue dots) compared to modeled values (black lines). Cyan lines show 2σ uncertainties.

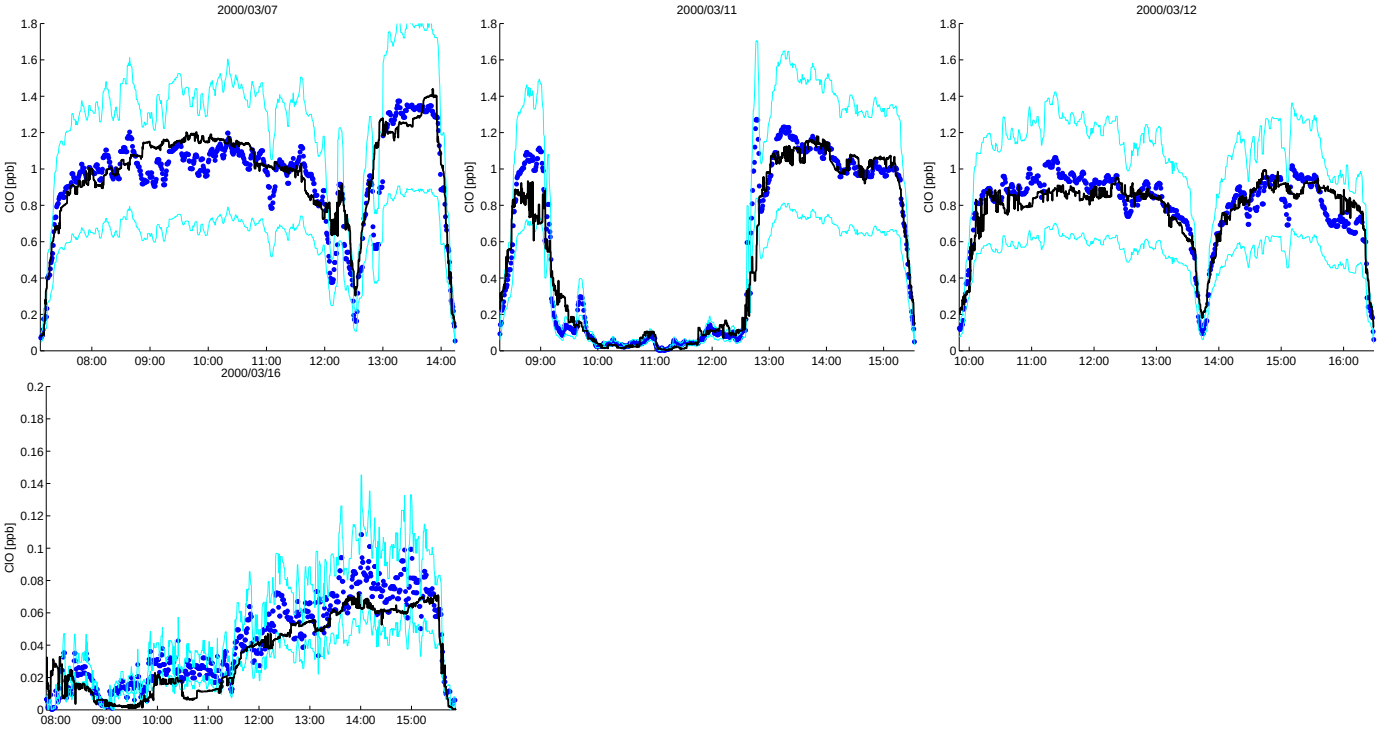

Figure 18: ClO as a function of flight time (UTC) from measurements of the Harvard $ClONO_2$-NO_2-ClO-Cl_2O_2 instrument (blue dots) compared to modeled values (black lines). Cyan lines show 2σ uncertainties.

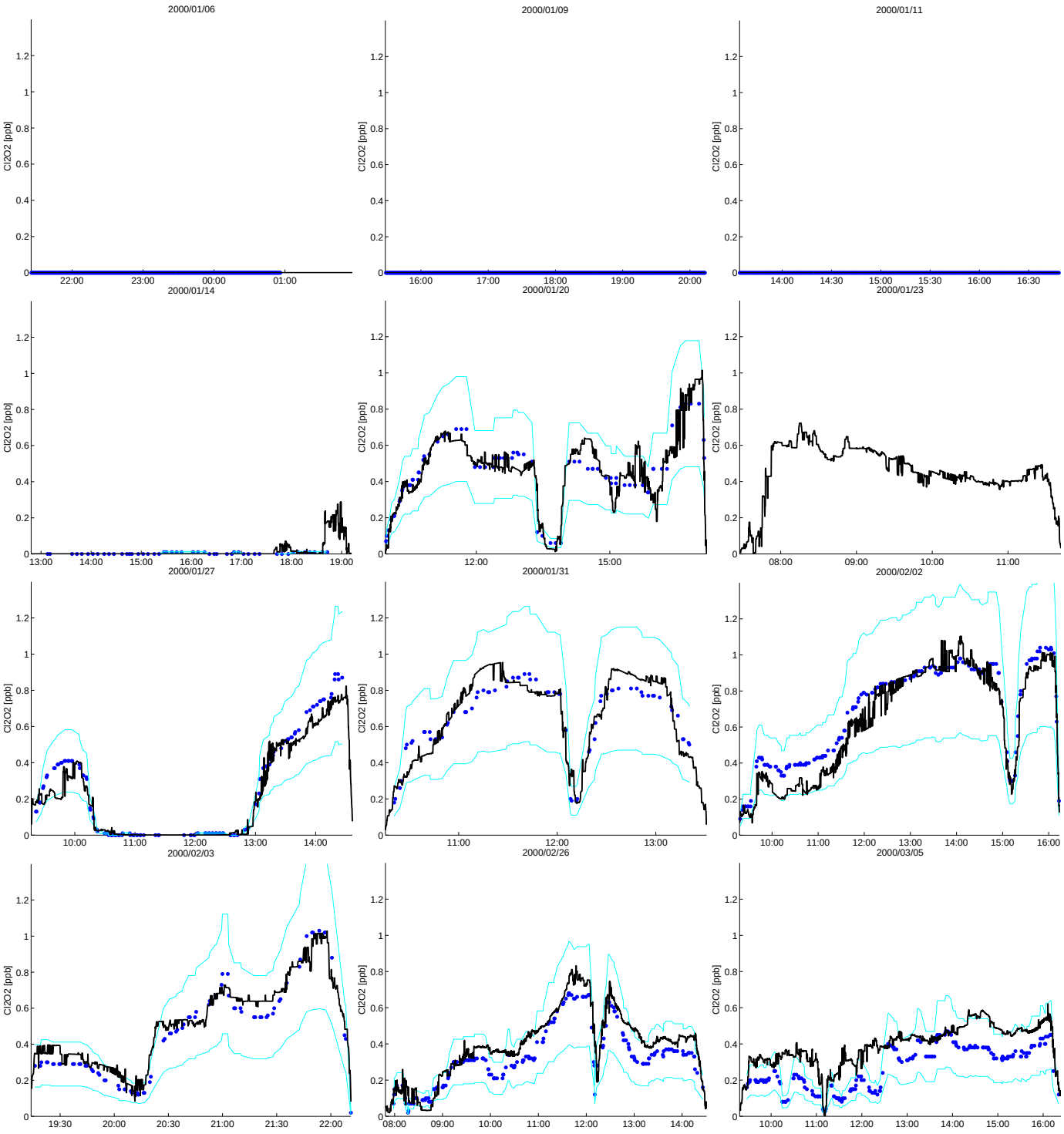

Figure 19: Cl_2O_2 as a function of flight time (UTC) from measurements of the Harvard $ClONO_2$-NO_2-ClO-Cl_2O_2 instrument (blue dots) compared to modeled values (black lines). Cyan lines show 2σ uncertainties.

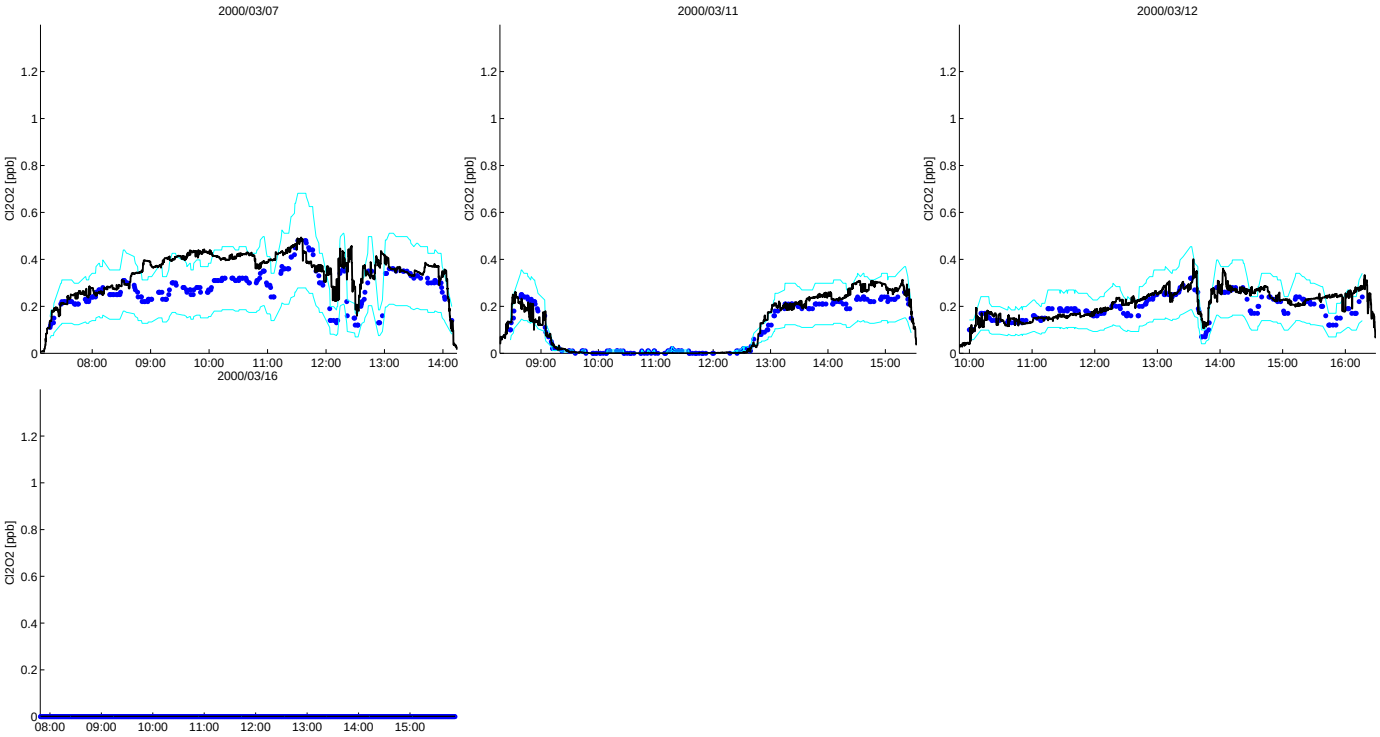

Figure 19: Cl_2O_2 as a function of flight time (UTC) from measurements of the Harvard $ClONO_2$-NO_2-ClO-Cl_2O_2 instrument (blue dots) compared to modeled values (black lines). Cyan lines show 2σ uncertainties.

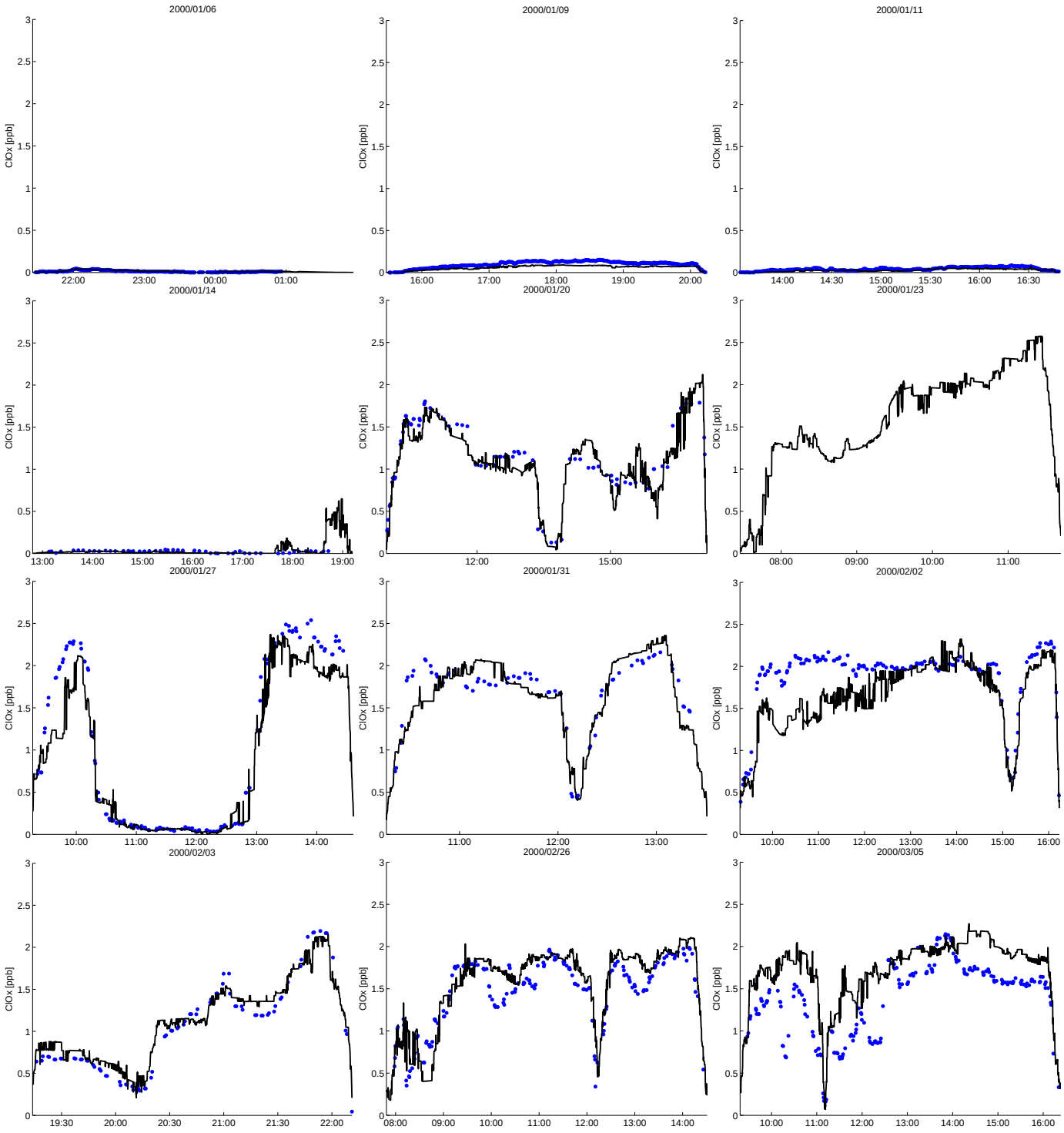

Figure 20: ClO_x=ClO+2 Cl_2O_2 as a function of flight time (UTC) from measurements of the Harvard $ClONO_2$-NO_2-ClO-Cl_2O_2 instrument (blue dots) compared to modeled values (black lines).

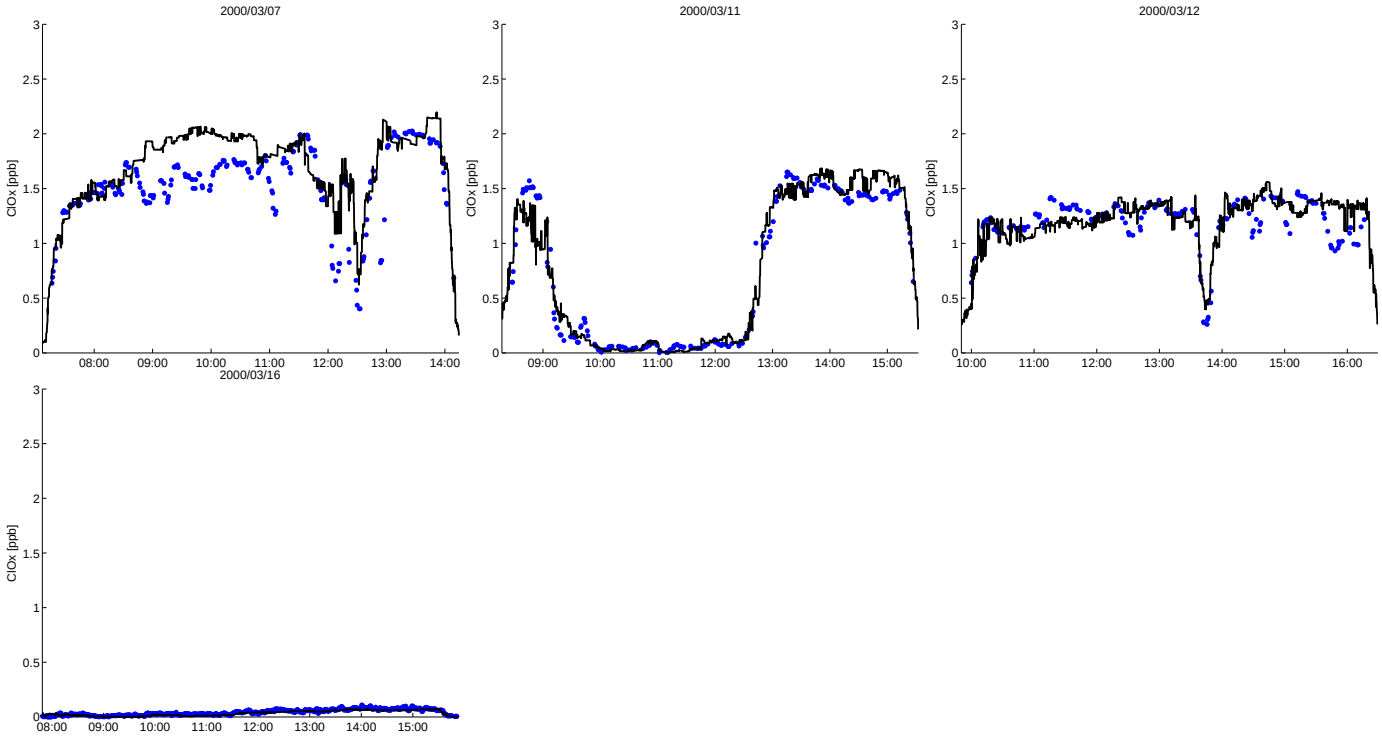

Figure 20: ClO_x=ClO+2 Cl_2O_2 as a function of flight time (UTC) from measurements of the Harvard $ClONO_2$-NO_2-ClO-Cl_2O_2 instrument (blue dots) compared to modeled values (black lines).

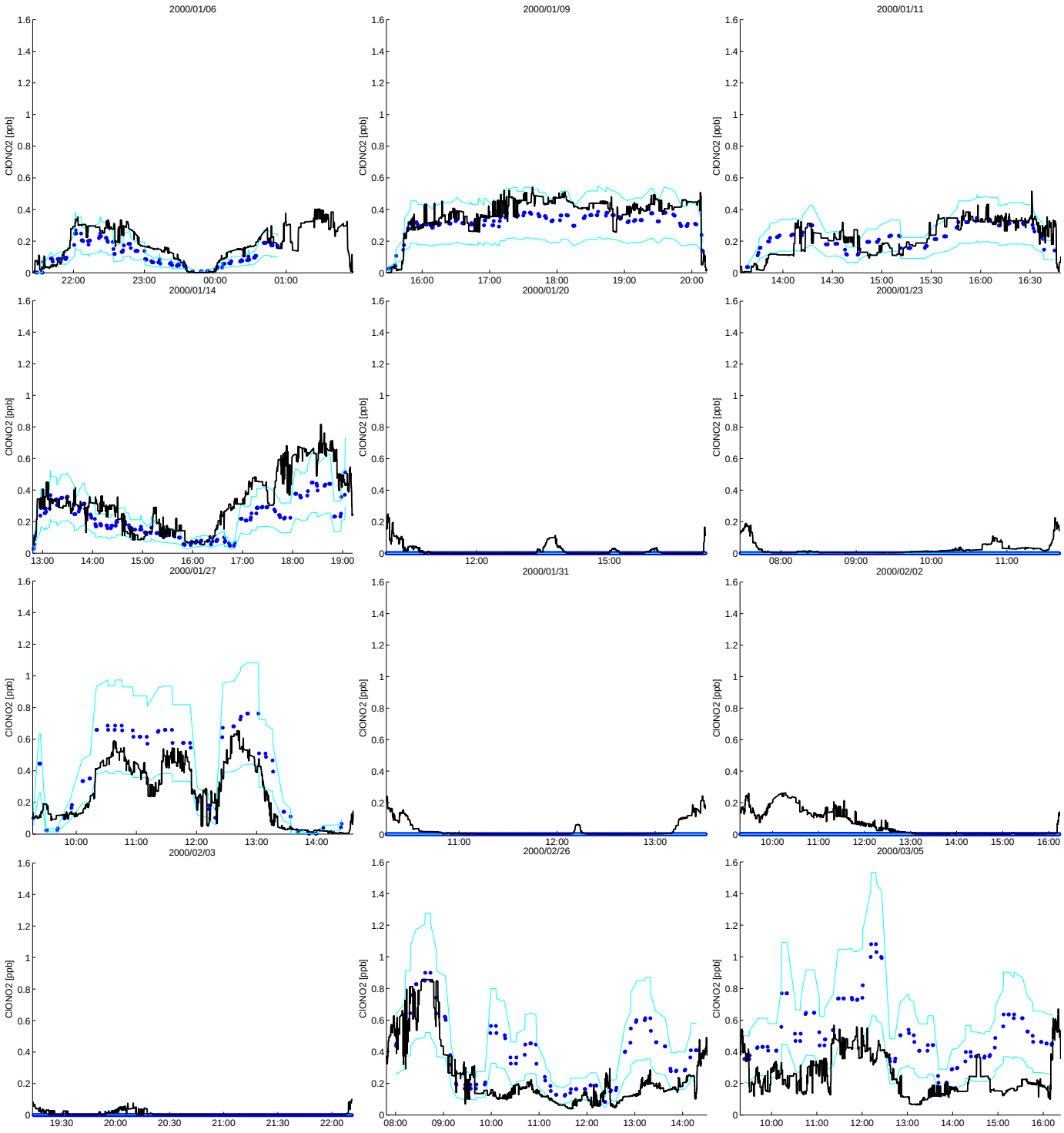

Figure 21: $ClONO_2$ as a function of flight time (UTC) from measurements of the Harvard $ClONO_2$-NO_2-ClO-Cl_2O_2 instrument (blue dots) compared to modeled values (black lines). Cyan lines show 2σ uncertainties.

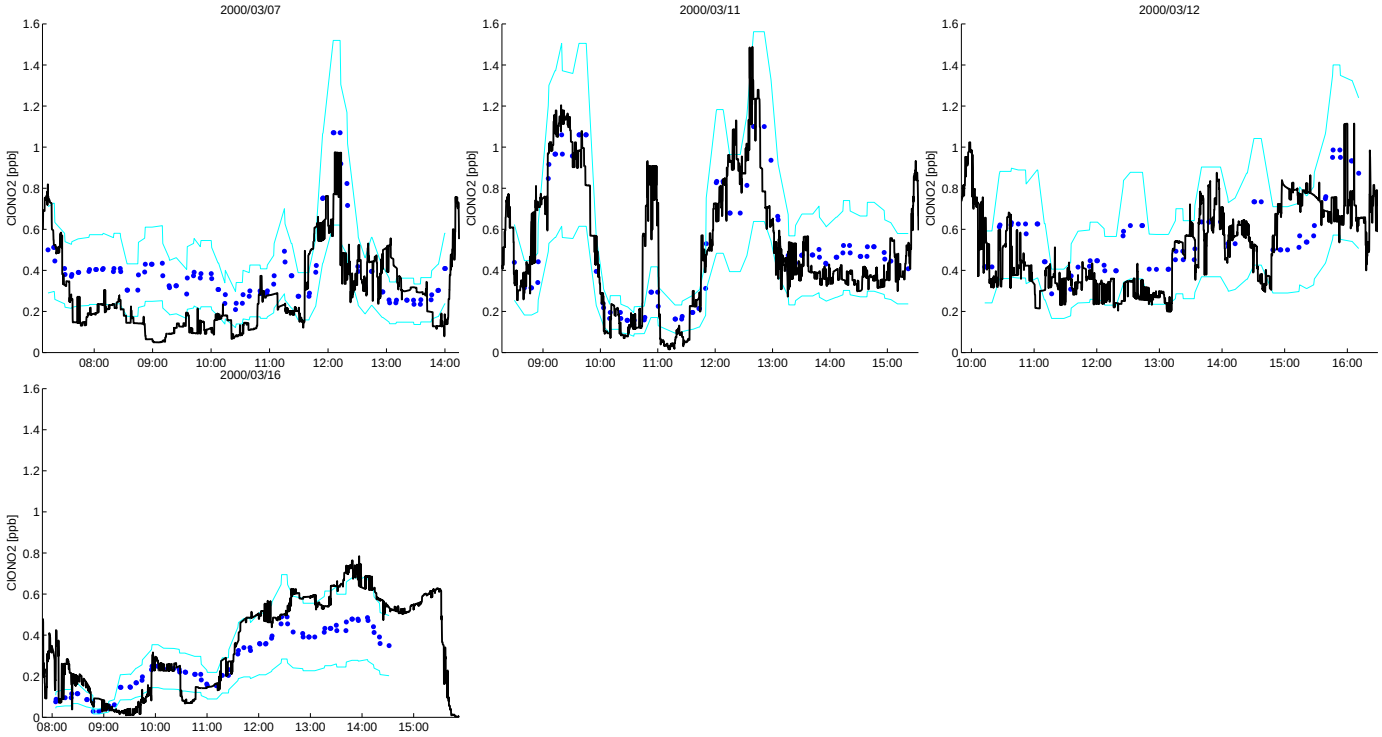

Figure 21: $ClONO_2$ as a function of flight time (UTC) from measurements of the Harvard $ClONO_2$-NO_2-ClO-Cl_2O_2 instrument (blue dots) compared to modeled values (black lines). Cyan lines show 2σ uncertainties.

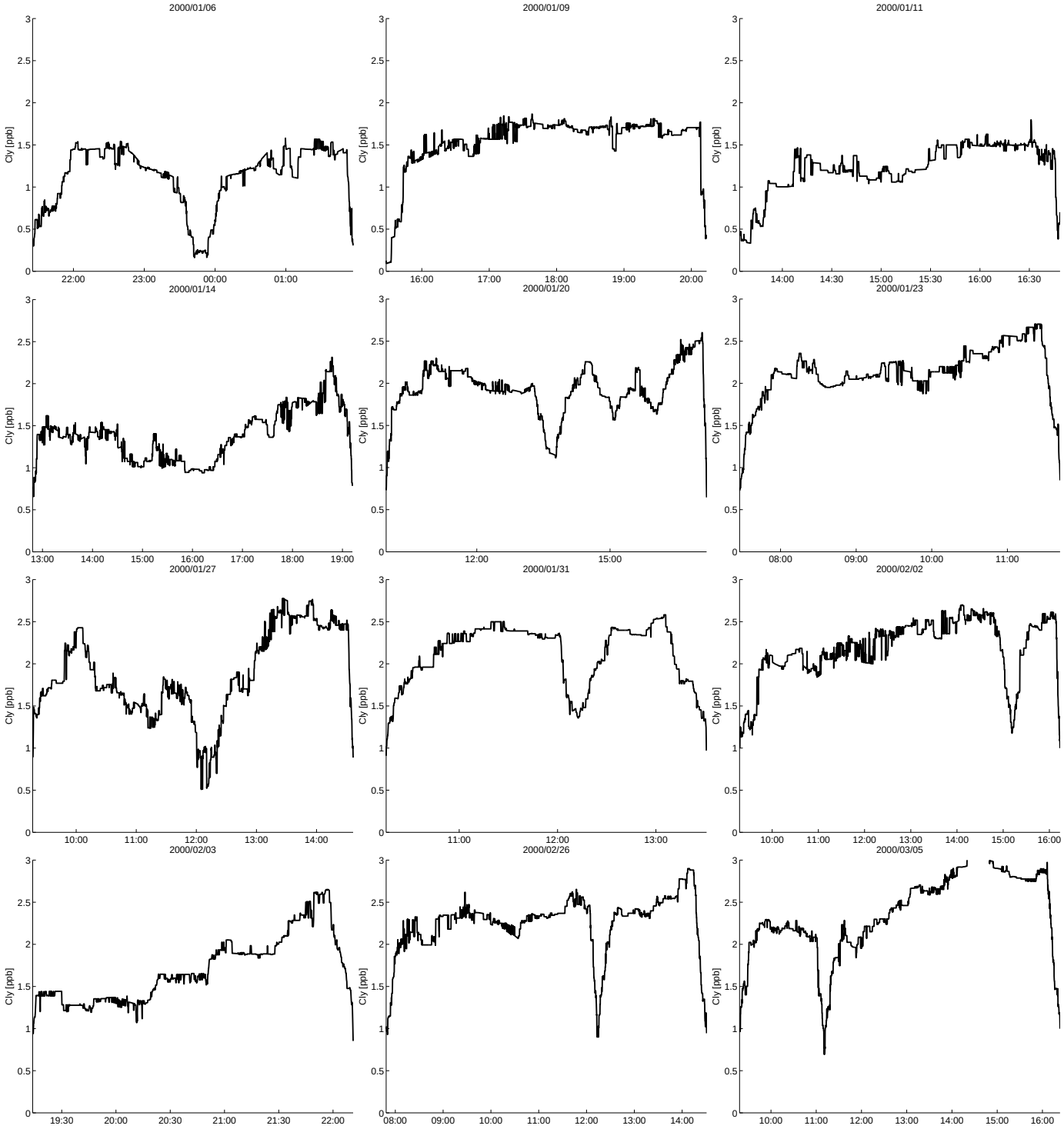

Figure 22: Cl_y as a function of flight time (UTC) from the sum of all modeled inorganic Cl species (black line).

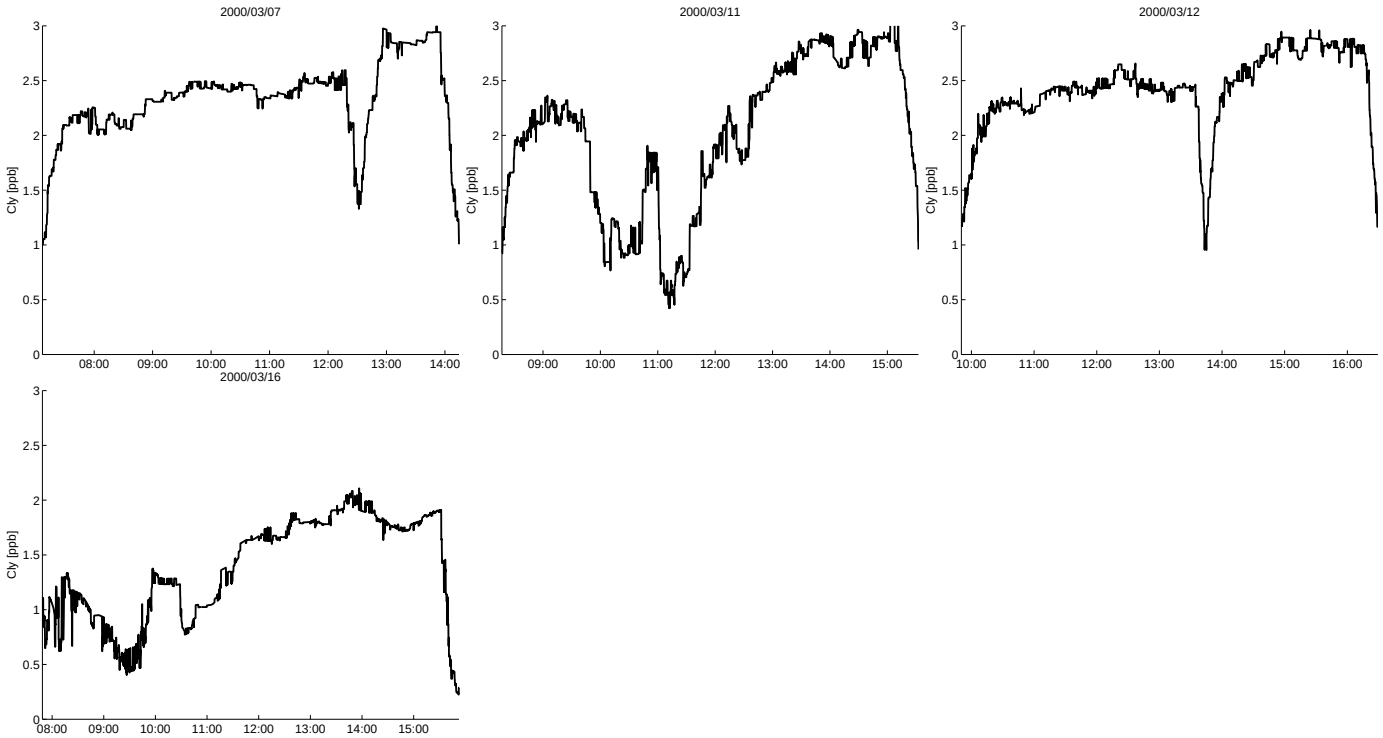

Figure 22: Cl_y as a function of flight time (UTC) from the sum of all modeled inorganic Cl species (black line).

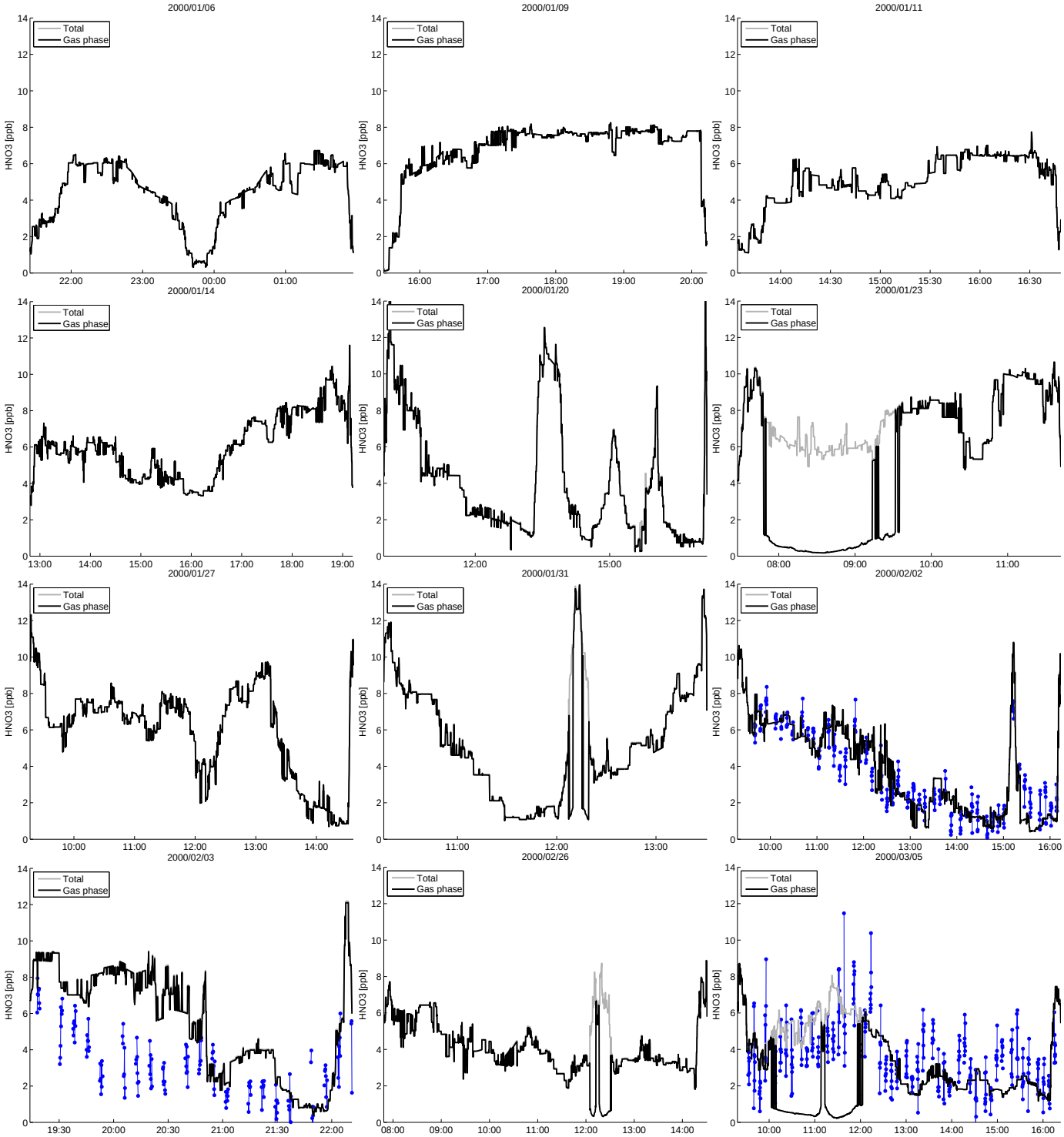

Figure 23: Gas phase HNO_3 as a function of flight time (UTC) from measurements of the CIMS instrument (blue dots) compared to modeled values. Grey lines show total (solid and gas phase) HNO_3 and black lines gas phase HNO_3.

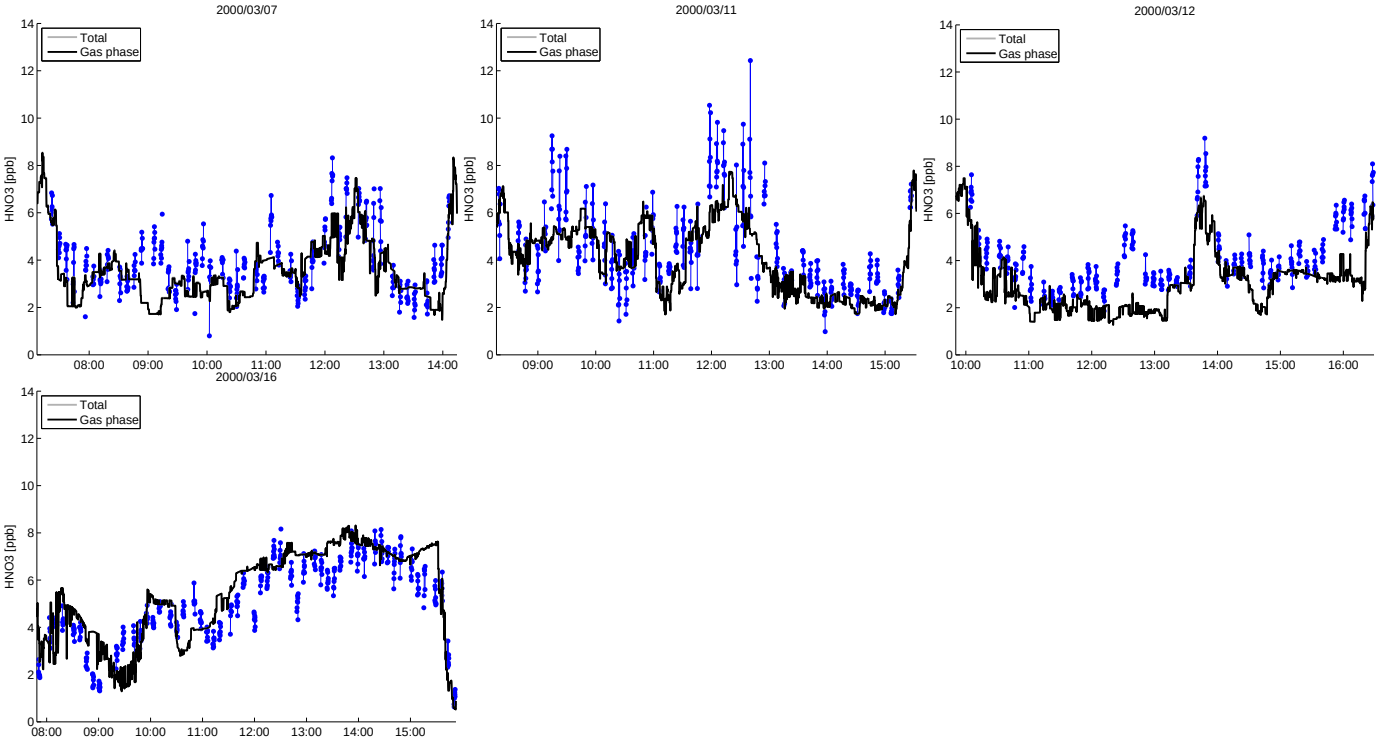

Figure 23: Gas phase HNO_3 as a function of flight time (UTC) from measurements of the CIMS instrument (blue dots) compared to modeled values. Grey lines show total (solid and gas phase) HNO_3 and black lines gas phase HNO_3.

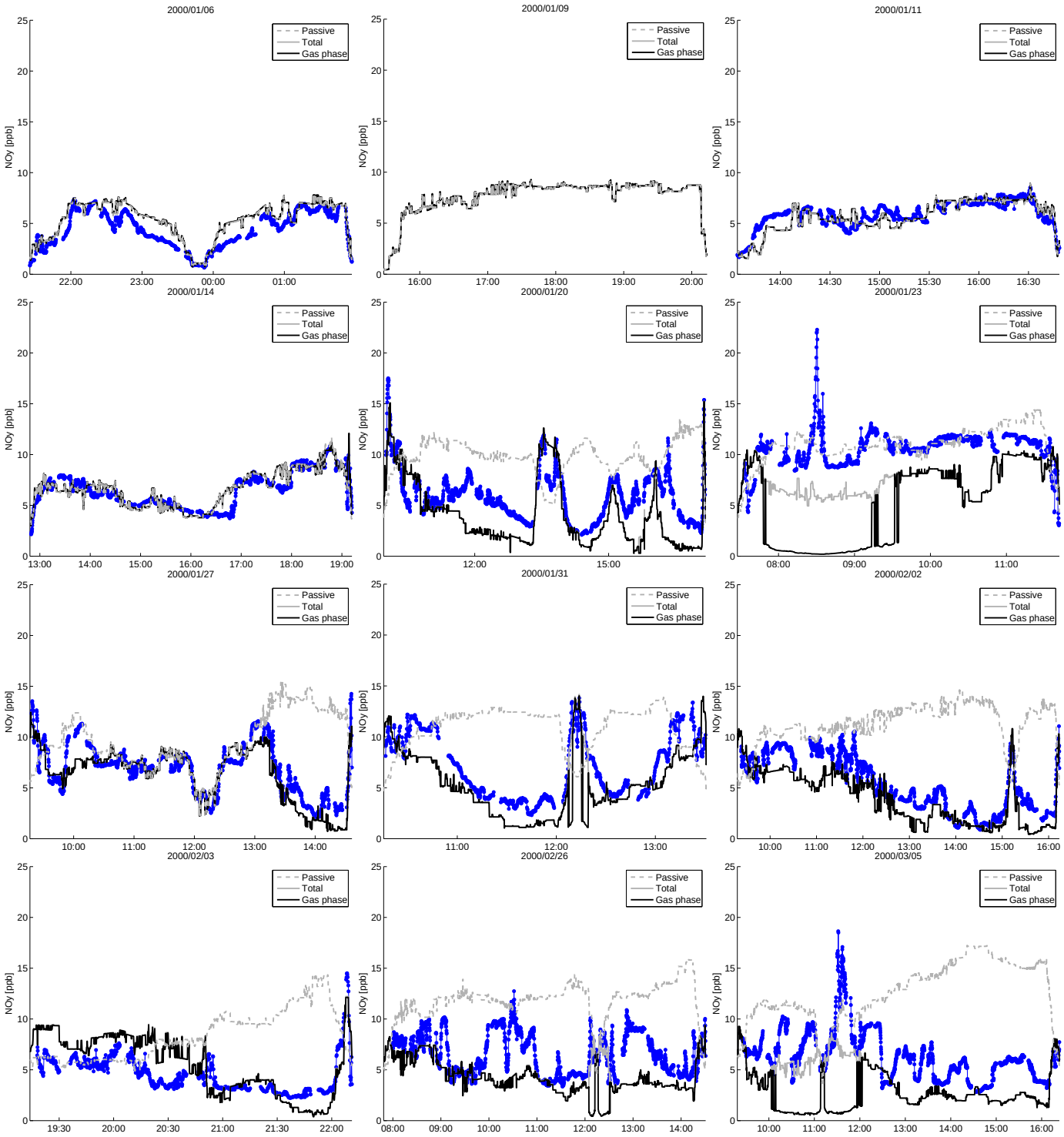

Figure 24: Total NO_y (solid and gas phase, for details see text) as a function of flight time (UTC) from measurements of the NOAA NO_y instrument (rear inlet, blue dots) compared to modeled values. Grey lines show total (solid and gas phase) NO_y and black lines gas phase NO_y. The dotted grey line shows the passive NO_y tracer.

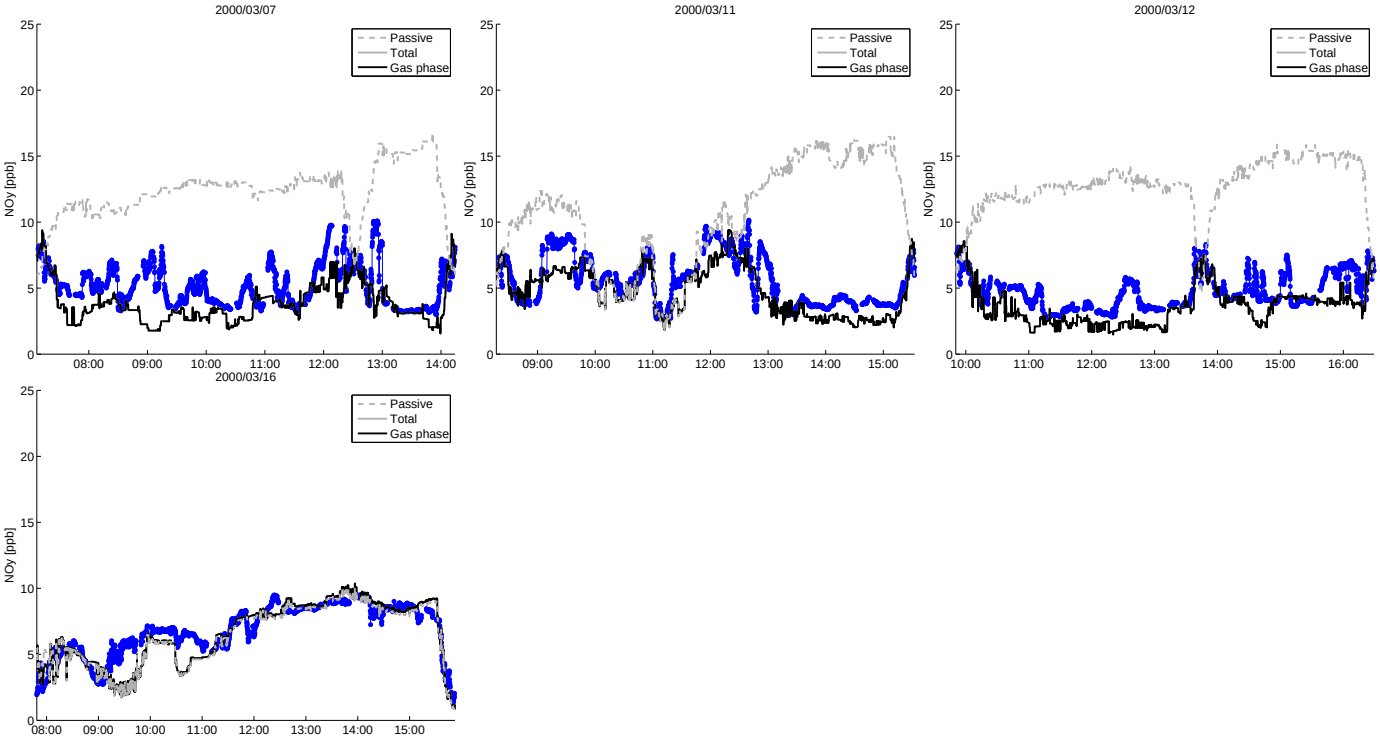

Figure 24: Total NO_y (solid and gas phase, for details see text) as a function of flight time (UTC) from measurements of the NOAA NO_y instrument (rear inlet, blue dots) compared to modeled values. Grey lines show total (solid and gas phase) NO_y and black lines gas phase NO_y. The dotted grey line shows the passive NO_y tracer.

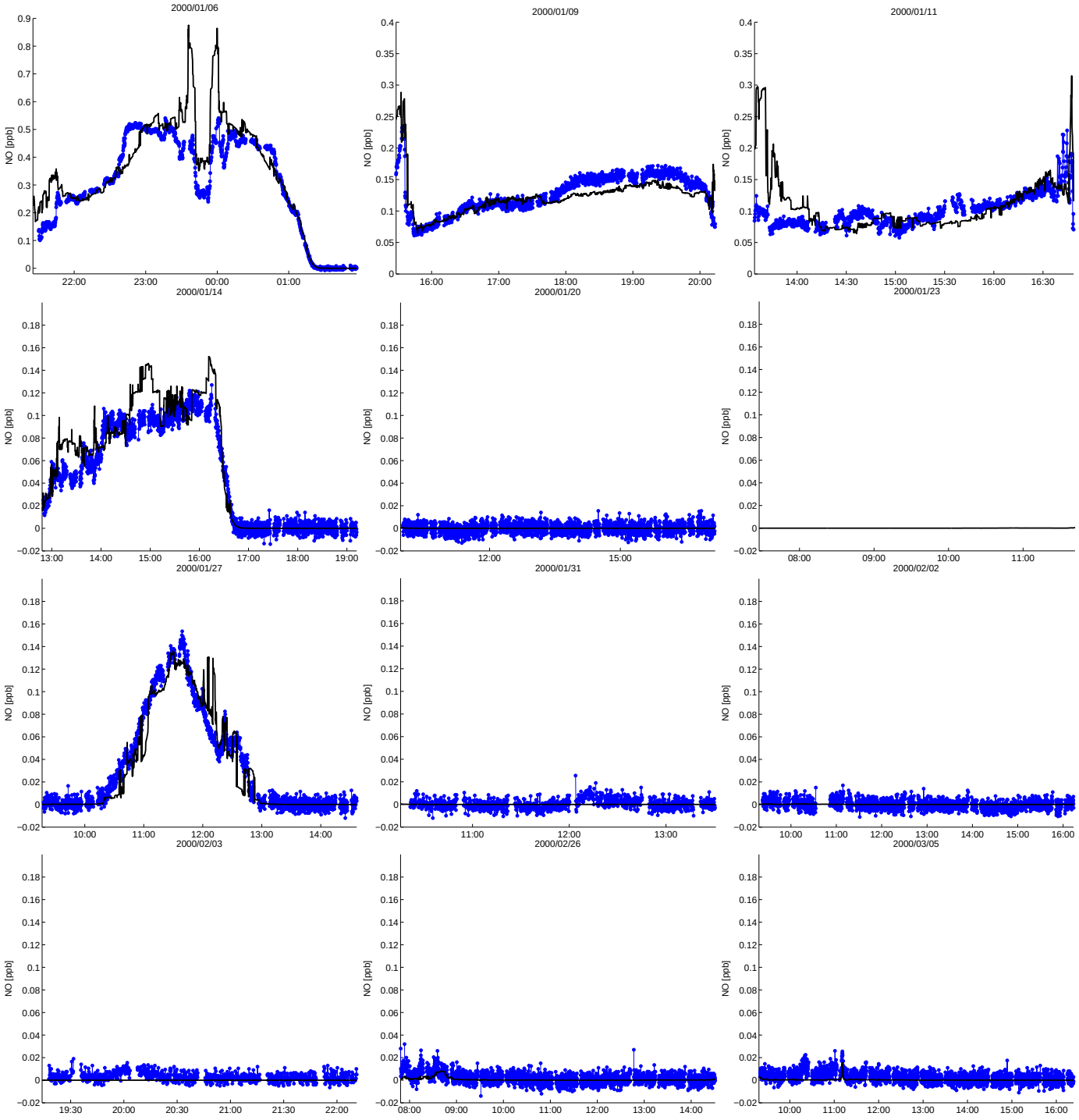

Figure 25: NO as a function of flight time (UTC) from measurements of the NOAA NO_y instrument (blue dots) compared to modeled values (black lines).

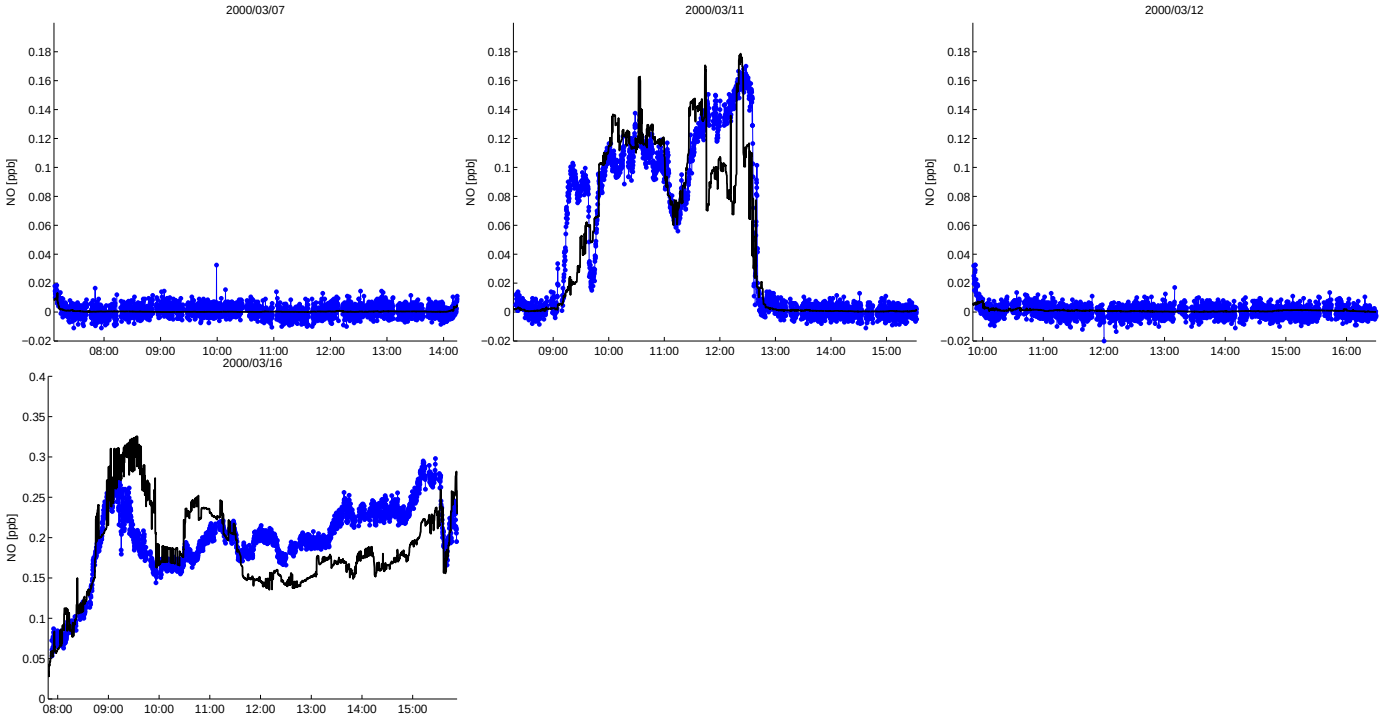

Figure 25: NO as a function of flight time (UTC) from measurements of the NOAA NO_y instrument (blue dots) compared to modeled values (black lines).

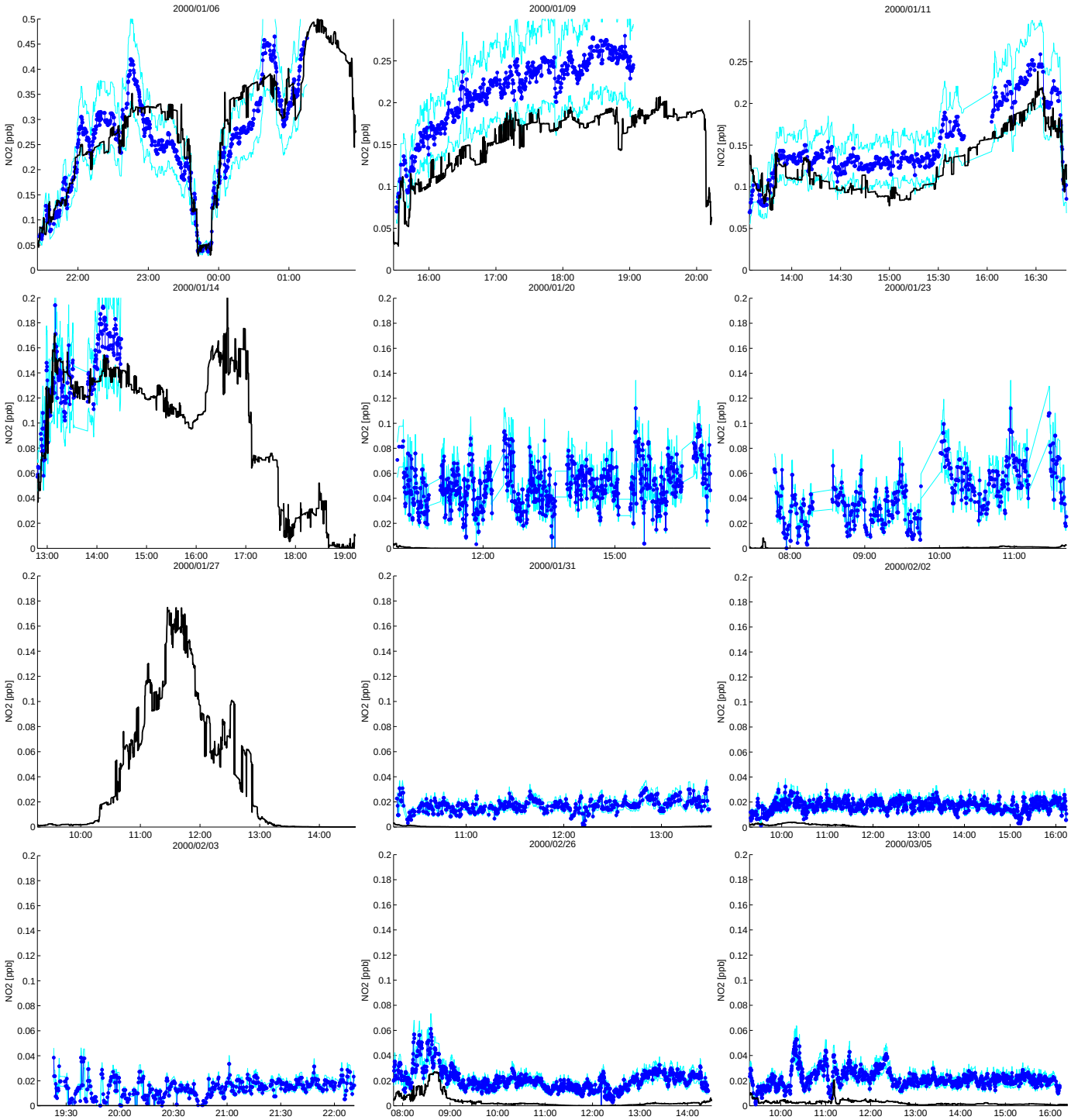

Figure 26: NO_2 as a function of flight time (UTC) from measurements of the Harvard $ClONO_2$-NO_2-ClO-Cl_2O_2 instrument (blue dots) compared to modeled values (black lines). Cyan lines show 2σ uncertainties.

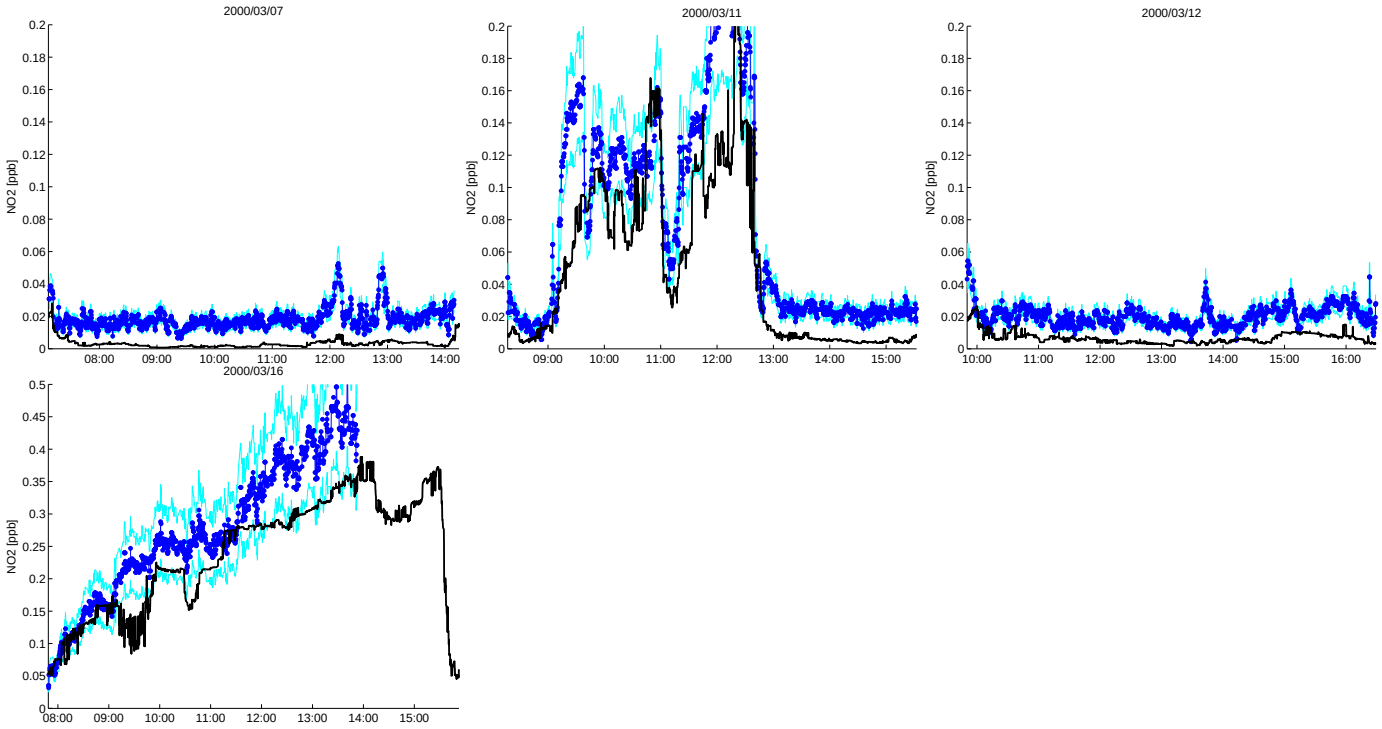

Figure 26: NO_2 as a function of flight time (UTC) from measurements of the Harvard $ClONO_2$-NO_2-ClO-Cl_2O_2 instrument (blue dots) compared to modeled values (black lines). Cyan lines show 2σ uncertainties.

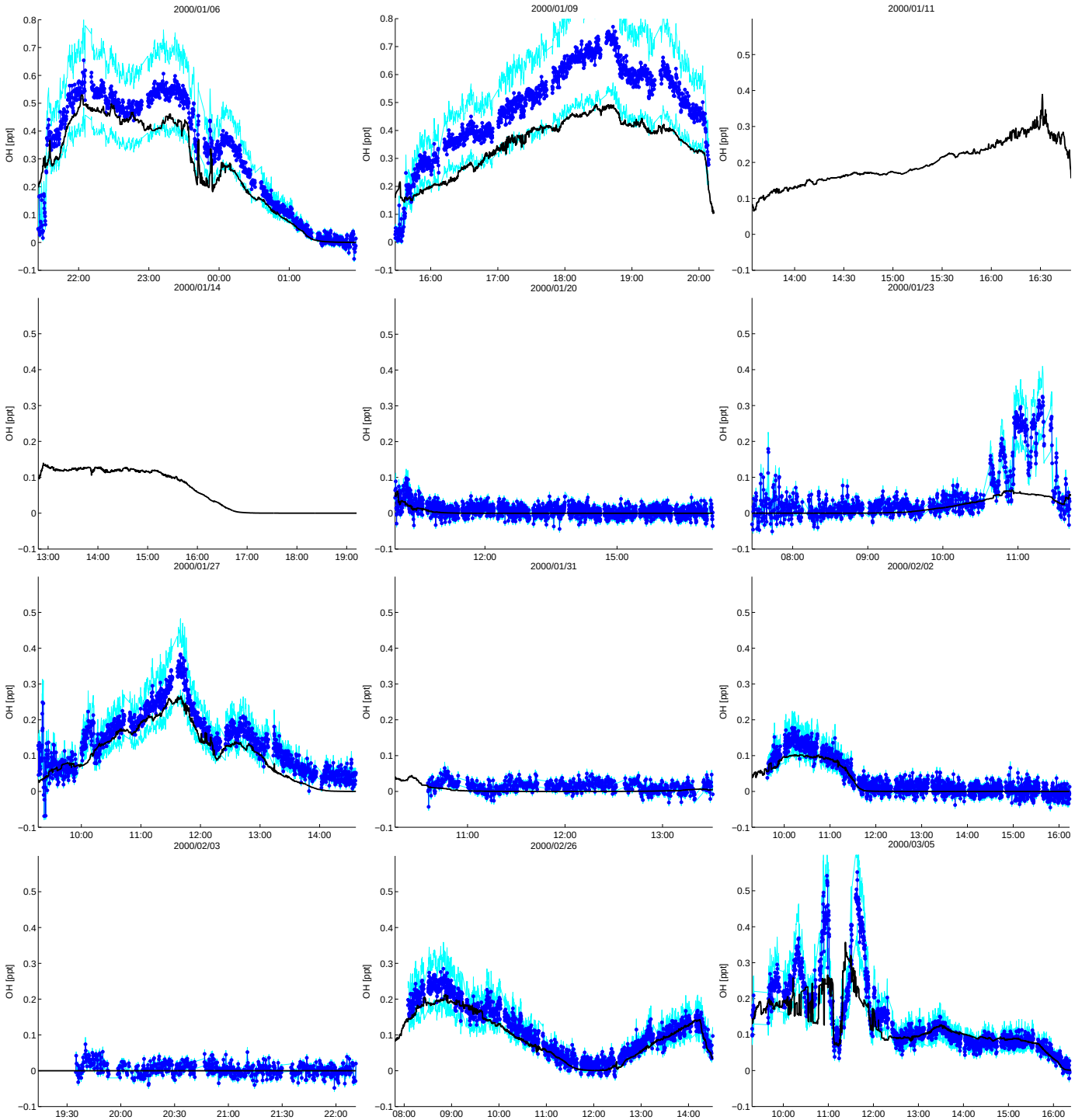

Figure 27: OH as a function of flight time (UTC) from measurements of the Harvard HO_x instrument (blue dots) compared to modeled values (black lines). Cyan lines show 2σ uncertainties.

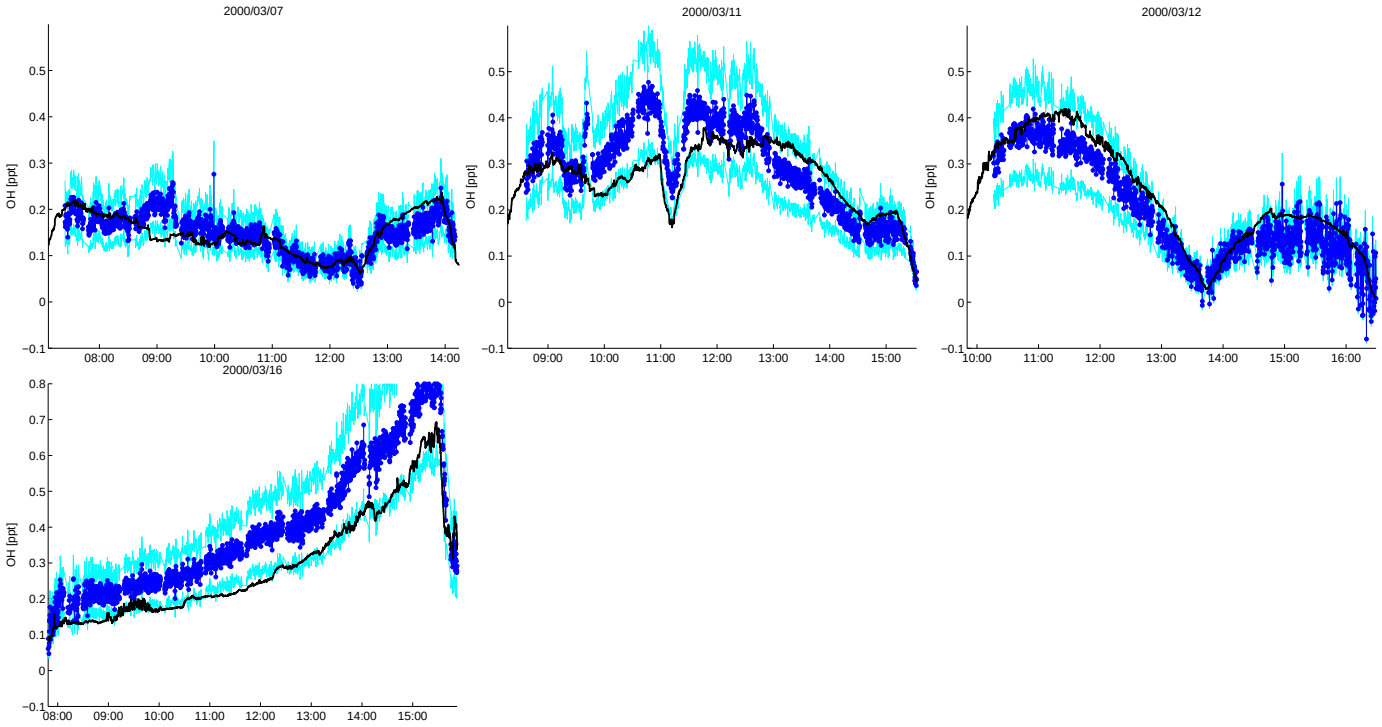

Figure 27: OH as a function of flight time (UTC) from measurements of the Harvard HO_x instrument (blue dots) compared to modeled values (black lines). Cyan lines show 2σ uncertainties.

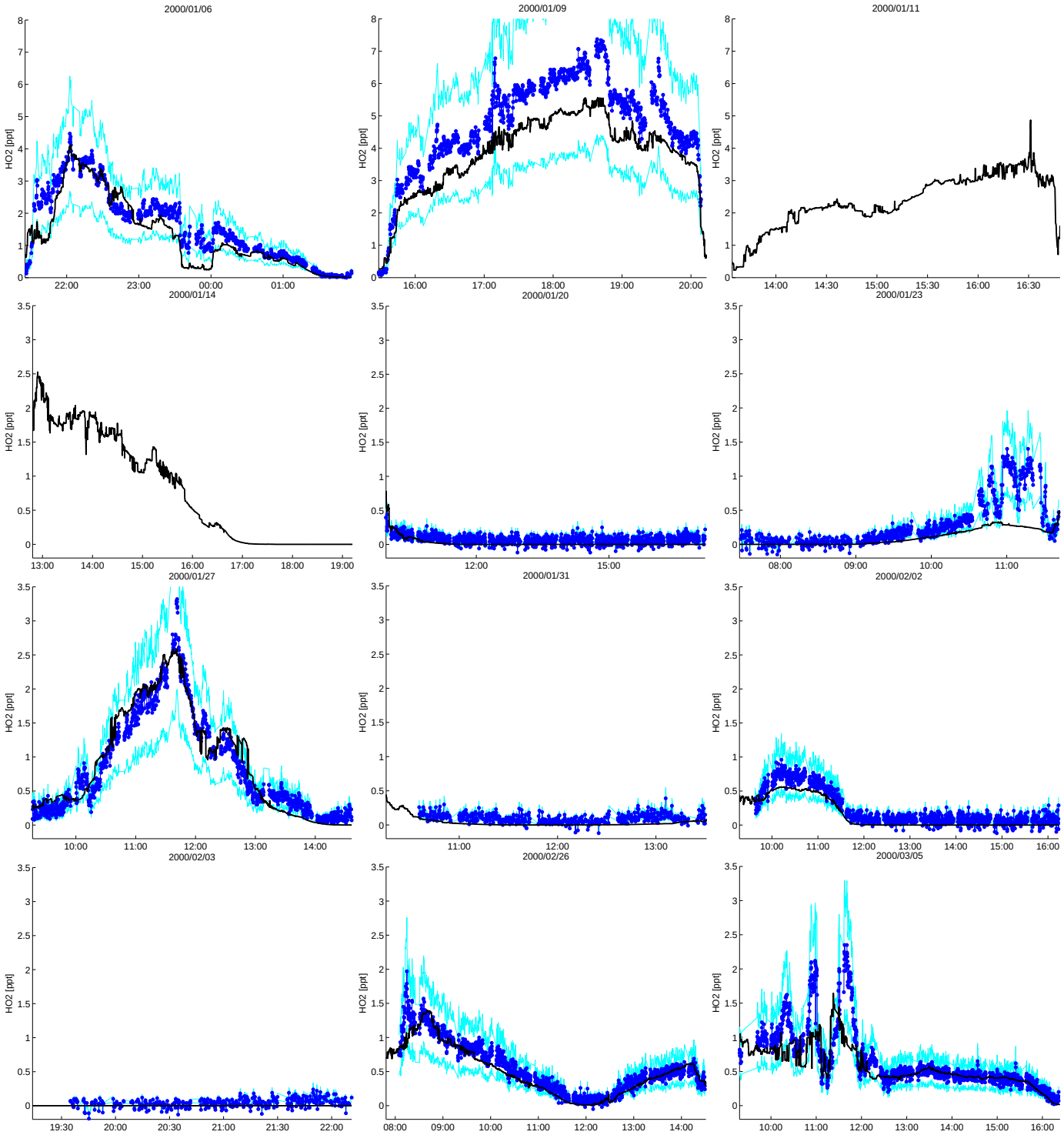

Figure 28: HO_2 as a function of flight time (UTC) from measurements of the Harvard HO_x instrument (blue dots) compared to modeled values (black lines). Cyan lines show 2σ uncertainties.

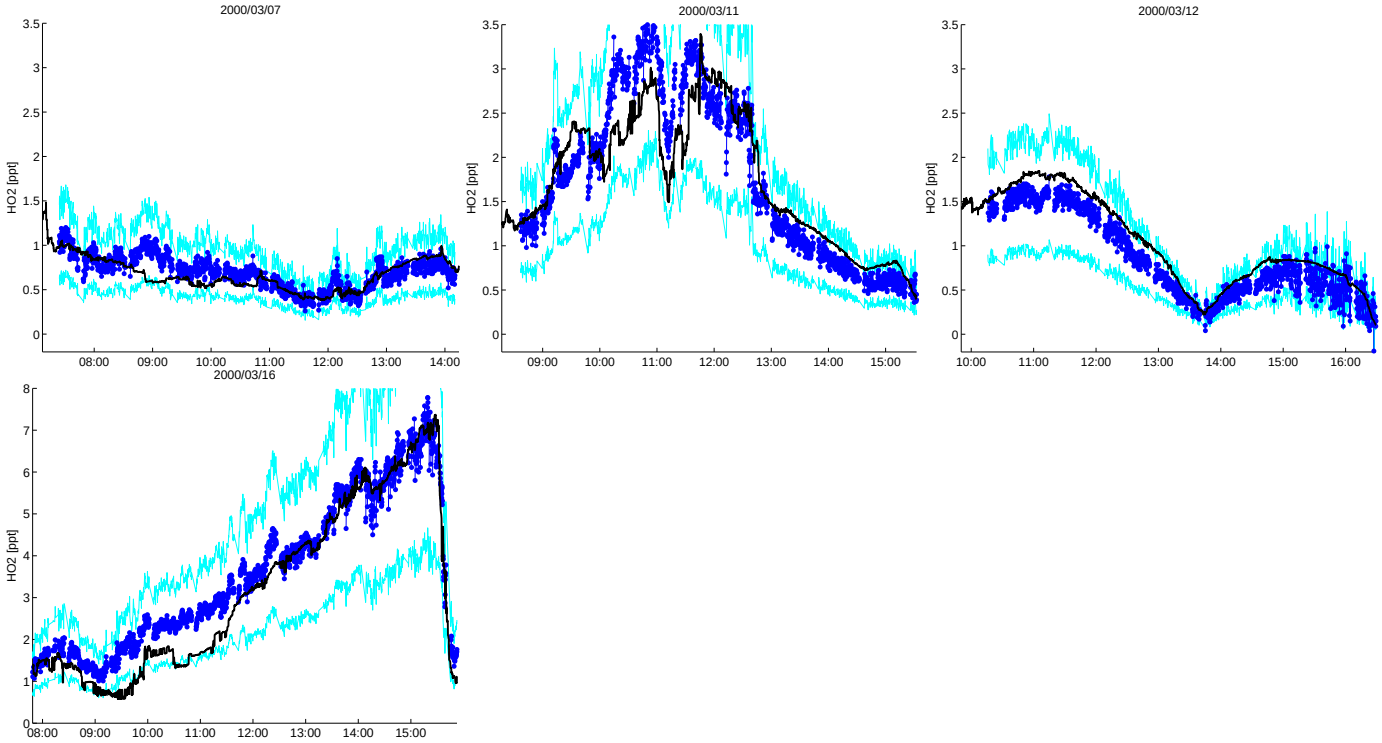

Figure 28: HO_2 as a function of flight time (UTC) from measurements of the Harvard HO_x instrument (blue dots) compared to modeled values (black lines). Cyan lines show 2σ uncertainties.

2 OMS remote balloon flights

The next figures show measurements of the Mark IV and the SLS instrument on the OMS remote balloon flights of 3 December 1999 (also used for initialization) and 15 March 2000. Note that the Mark IV and SLS instruments have different viewing geometries and measurement times. The first set of figures is interpolated to the Mark IV instrument, but shows additionally the SLS measurements, if available. The second set is interpolated to the SLS instrument, but shows additionally the Mark IV instrument.

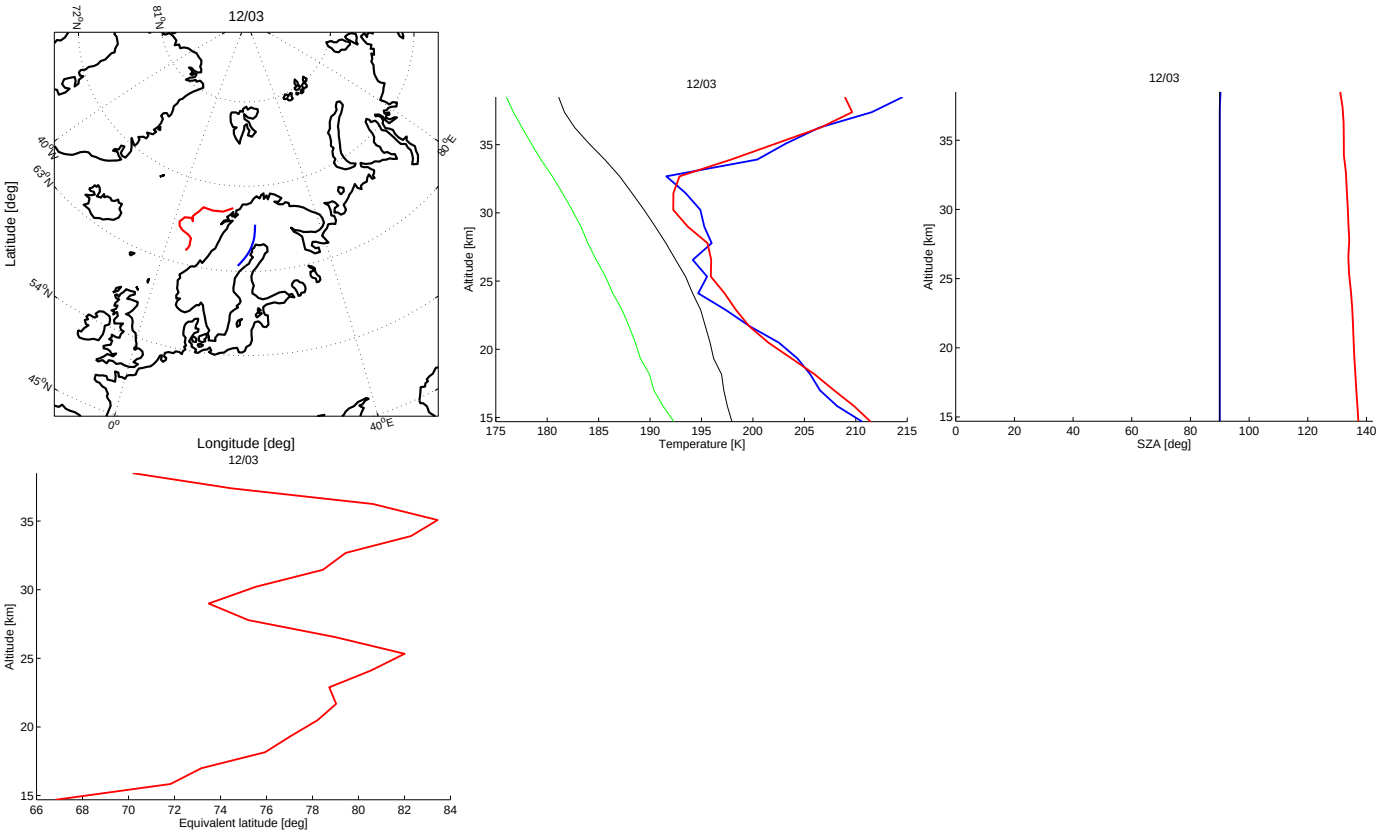

Figure 29: Flight parameters for the Mark IV instrument on 3 December 1999. From upper left to lower right: (1) Flight path of the balloon. The blue line shows the actual flight path and the red line is the position of the probed air parcels at the last model time step before the flight. (2) Temperature as a function of pressure altitude. The blue line shows the measured temperature and the red line shows the temperature on the position of the probed air parcels at the last model time step before the flight (from the ERA Interim reanalysis). The thin black and green lines show the NAT and ice formation temperatures. (3) Solar zenith angle as a function of pressure altitude. (4) Equivalent latitude as a function of pressure altitude.

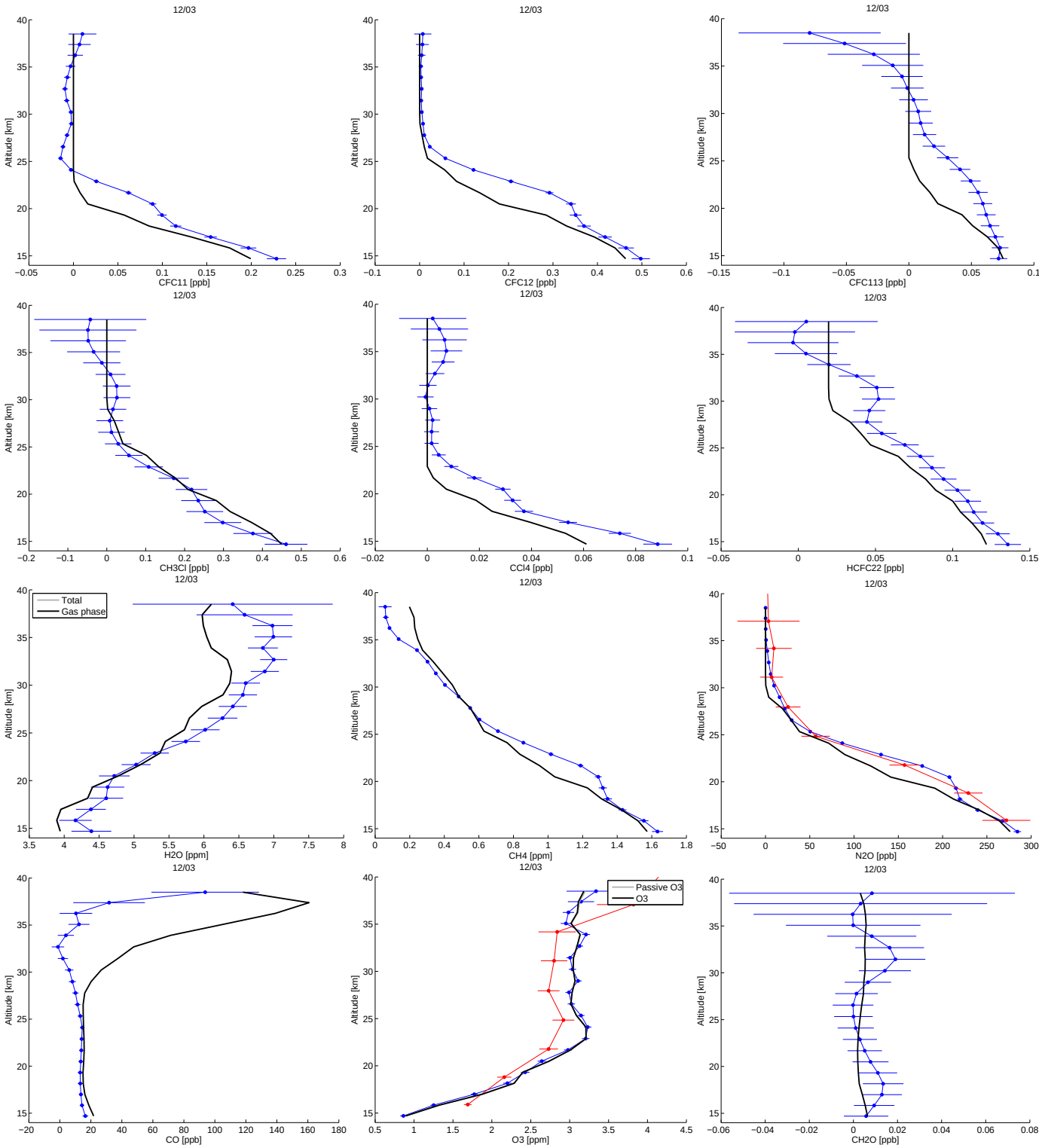

Figure 29: Several species as a function of pressure altitude for measurements of the Mark IV instrument and the SLS instrument on 3 December 1999 (blue and red lines with error bars) compared to modeled values interpolated to the Mark IV viewing geometry (black lines). Grey lines show total (solid and gas phase) modeled values or passive ozone. Species are (from upper left to lower right): CFC-11, CFC-12, CFC-113, CH_3Cl, CCl_4, HCFC-22, H_2O, CH_4, N_2O, CO, O_3, CH_2O.

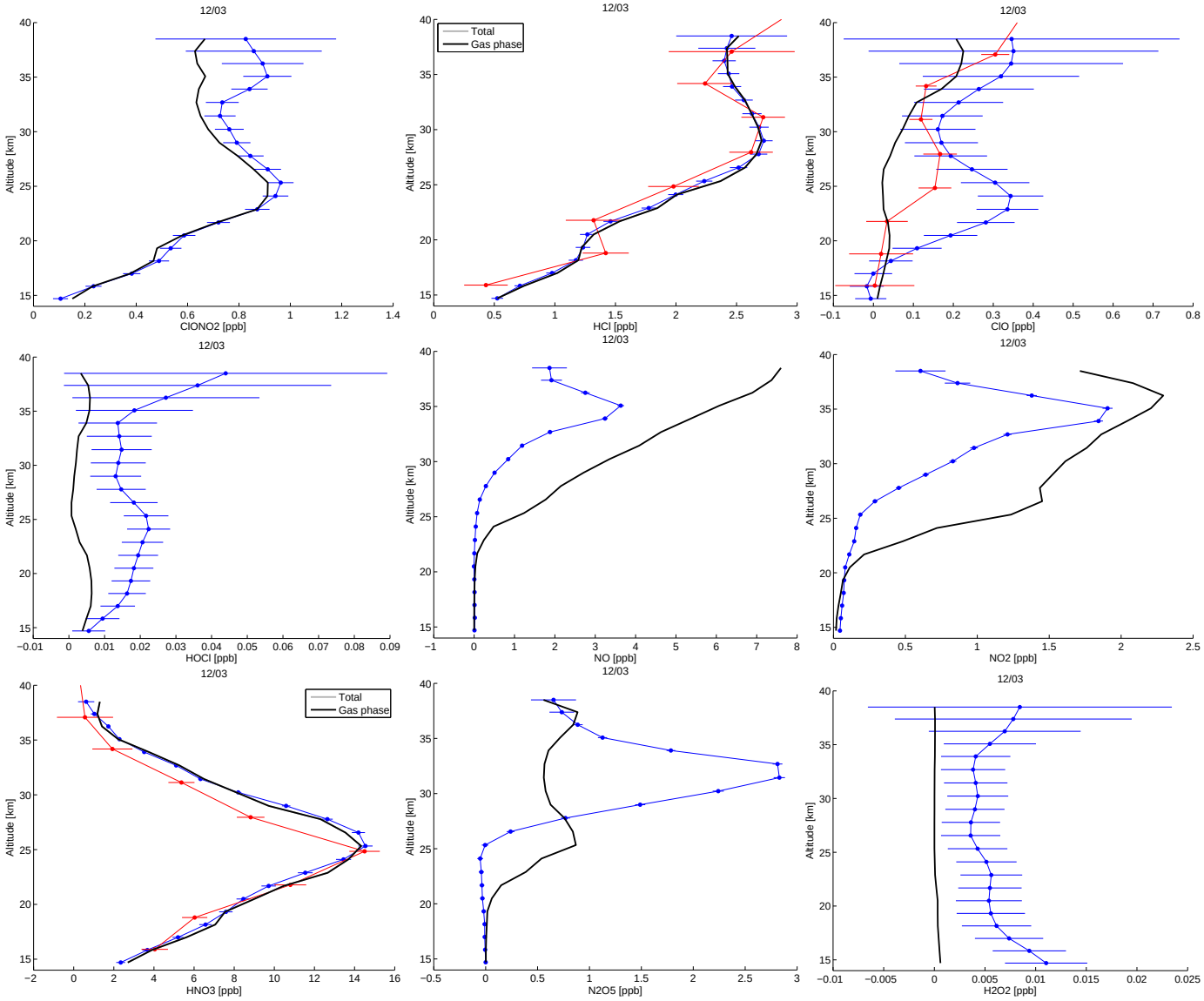

Figure 29: Several species as a function of pressure altitude for measurements of the Mark IV instrument and the SLS instrument on 3 December 1999 (blue and red lines with error bars) compared to modeled values interpolated to the Mark IV viewing geometry (black lines). Grey lines show total (solid and gas phase) modeled values. Species are (from upper left to lower right): $ClONO_2$, HCl, ClO, HOCl, NO, NO_2, HNO_3, N_2O_5, H_2O_2.

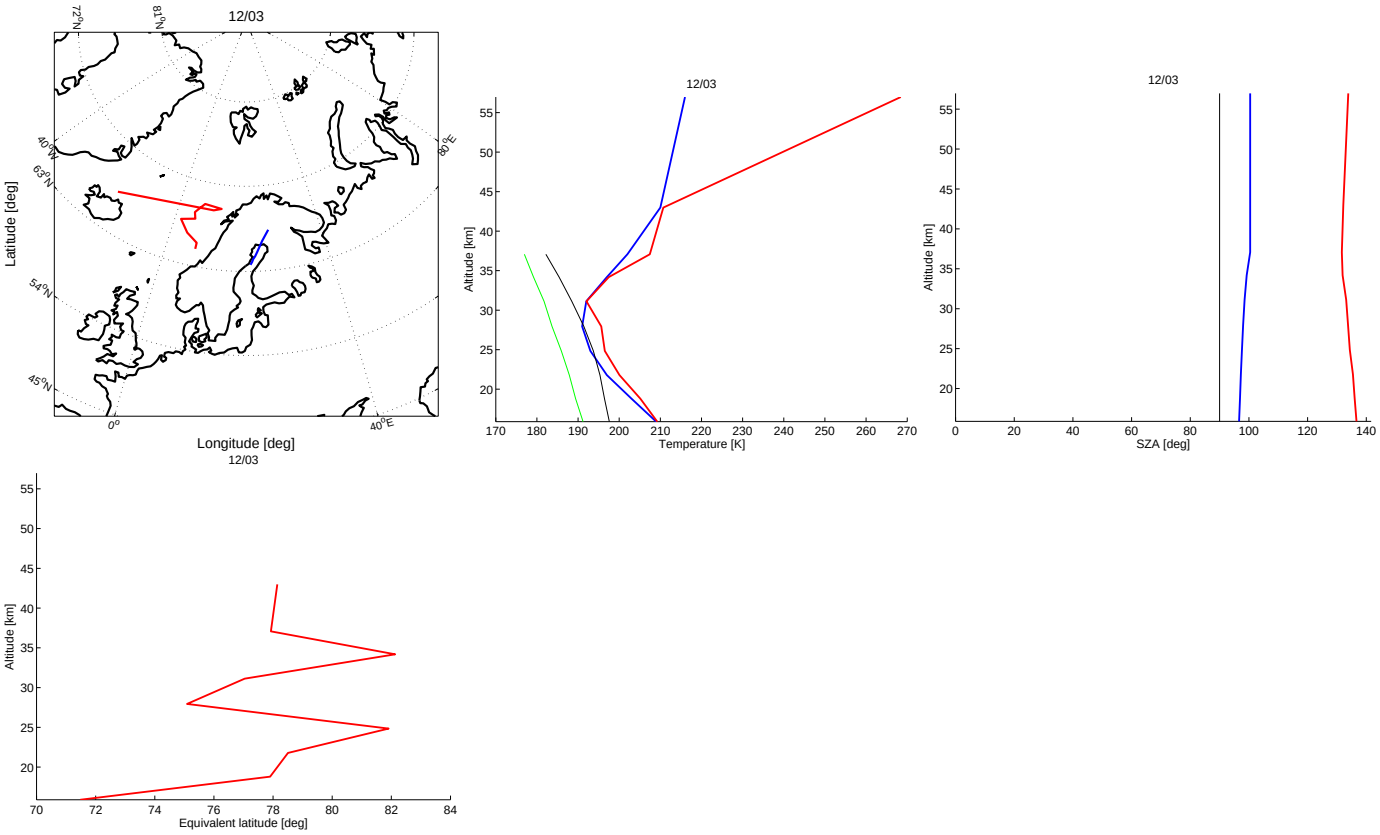

Figure 30: Flight parameters for the SLS instrument on 3 December 1999. From upper left to lower right: (1) Flight path of the balloon. The blue line shows the actual flight path and the red line is the position of the probed air parcels at the last model time step before the flight. (2) Temperature as a function of pressure altitude. The blue line shows the measured temperature and the red line shows the temperature on the position of the probed air parcels at the last model time step before the flight (from the ERA Interim reanalysis). The thin black and green lines show the NAT and ice formation temperatures. (3) Solar zenith angle as a function of pressure altitude. (4) Equivalent latitude as a function of pressure altitude.

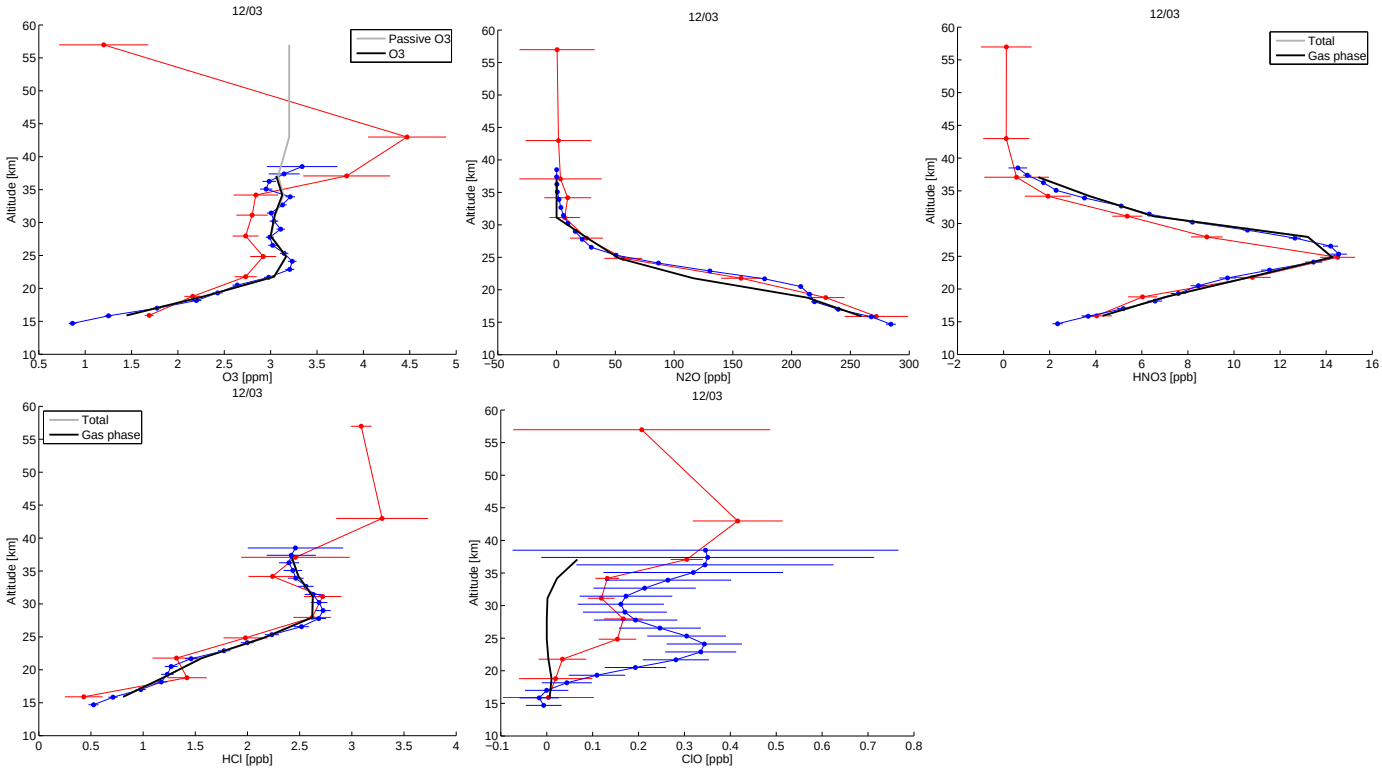

Figure 30: Several species as a function of pressure altitude for measurements of the Mark IV instrument and the SLS instrument on 3 December 1999 (blue and red lines with error bars) compared to modeled values interpolated to the SLS viewing geometry (black lines). Grey lines show total (solid and gas phase) modeled values or passive ozone. Species are (from upper left to lower right): O_3, N_2O, HNO_3, HCl, ClO

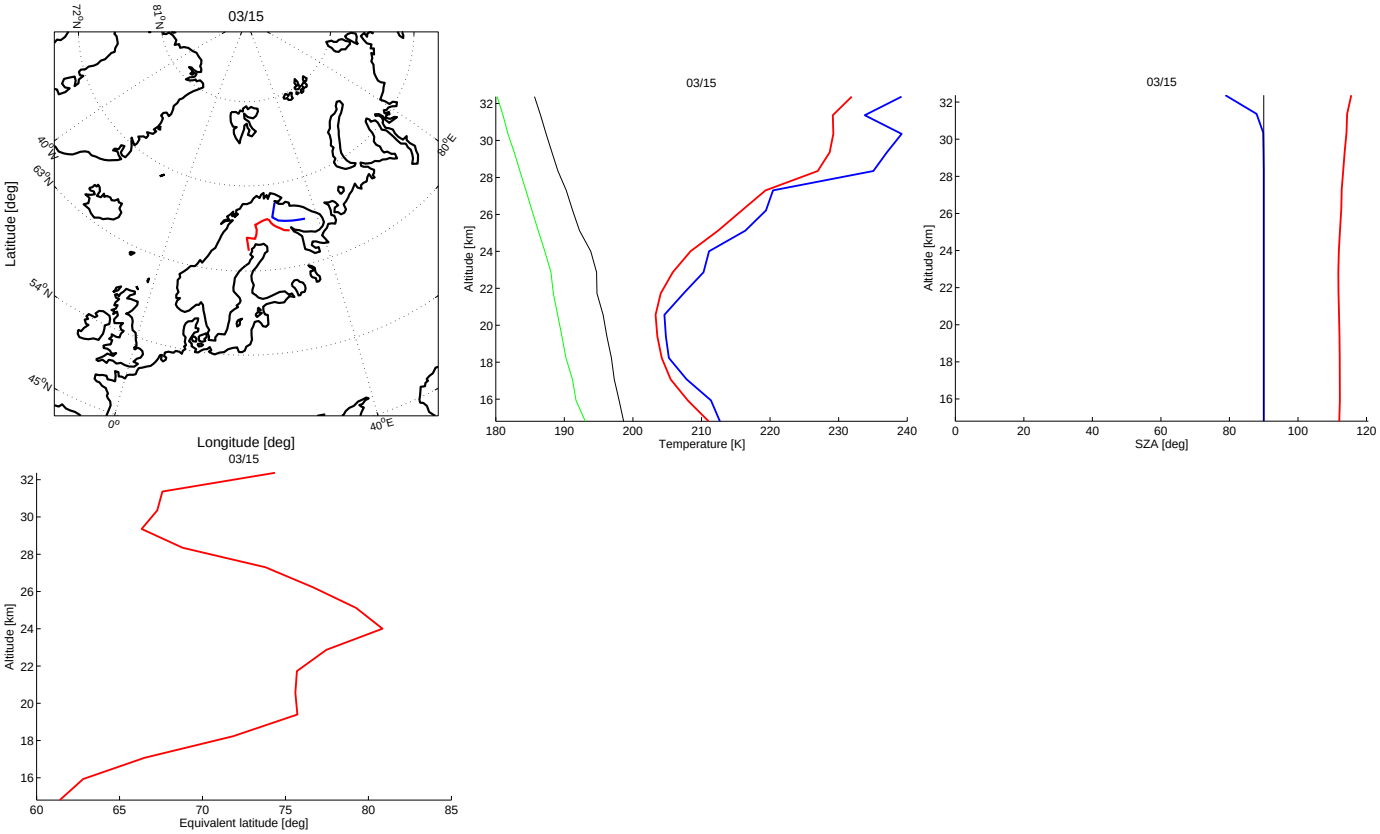

Figure 31: Flight parameters for the Mark IV instrument on 15 March 2000. From upper left to lower right: (1) Flight path of the balloon. The blue line shows the actual flight path and the red line is the position of the probed air parcels at the last model time step before the flight. (2) Temperature as a function of pressure altitude. The blue line shows the measured temperature and the red line shows the temperature on the position of the probed air parcels at the last model time step before the flight (from the ERA Interim reanalysis). The thin black and green lines show the NAT and ice formation temperatures. (3) Solar zenith angle as a function of pressure altitude. (4) Equivalent latitude as a function of pressure altitude.

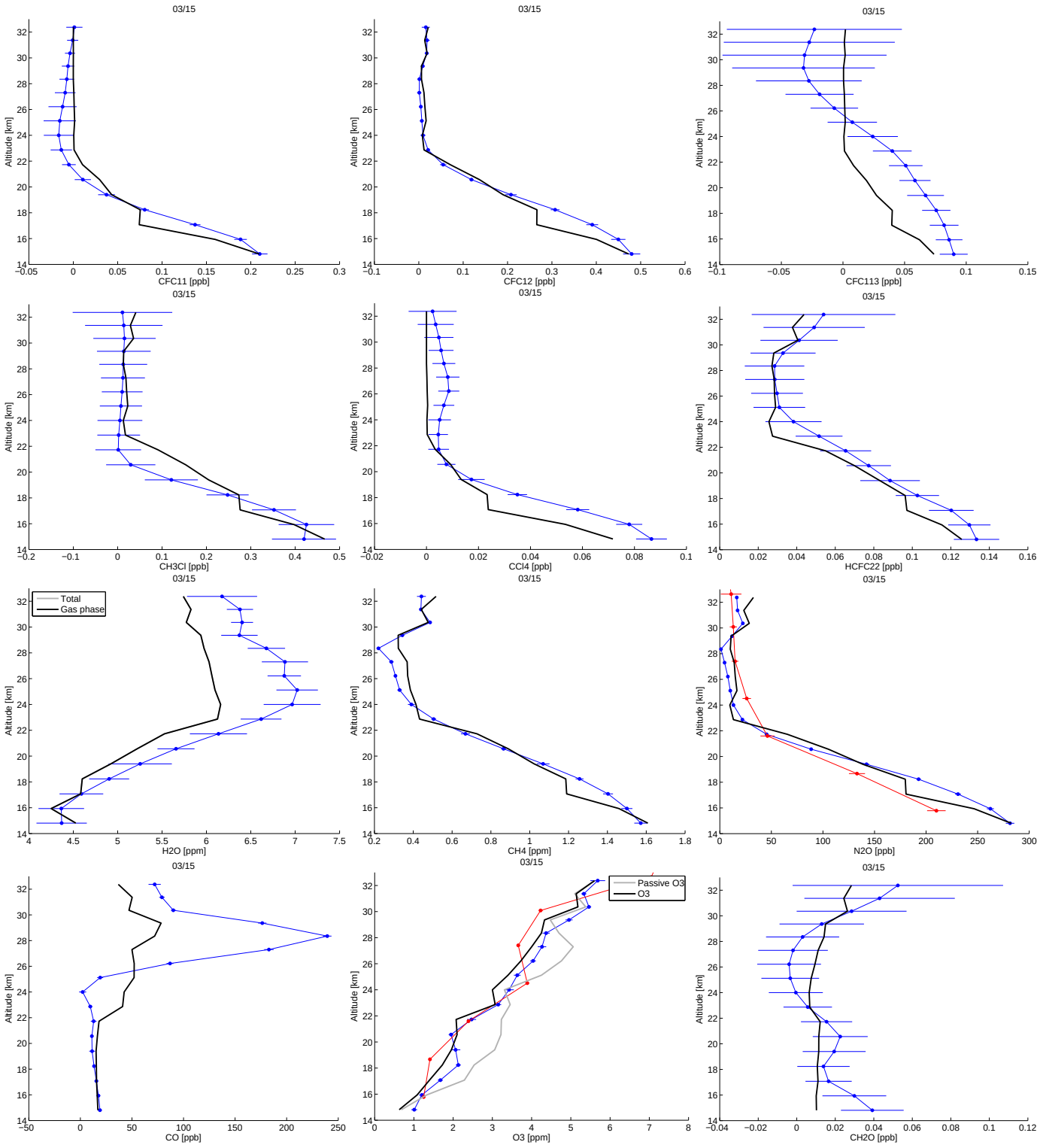

Figure 31: Several species as a function of pressure altitude for measurements of the Mark IV instrument and the SLS instrument on 15 March 2000 (blue and red lines with error bars) compared to modeled values interpolated to the Mark IV viewing geometry (black lines). Grey lines show total (solid and gas phase) modeled values or passive ozone. Species are (from upper left to lower right): CFC-11, CFC-12, CFC-113, CH_3Cl, CCl_4, HCFC-22, H_2O, CH_4, N_2O, CO, O_3, CH_2O.

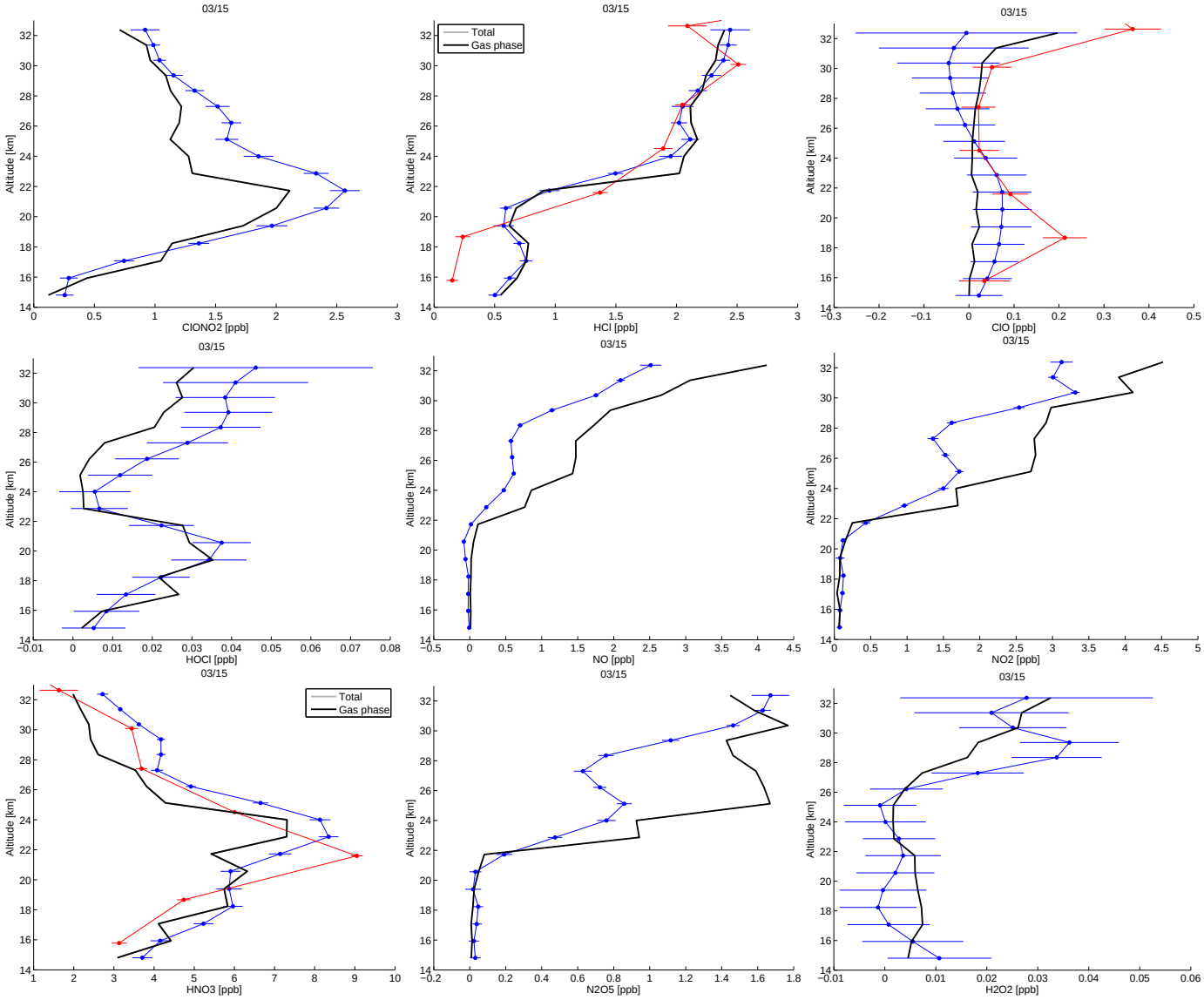

Figure 31: Several species as a function of pressure altitude for measurements of the Mark IV instrument and the SLS instrument on 15 March 2000 (blue and red lines with error bars) compared to modeled values interpolated to the Mark IV viewing geometry (black lines). Grey lines show total (solid and gas phase) modeled values. Species are (from upper left to lower right): $ClONO_2$, HCl, ClO, HOCl, NO, NO_2, HNO_3, N_2O_5, H_2O_2.

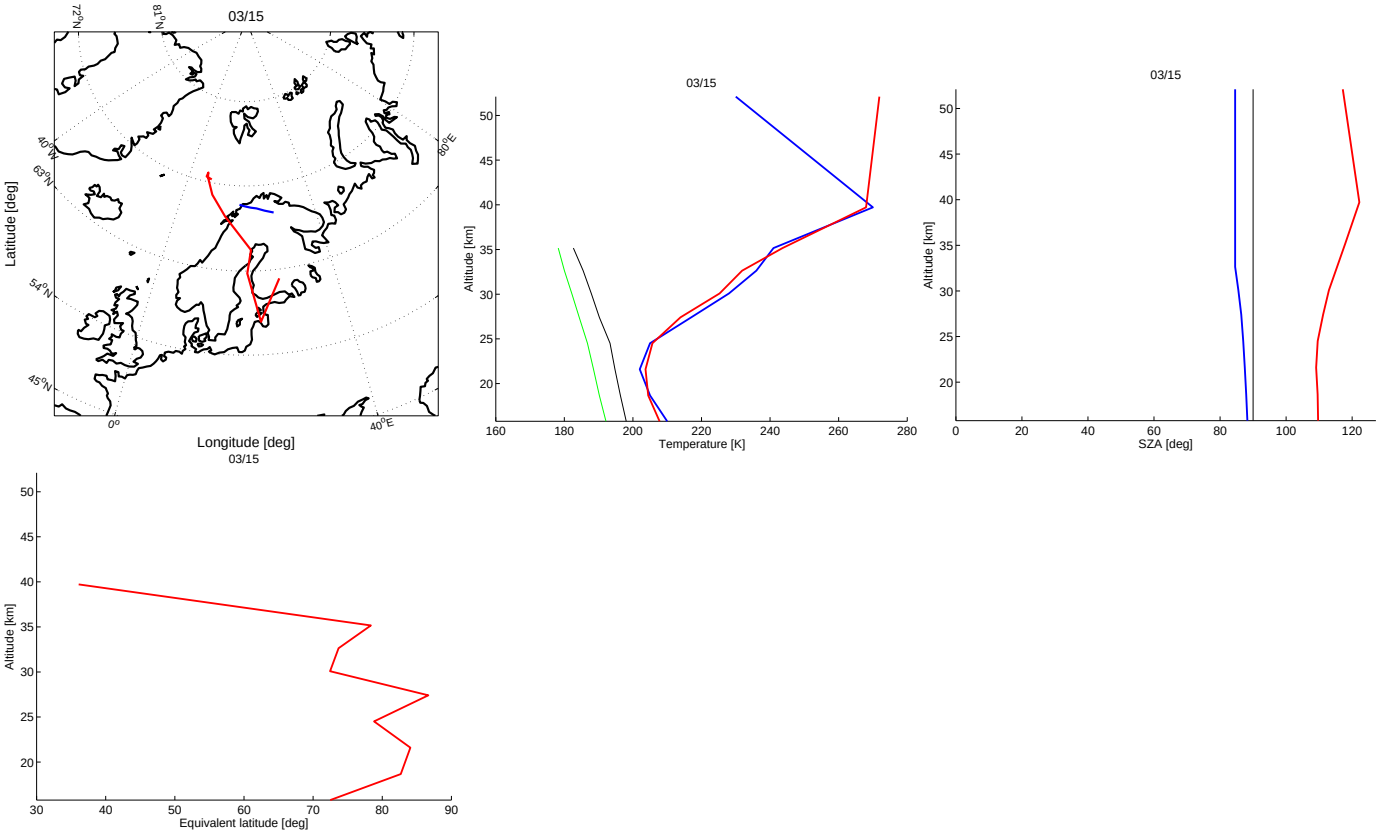

Figure 32: Flight parameters for the SLS instrument on 15 March 2000. From upper left to lower right: (1) Flight path of the balloon. The blue line shows the actual flight path and the red line is the position of the probed air parcels at the last model time step before the flight. (2) Temperature as a function of pressure altitude. The blue line shows the measured temperature and the red line shows the temperature on the position of the probed air parcels at the last model time step before the flight (from the ERA Interim reanalysis). The thin black and green lines show the NAT and ice formation temperatures. (3) Solar zenith angle as a function of pressure altitude. (4) Equivalent latitude as a function of pressure altitude.

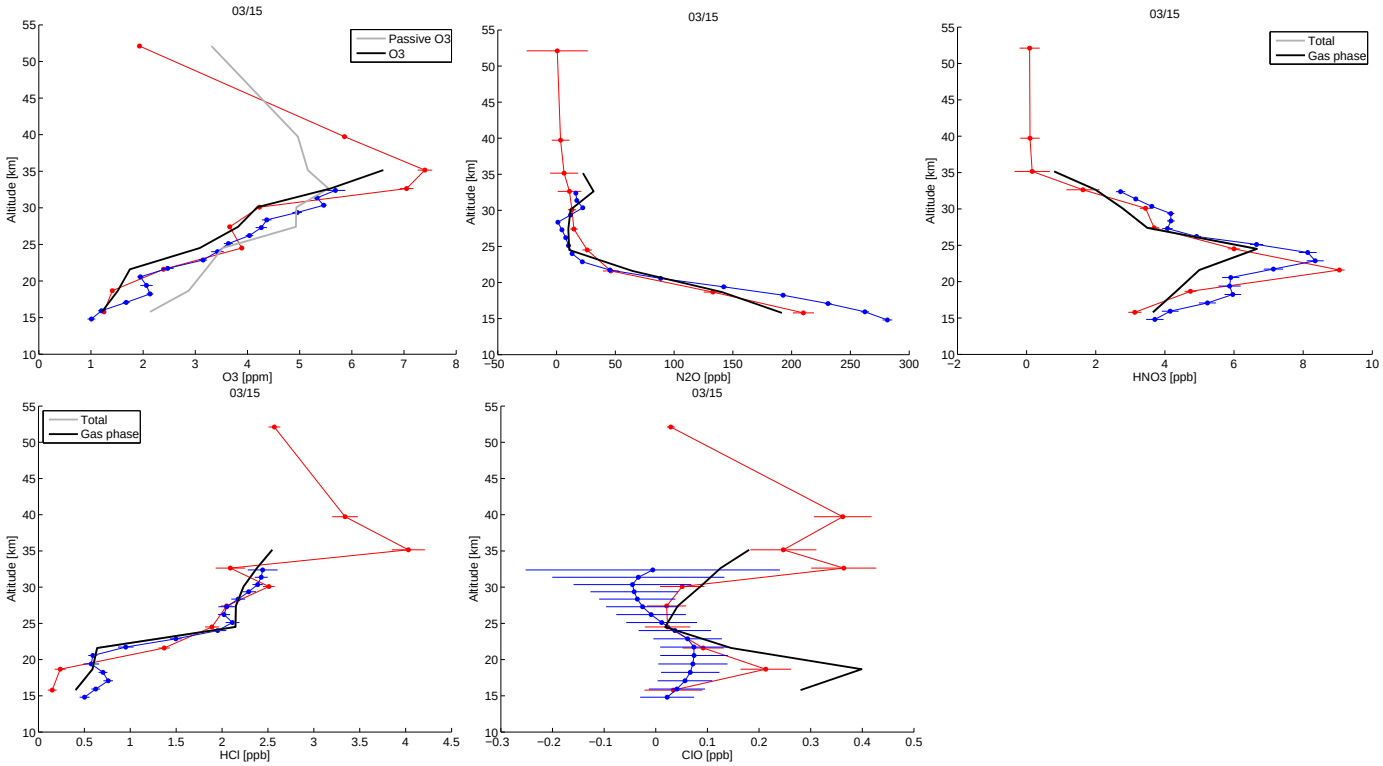

Figure 32: Several species as a function of pressure altitude for measurements of the Mark IV instrument and the SLS instrument on 15 March 2000 (blue and red lines with error bars) compared to modeled values interpolated to the SLS viewing geometry (black lines). Grey lines show total (solid and gas phase) modeled values or passive ozone. Species are (from upper left to lower right): O_3, N_2O, HNO_3, HCl, ClO

3 OMS in situ balloon flight

The next figures show measurements of the LACE instrument on the OMS in situ balloon flight of 5 March 2000.

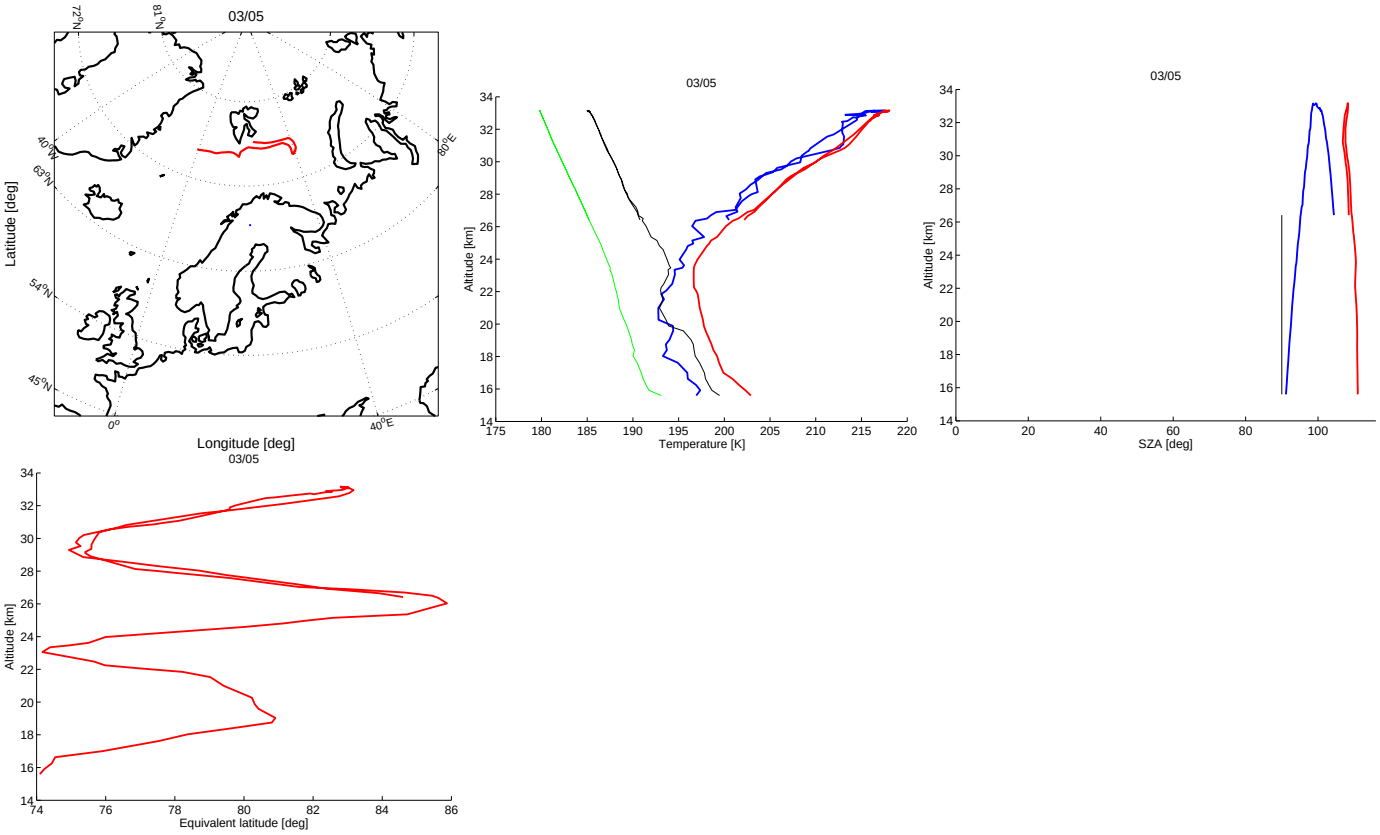

Figure 33: From upper left to lower right: (1) Flight path of the balloon. The blue line shows the actual flight path and the red line is the position of the probed air parcels at the last model time step before the flight. (2) Temperature as a function of pressure altitude. The blue line shows the measured temperature and the red line shows the temperature on the position of the probed air parcels at the last model time step before the flight (from the ERA Interim reanalysis). The thin black and green lines show the NAT and ice formation temperatures. (3) Solar zenith angle as a function of pressure altitude. (4) Equivalent latitude as a function of pressure altitude.

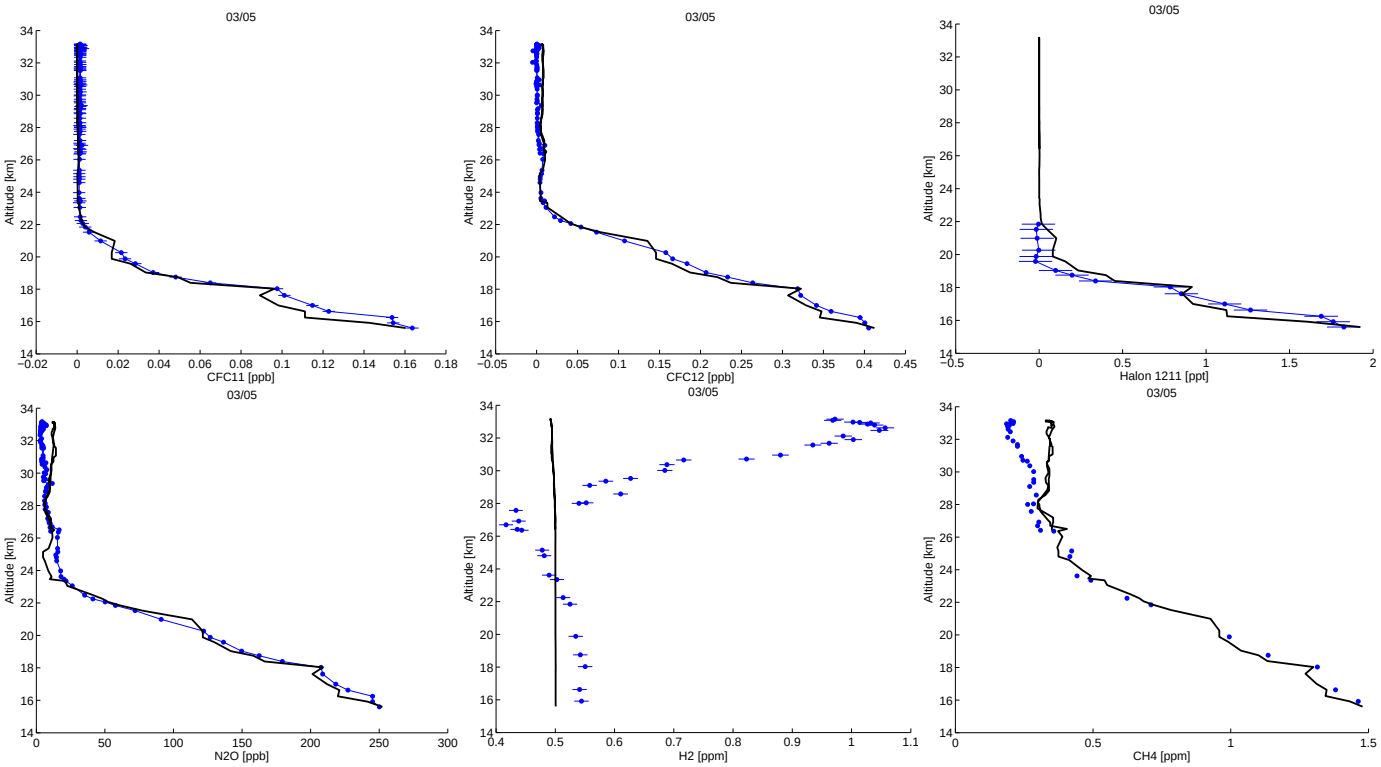

Figure 33: Several species as a function of pressure altitude for measurements of the LACE instrument on 5 March 2000 (blue lines with error bars) compared to modeled values (black lines). Species are (from upper left to lower right): CFC-11, CFC-12, Halon-1211, N_2O, H_2, CH_4

4 Ozone sondes

The next figures show measurements of ozone sondes from the stations Ny-Alesund (polar), Hohenpeissenberg (mid-latitudes), Samoa and Paramaribo (tropical) between December 1999 and March 2000. The legend of all figures is the same and only given here:

From upper left to lower right: (1) Flight path of the balloon. The blue line shows the actual flight path and the red line is the position of the probed air parcels at the last model time step before the flight. (2) Temperature as a function of pressure altitude. The blue line shows the measured temperature and the red line shows the temperature on the position of the probed air parcels at the last model time step before the flight (from the ERA Interim reanalysis). The thin black and green lines show the NAT and ice formation temperatures. (3) Solar zenith angle as a function of pressure altitude. (4) Equivalent latitude as a function of pressure altitude. (5) Measured ozone profile (blue dots) as a function of presure altitude compared to modeled values (black line). The grey line is the passive ozone profile.

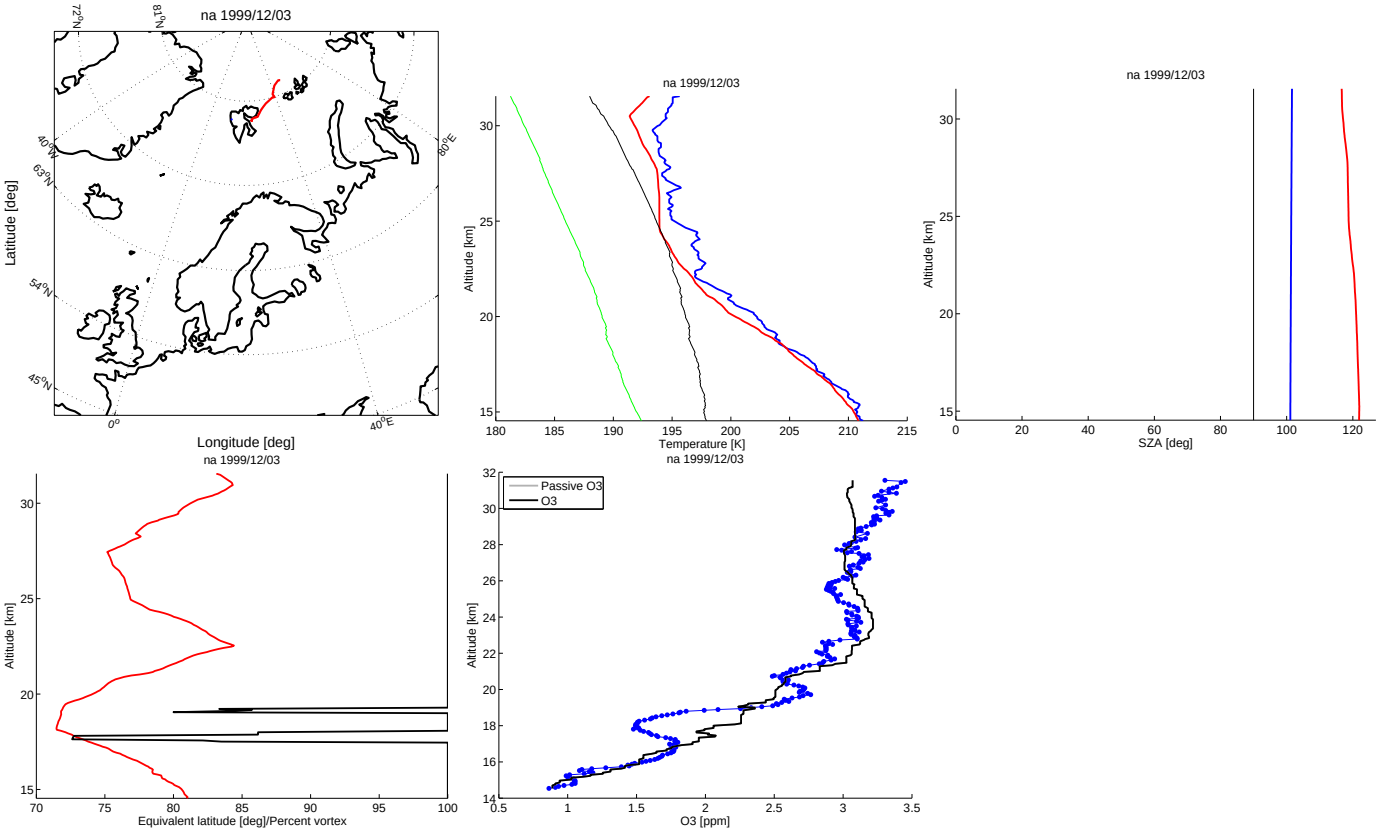

Figure 34: Ny-Alesund 3 December 1999

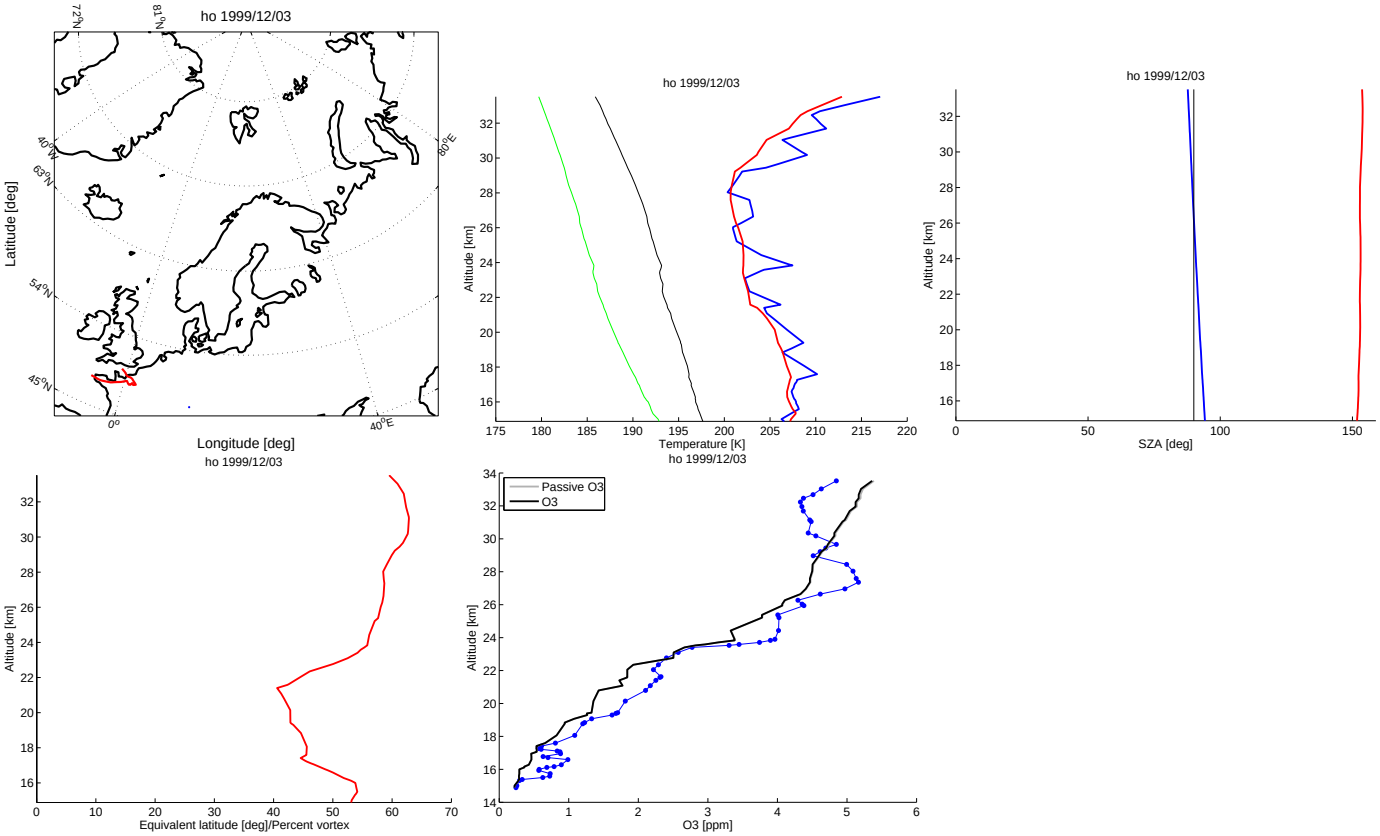

Figure 35: Hohenpeissenberg 3 December 1999

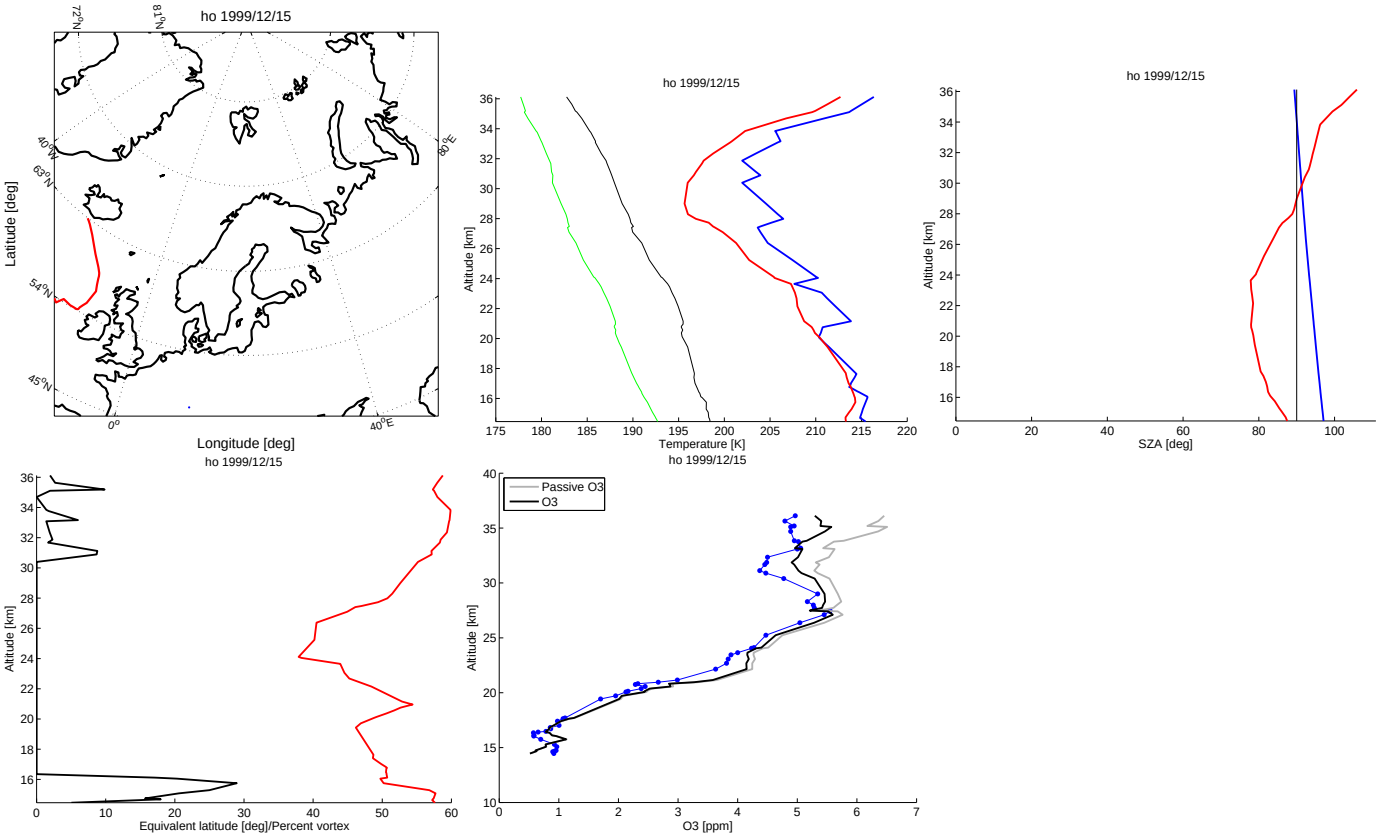

Figure 36: Hohenpeissenberg 15 December 1999

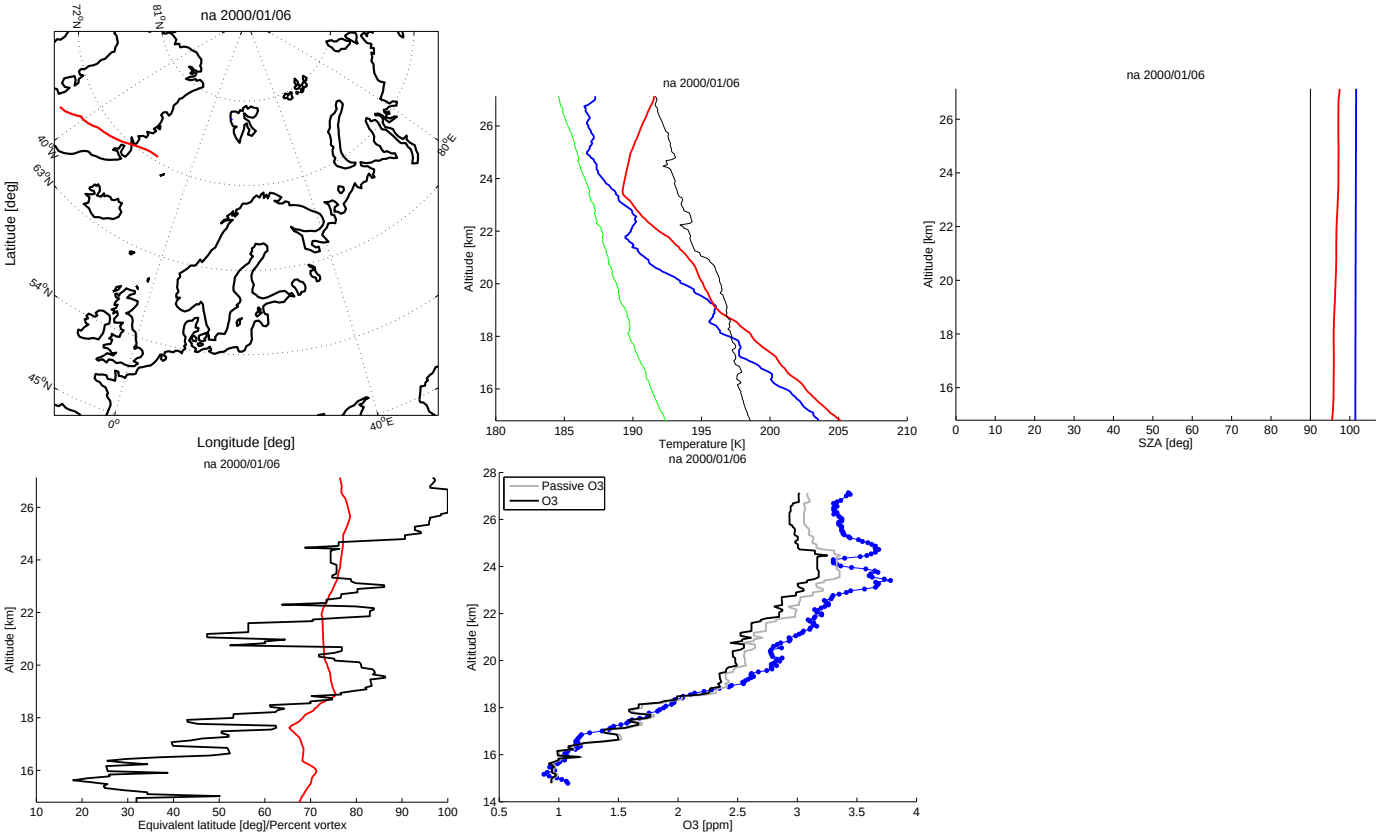

Figure 37: Ny-Alesund 6 January 2000

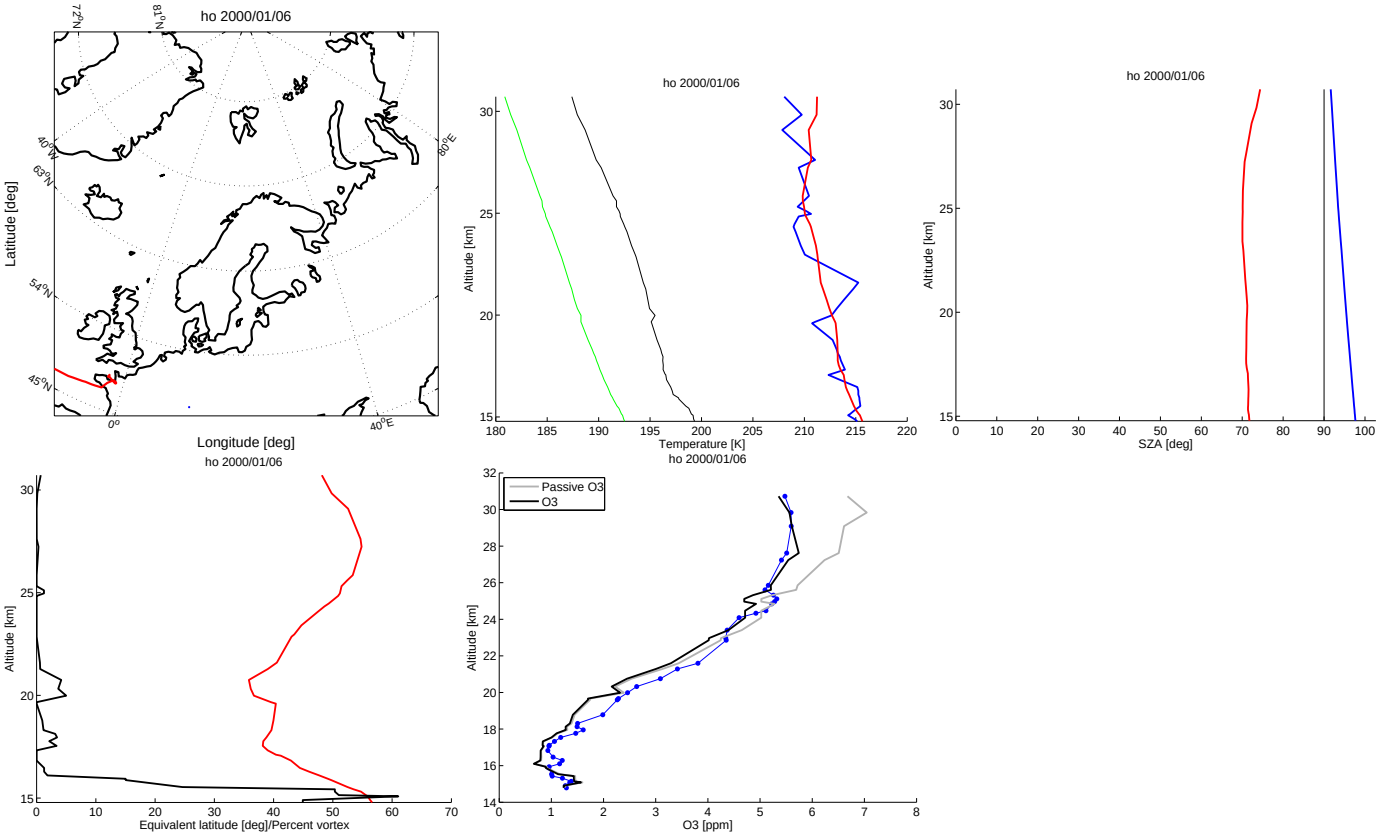

Figure 38: Hohenpeissenberg 6 January 2000

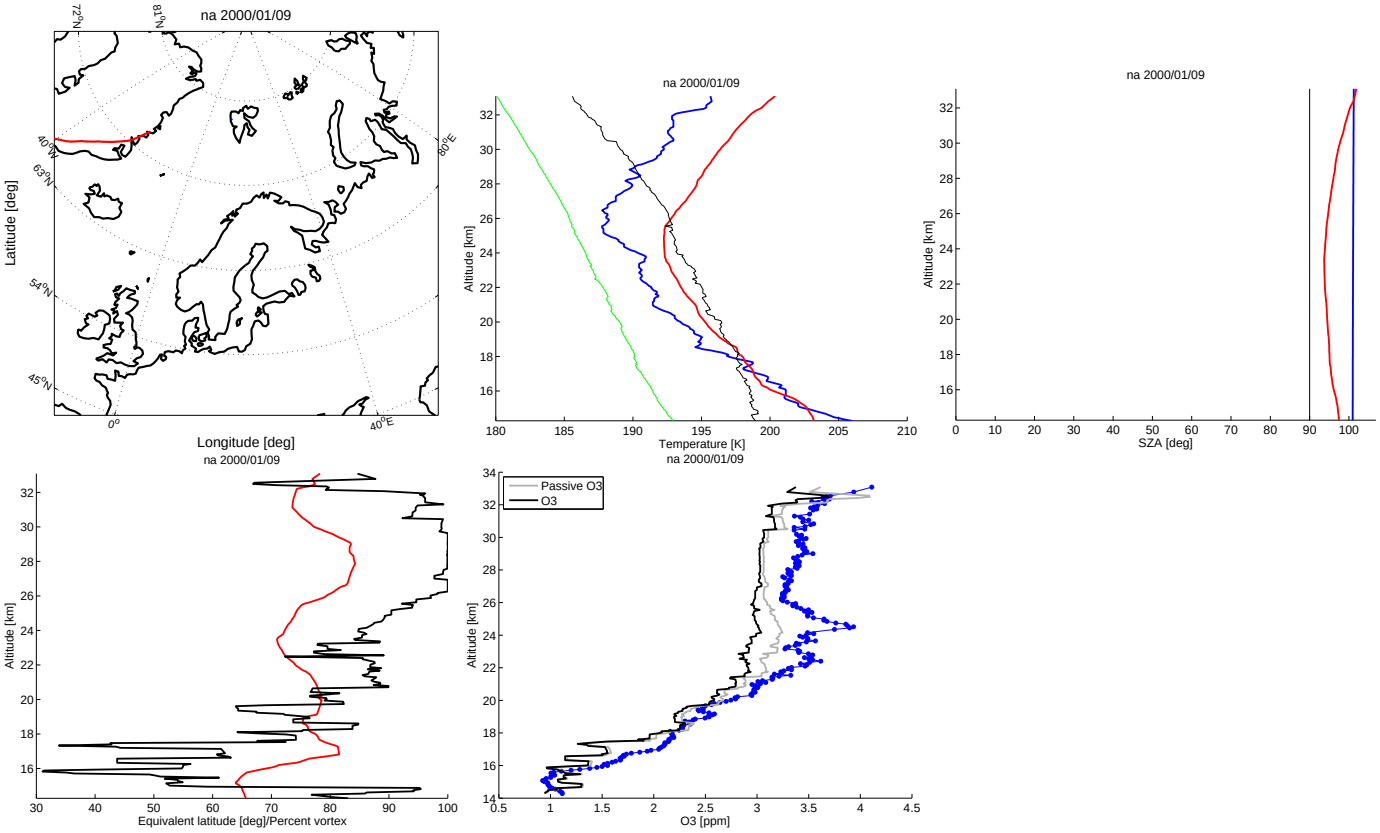

Figure 39: Ny-Alesund 9 January 2000

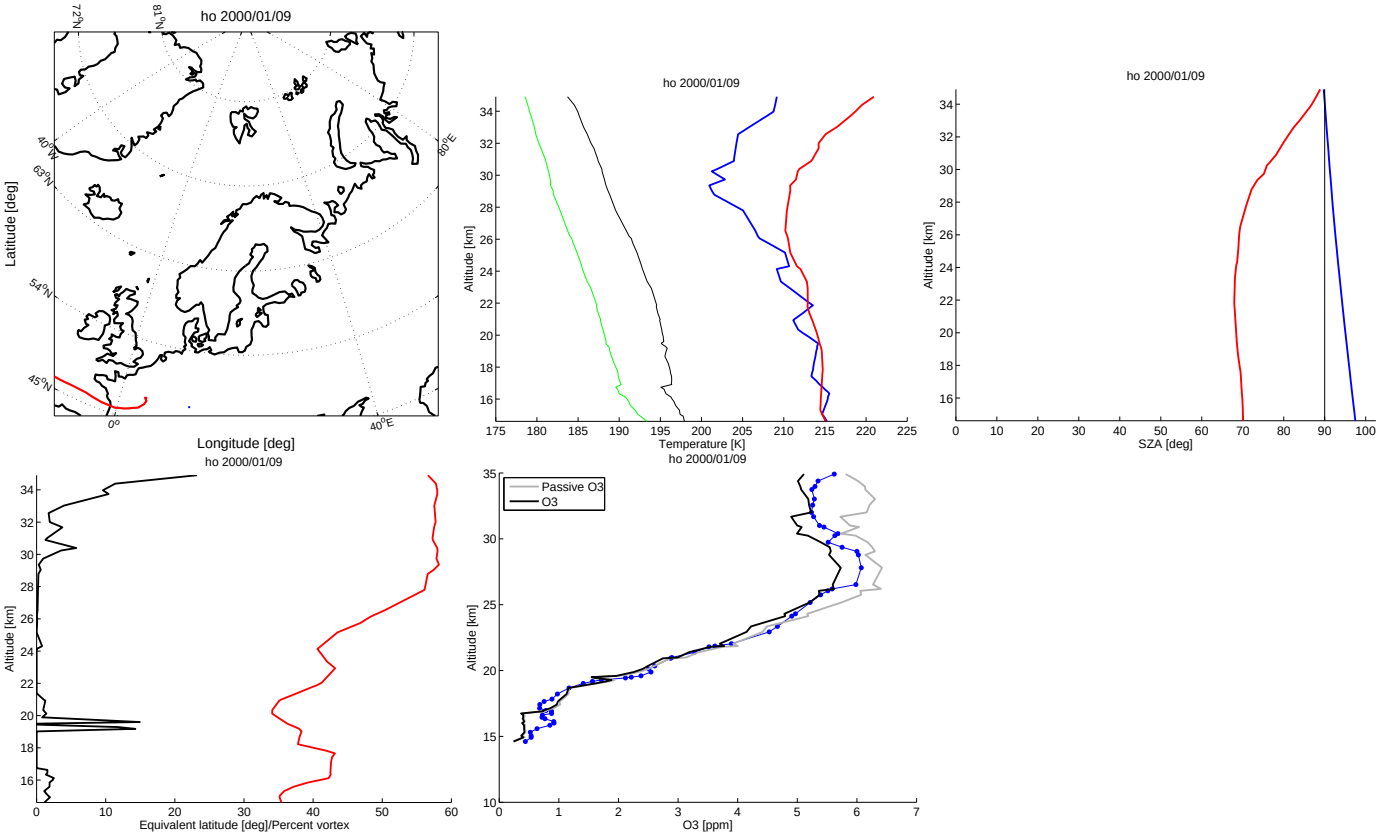

Figure 40: Hohenpeissenberg 9 January 2000

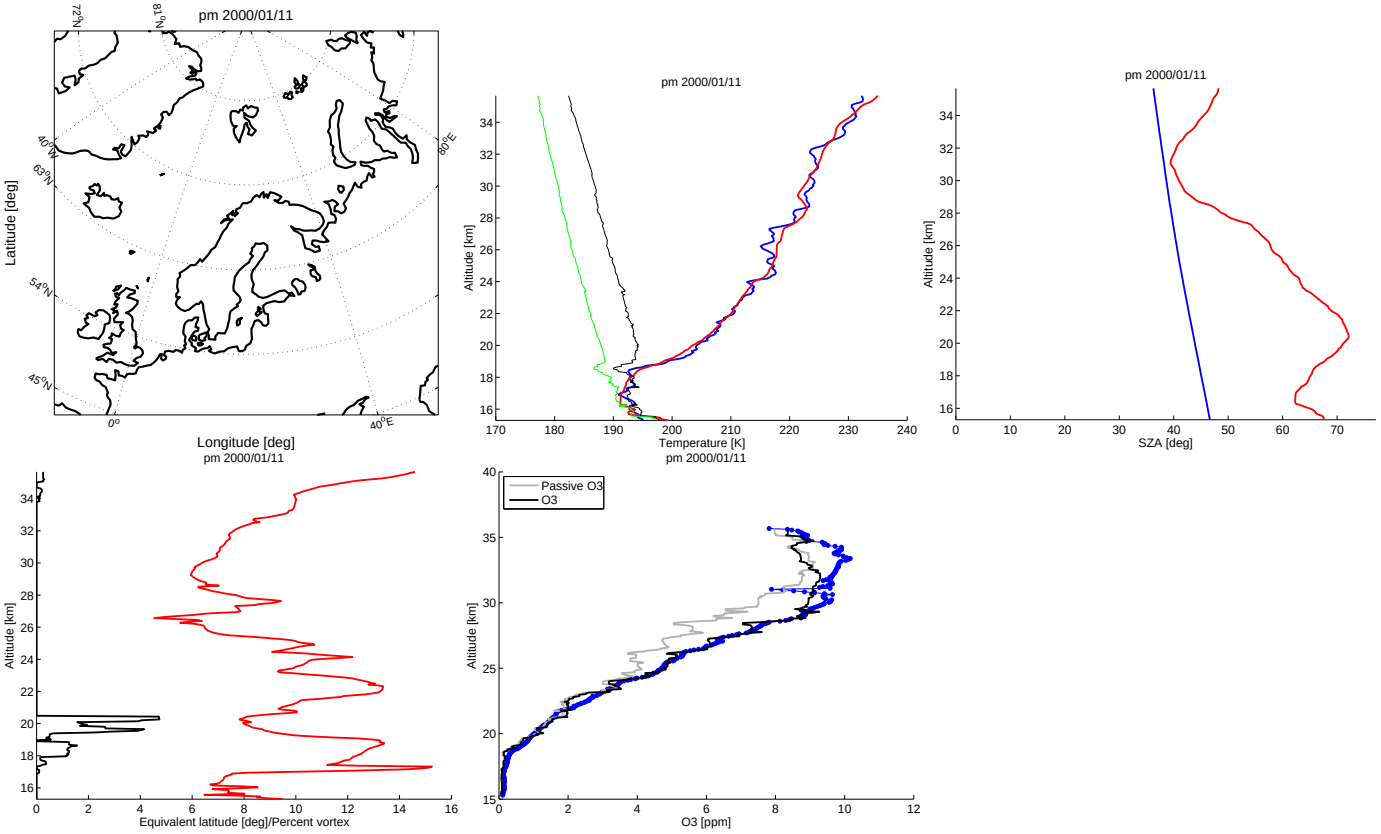

Figure 41: Paramaribo 11 January 2000

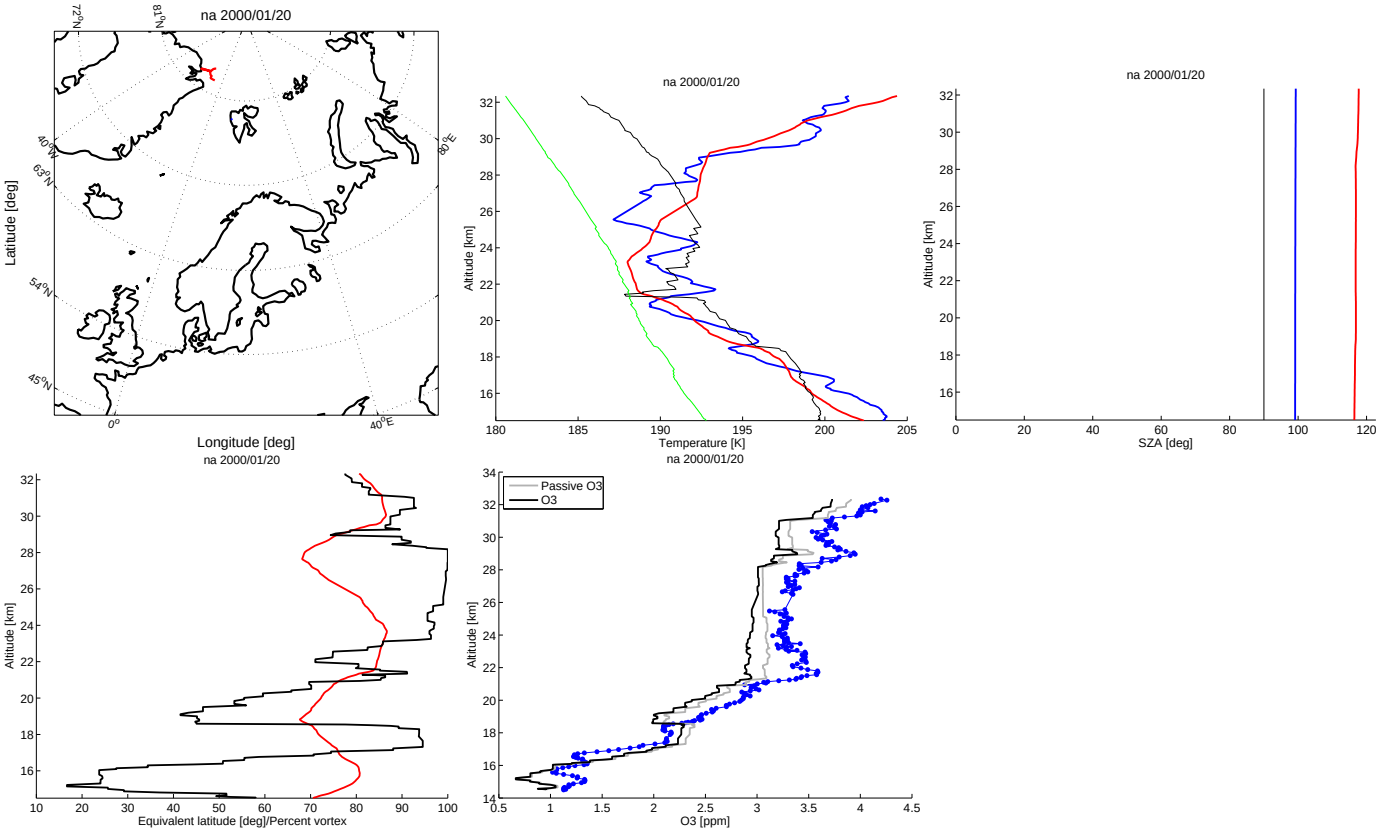

Figure 42: Ny-Alesund 20 January 2000

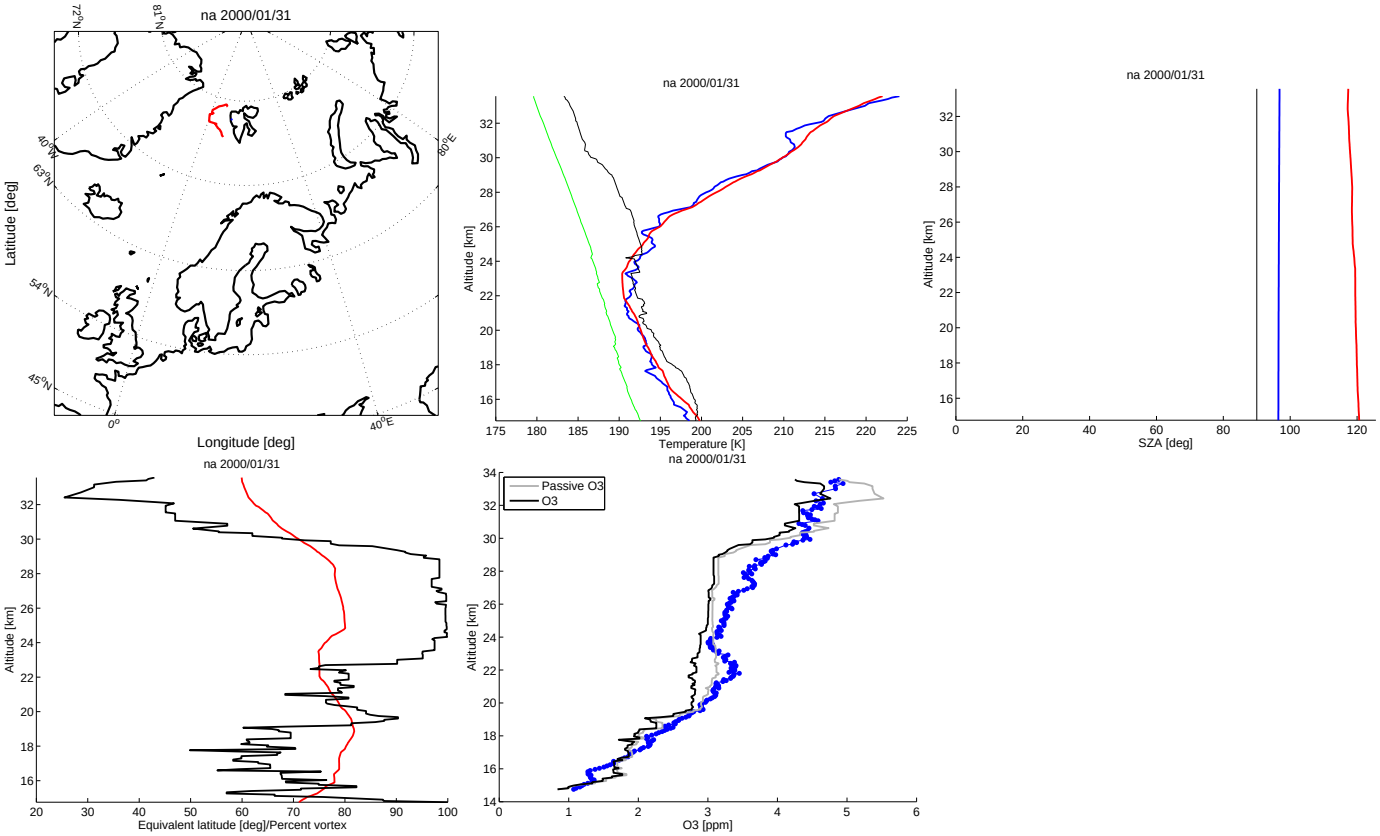

Figure 43: Ny-Alesund 31 January 2000

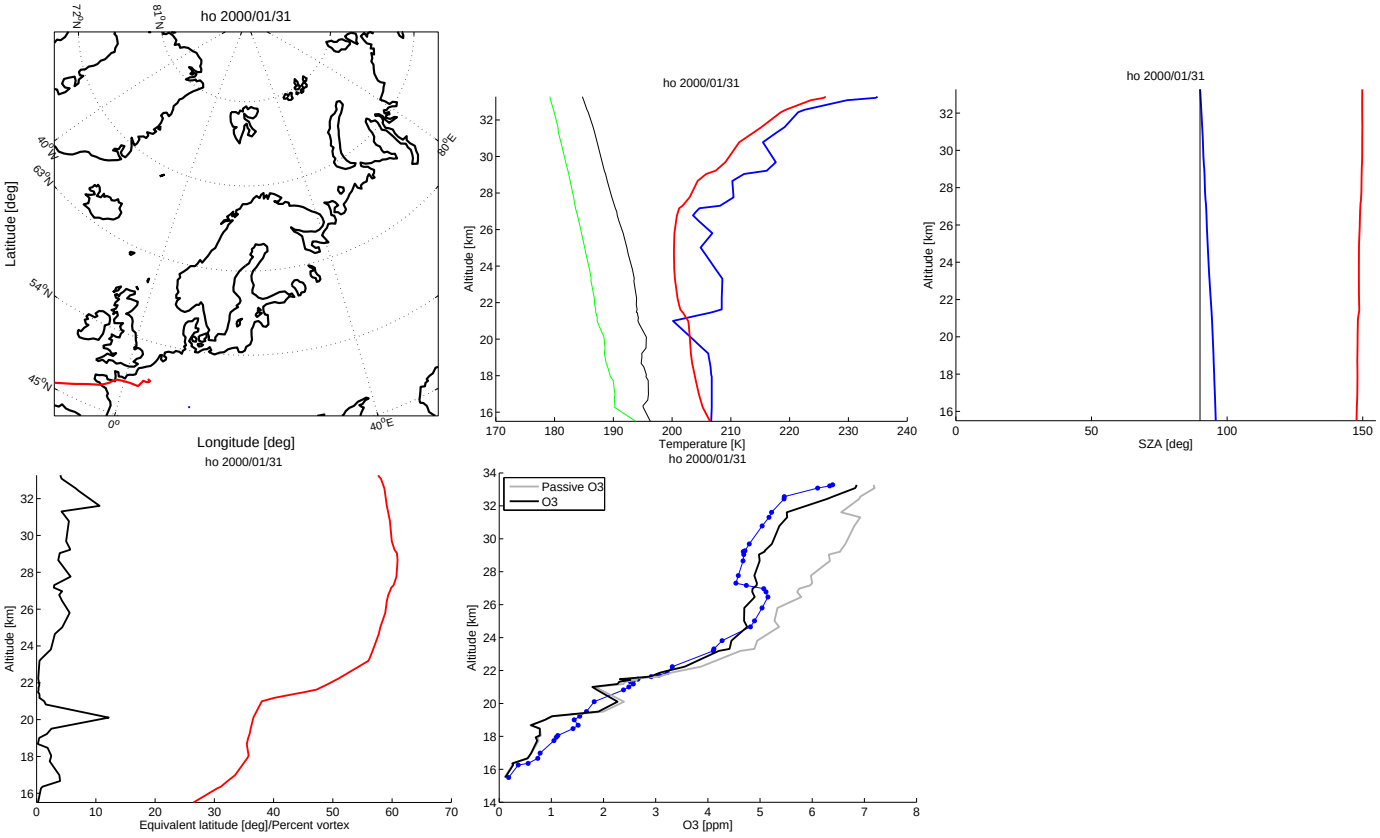

Figure 44: Hohenpeissenberg 31 January 2000

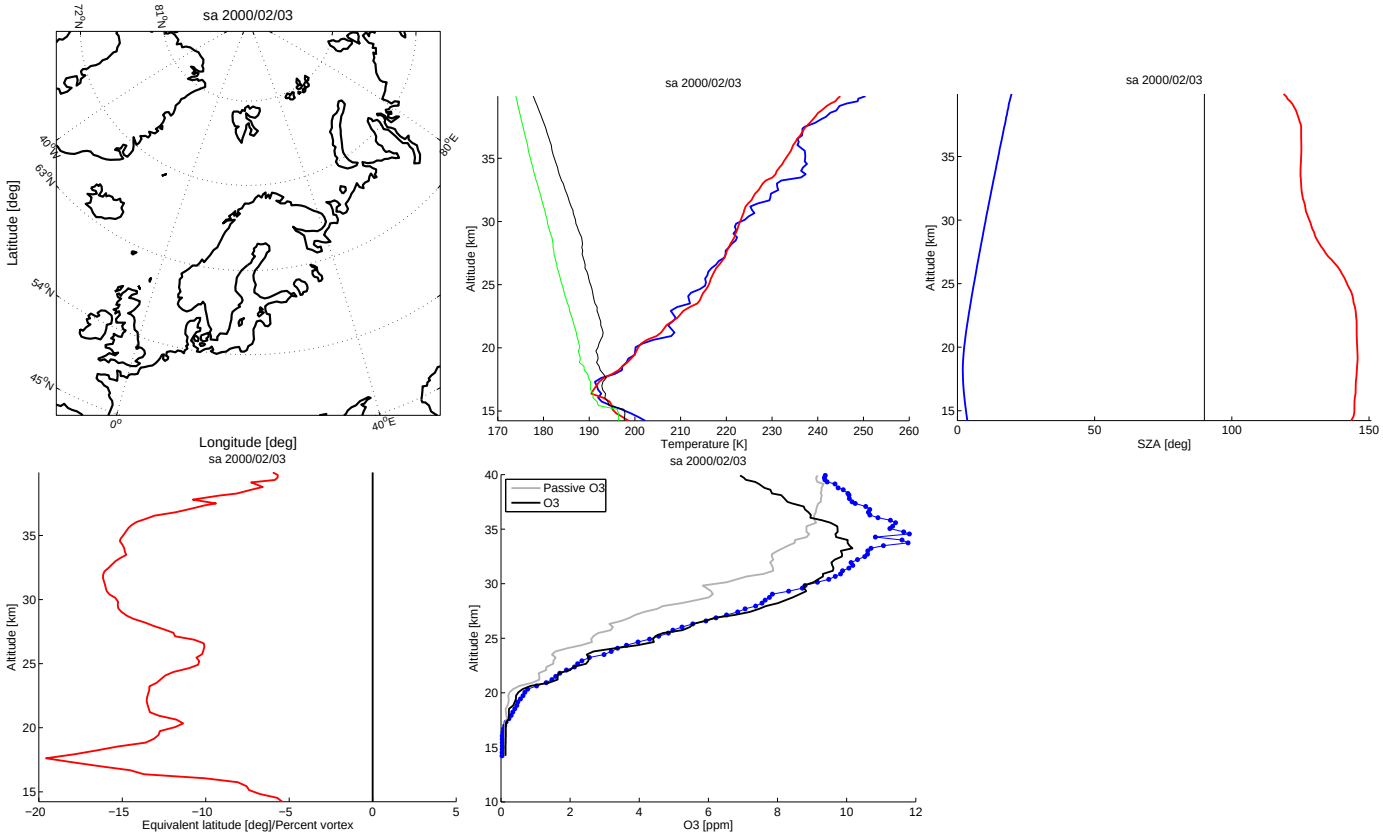

Figure 45: Samoa 3 February 2000

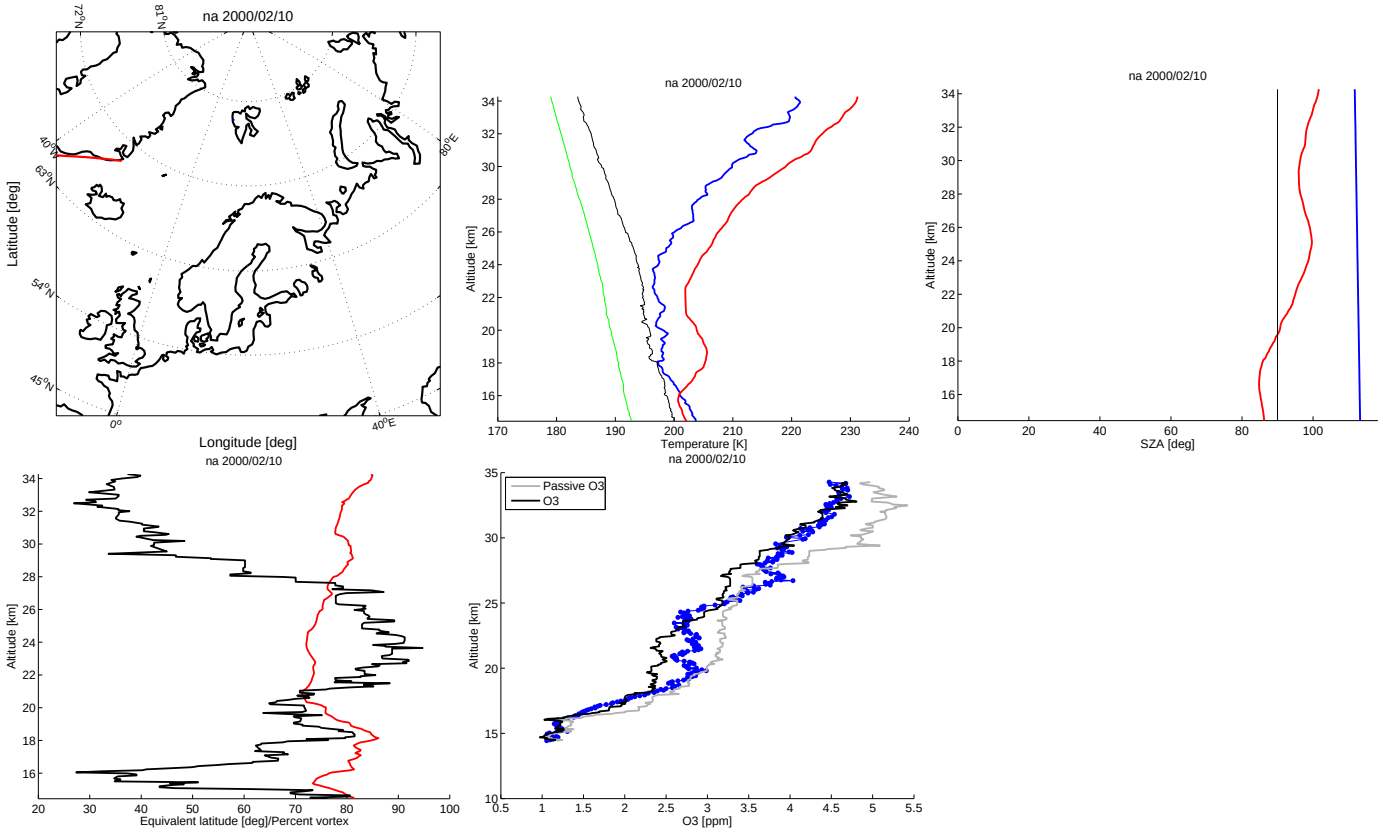

Figure 46: Ny-Alesund 10 February 2000

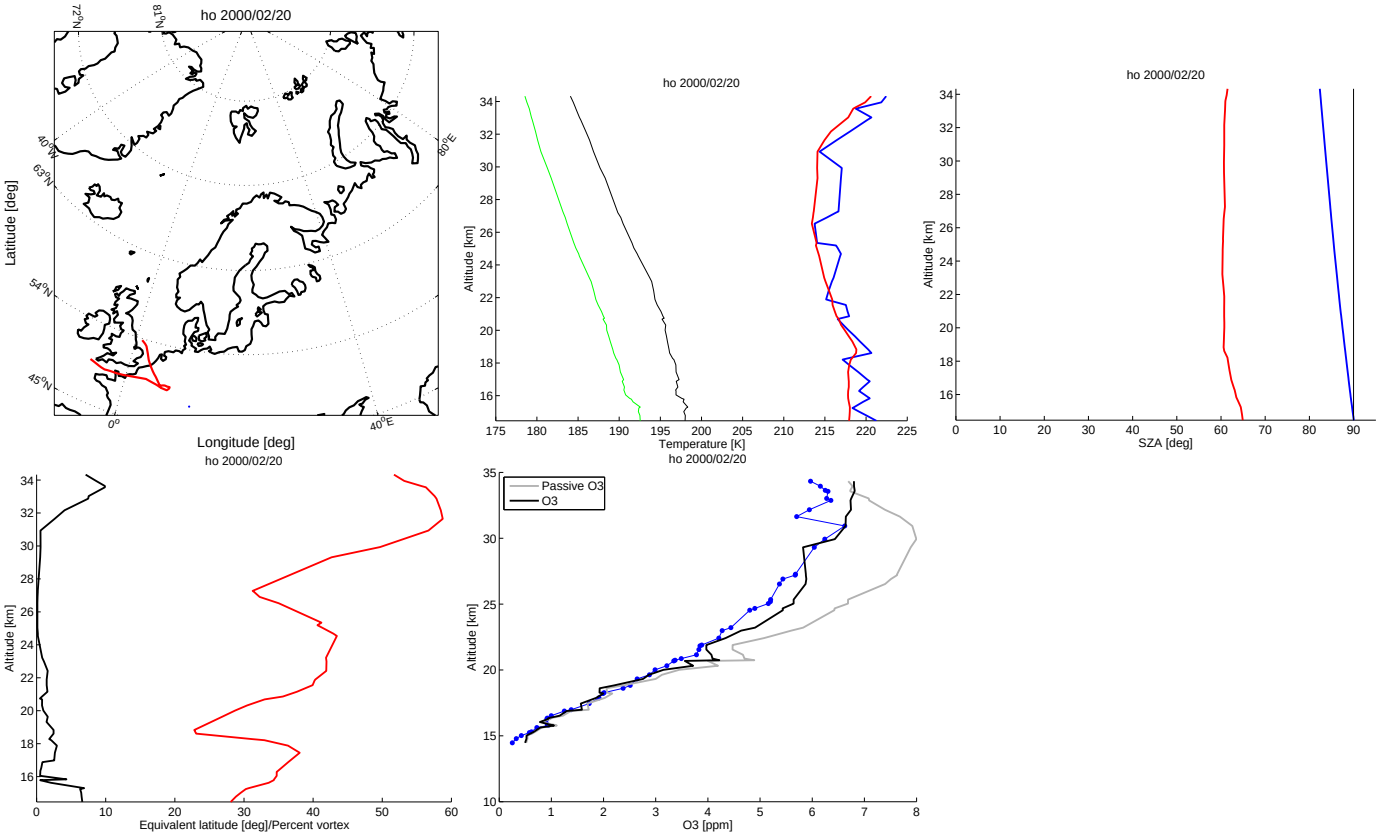

Figure 47: Hohenpeissenberg 20 February 2000

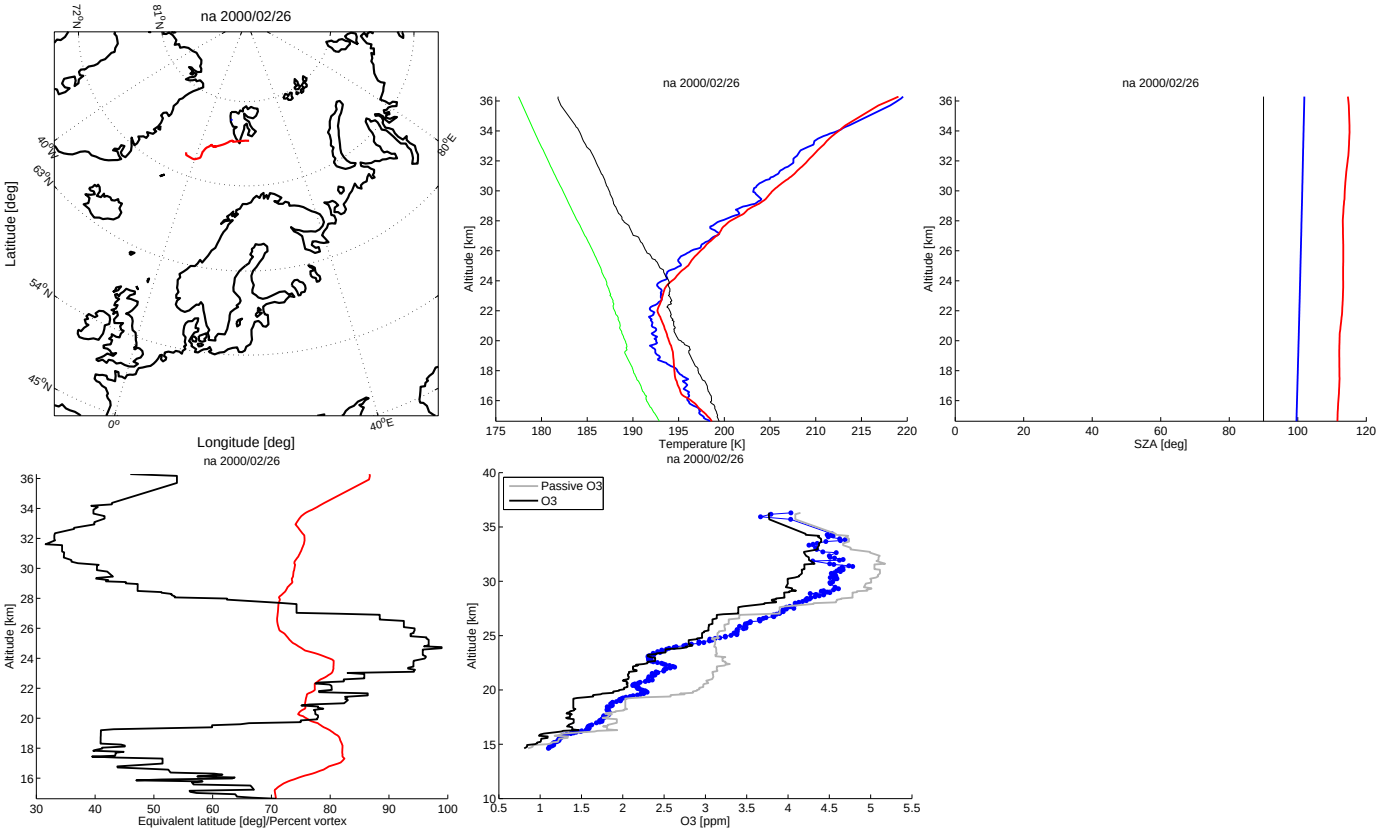

Figure 48: Ny-Alesund 26 February 2000

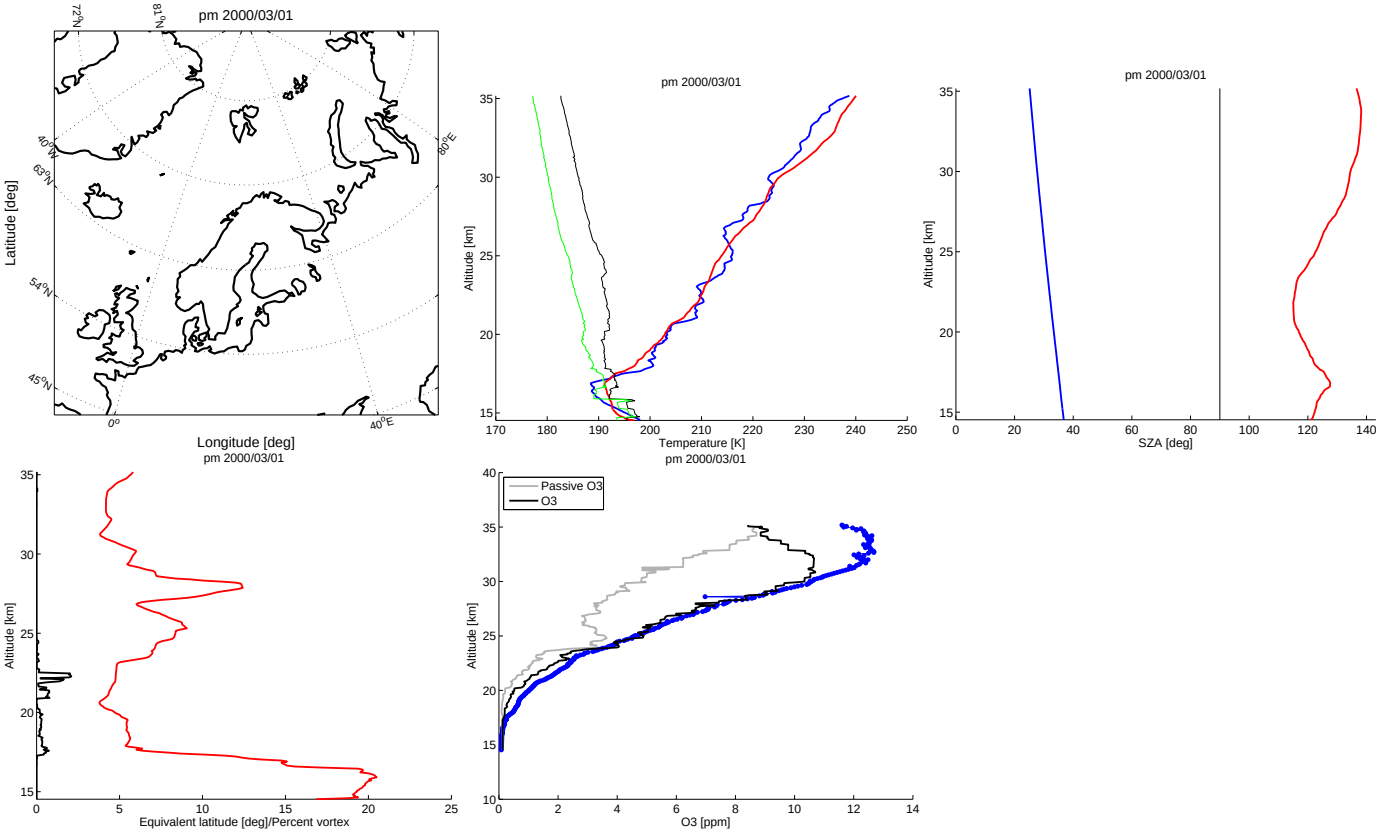

Figure 49: Paramaribo 1 March 2000

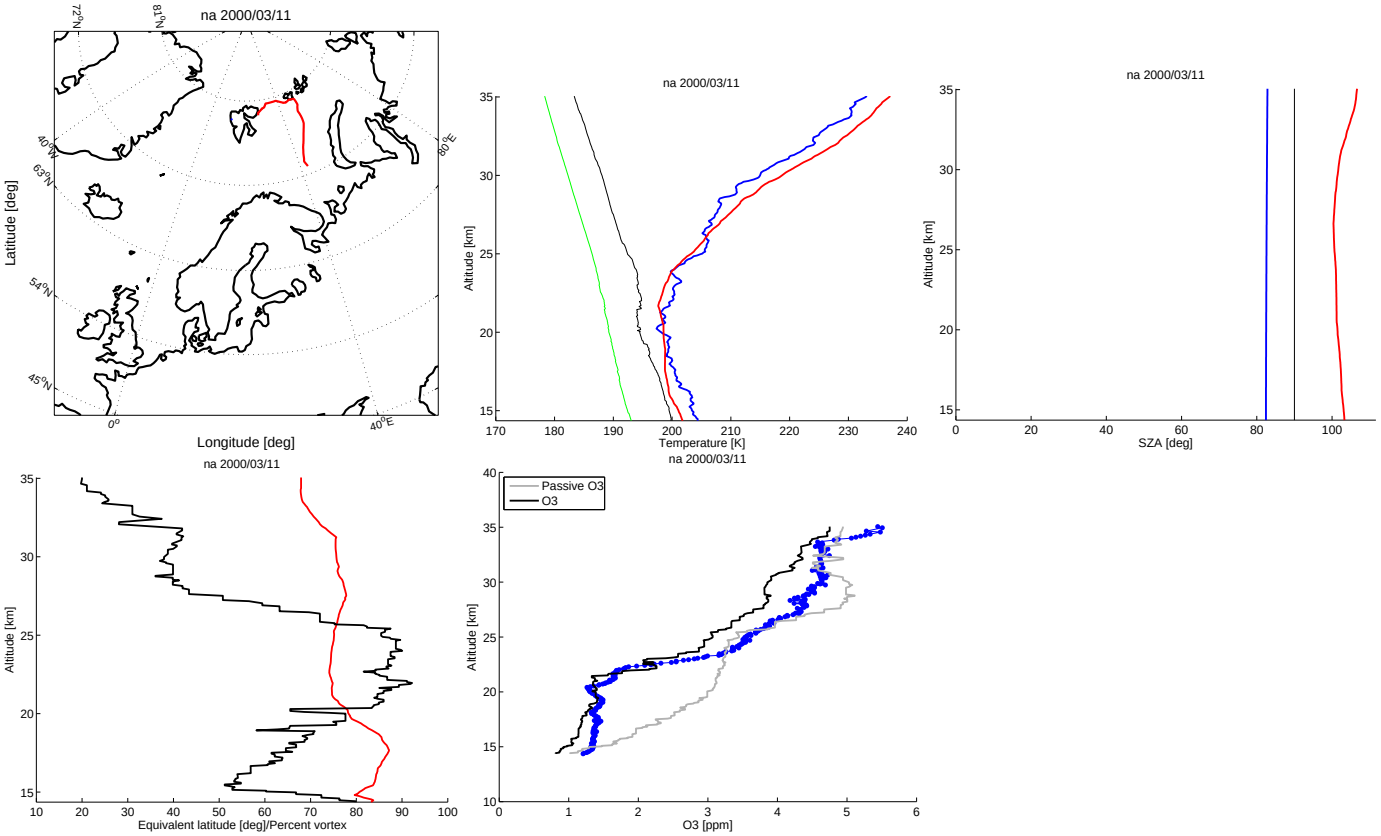

Figure 50: Ny-Alesund 11 March 2000

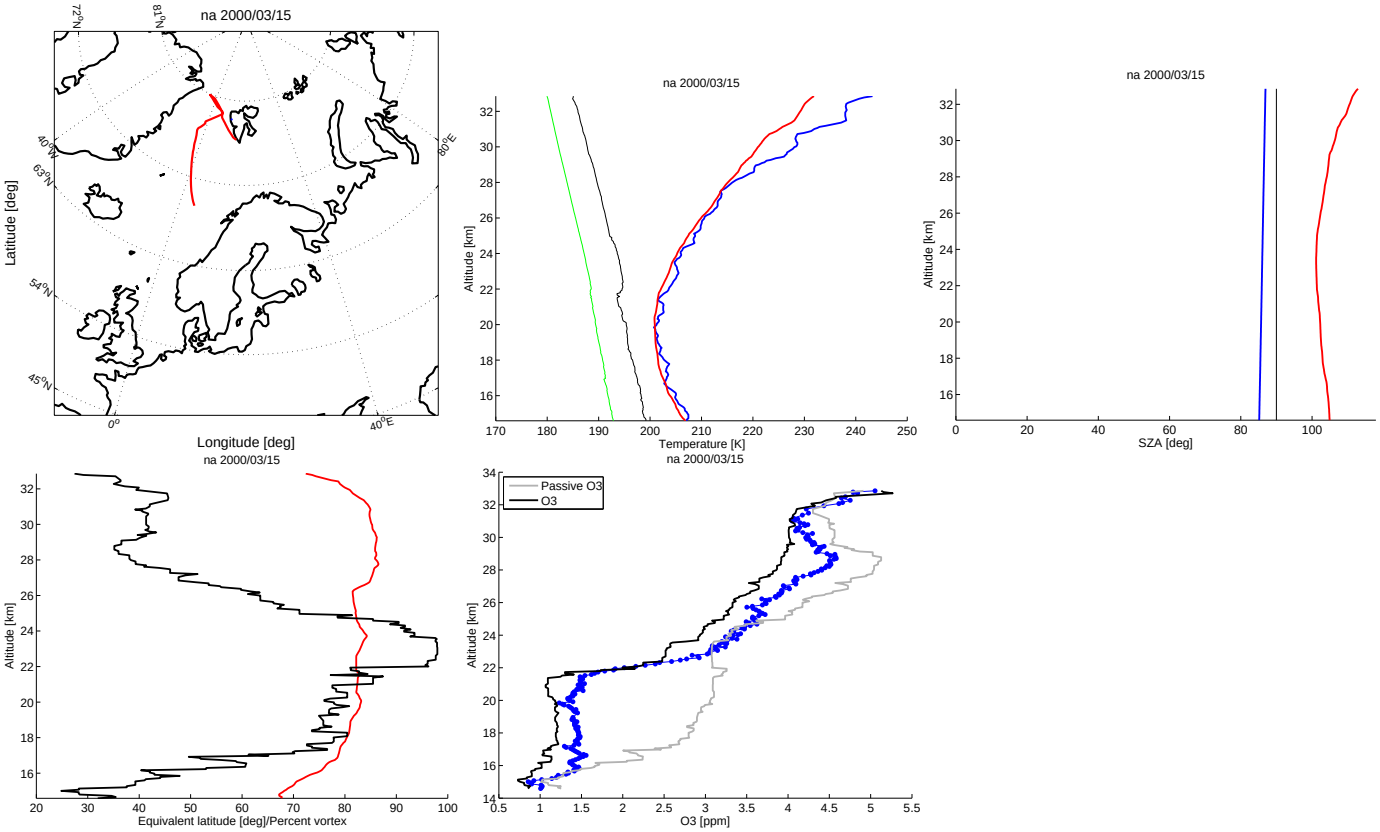

Figure 51: Ny-Alesund 15 March 2000

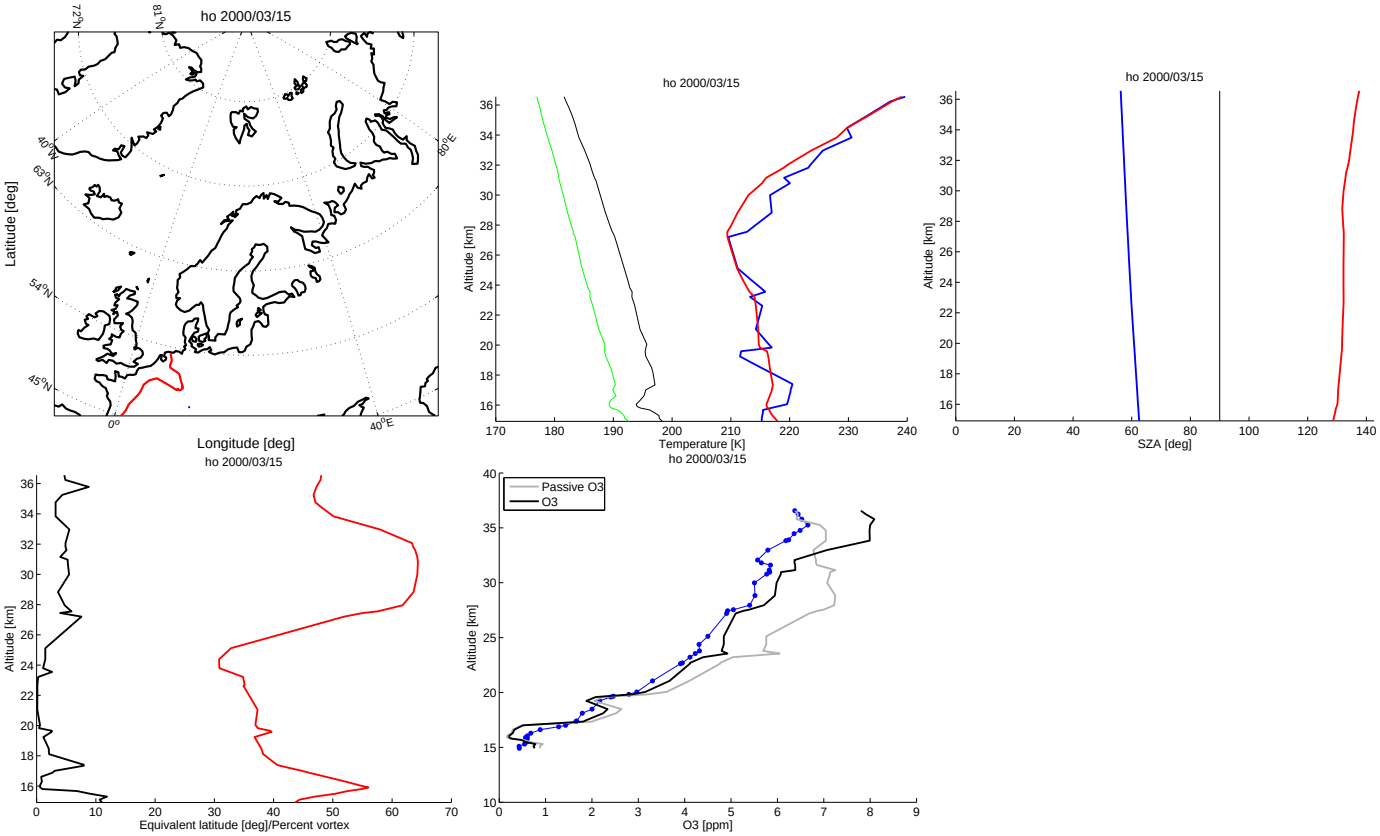

Figure 52: Hohenpeissenberg 15 March 2000

5 Vortex means

The next figures show vortex means averaged over all air parcels inside the inner vortex boundary according to the Nash criterion and over several hybrid coordinate (i.e. potential temperature) intervals equivalent to the mixing depth of the model. From upper left to lower right: Ozone, ozone loss as difference between chemically active ozone and the passive ozone tracer, denitrification as difference between NO_y and the passive NO_y tracer, ClO and NO_x.

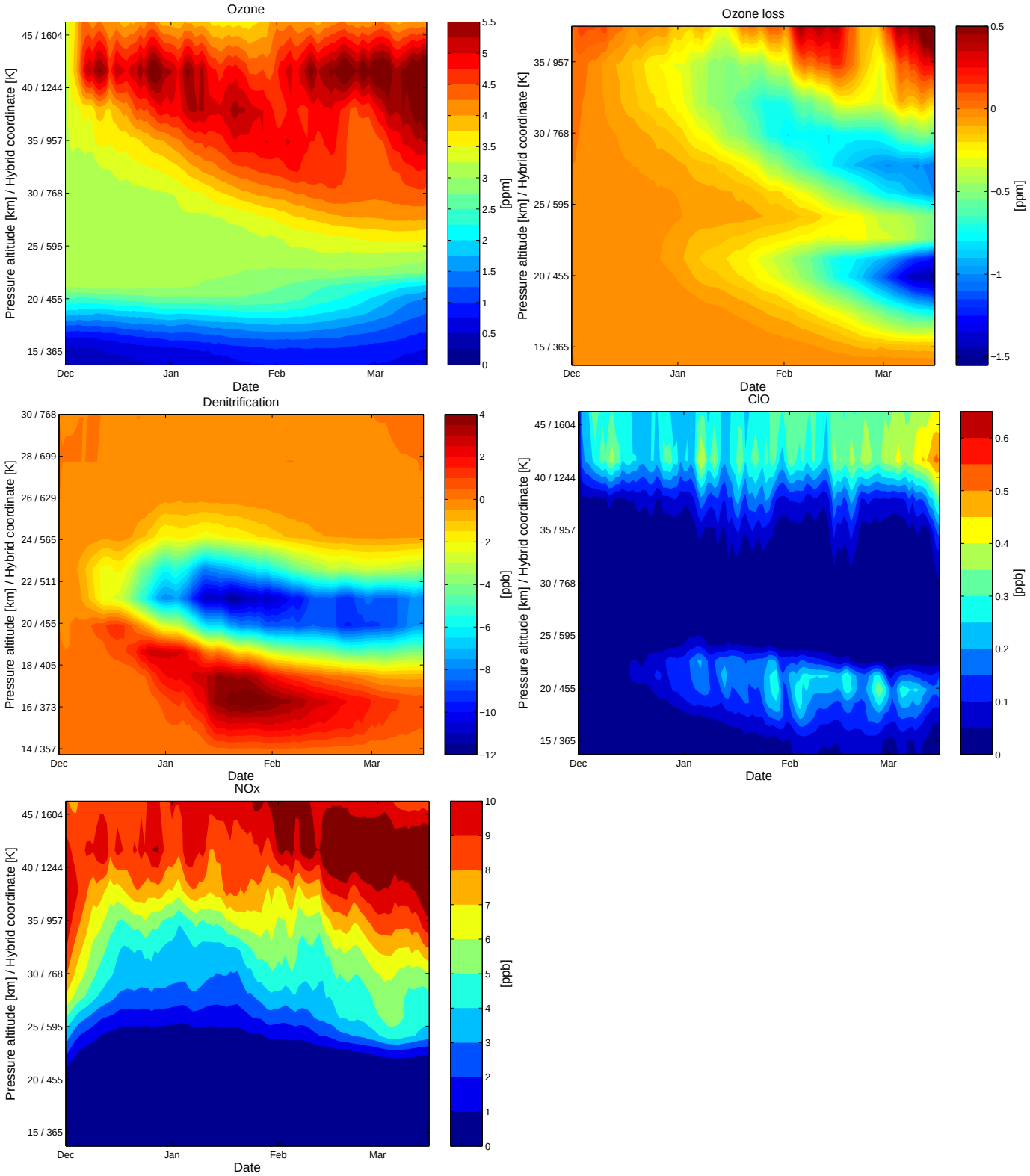

Figure 53: Vortex means of ozone, ozone loss, denitrification, ClO and NO_x inside the inner vortex boundary according to Nash.

6 HALOE zonal means

The next figures show zonal and monthly mean mixing ratios for HCl, O_3, CH_4, H_2O and NO_x as a function of pressure altitude and equivalent latitude for February 2000. Left: HALOE measurements, right: modeled values.

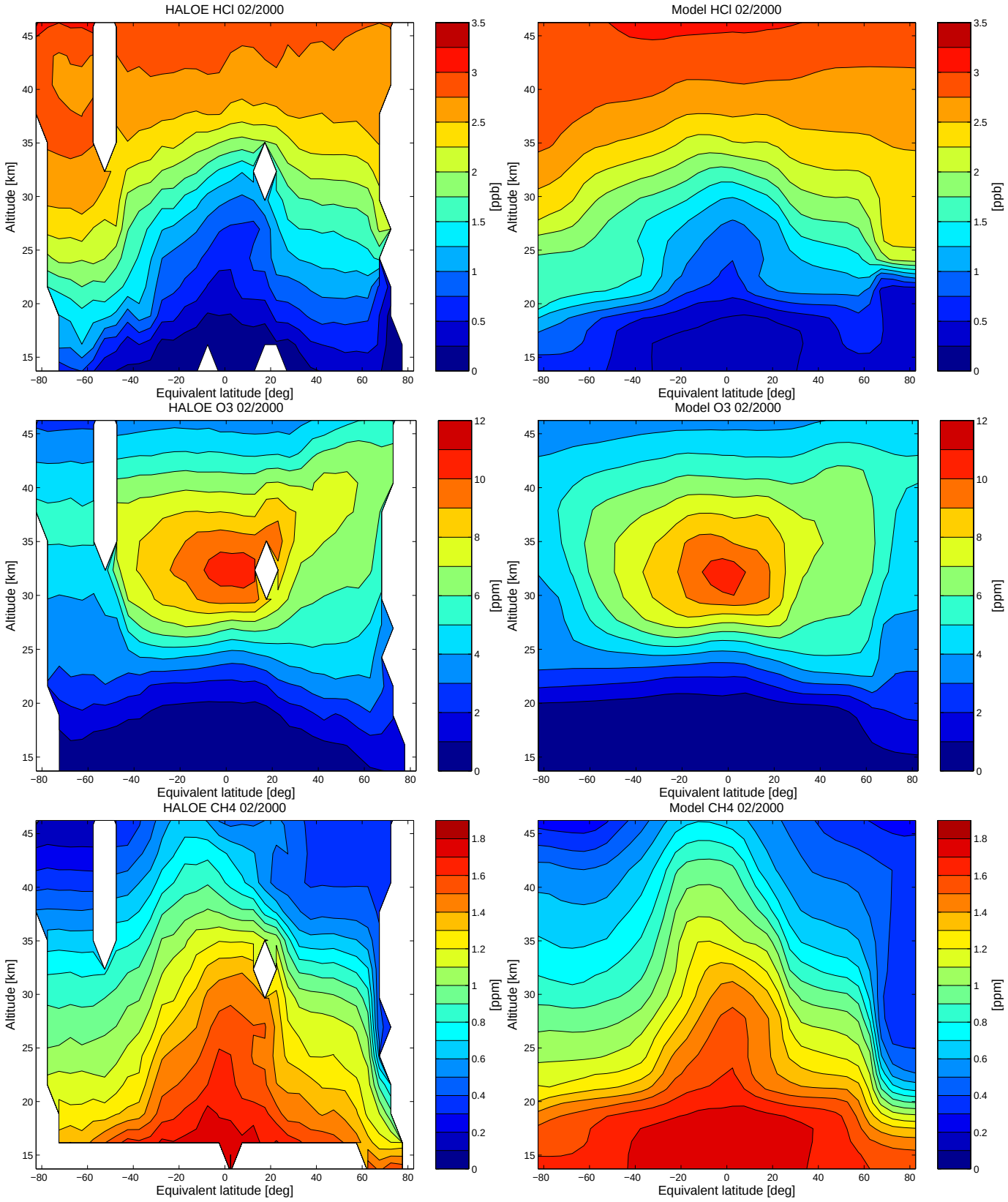

Figure 54: Zonal and monthly mean mixing ratios of HCl, O_3 and CH_4 as a function of pressure altitude and equivalent latitude for February 2000. Left: HALOE measurements, right: modeled values.

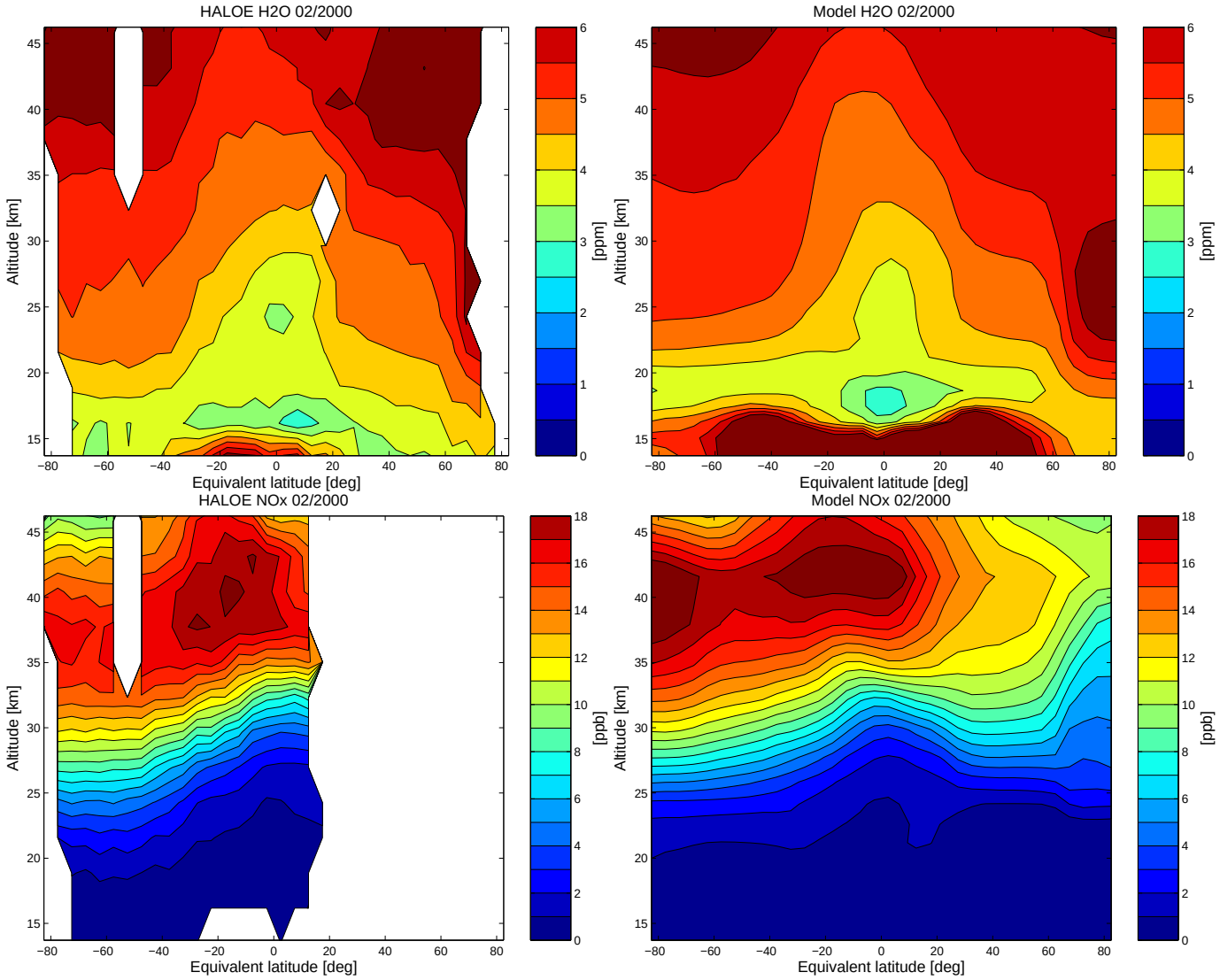

Figure 54: Zonal and monthly mean mixing ratios of H_2O and NO_x as a function of pressure altitude and equivalent latitude for February 2000. Left: HALOE measurements, right: modeled values.